HELLENIC REPUBLIC

National and Kapodistrian University of Athens

EST. 1837

SLIP DISTRIBUTION OF LARGE EARTHQUAKES IN GREECE

Christos Millas

MSc Thesis

Examination Committee

Dr. Kaviris George (Assistant Professor, Supervisor)

Dr. Karakostas Vasileios (Professor)

Dr. Papadimitriou Panayotis (Professor)

Keywords: Slip Distribution; Slip Inversion; Crustal Deformation; Earthquakes in Greece

ATHENS 2018

Table of Contents

Acknowledgements

The present Master Thesis was conducted in the framework of the Postgraduate Program of the Faculty of Geology and Geoenvironment of the National and Kapodistrian University of Athens, in the specialization field of Seismology. It is my moral obligation and will to thank all these individuals who supported and taught me throughout my entire academic years. First and foremost, I would like to say special thanks to my supervisor/mentor Dr. George Kaviris, who gave me motive and moral support. He was always willing to spend his time and his almost unlimited patience in order to teach and guide me, from my second year of Undergraduate Studies, until now. I would strongly like to express my gratitude to Dr. Vasileios Karakostas for his guidance throughout my Thesis. His assistance and suggestions in general, but especially in his area of expertise was vital to me. For the third member of my three-member committee, Dr. Panayotis Papadimitriou, I am grateful for his suggestions and the challenges that he put on me, in order to guide me in a path to defy and surpass my limits. Dr. Papadimitriou is one of the reasons that made me try my best and eventually succeed in this endeavor and thus he has my gratitude.

I would like to express my gratitude towards Dr. Nicholas Voulgaris for his trust, his important lessons and his guidance along my Under and Postgraduate years. Of course, I should also thank Dr. Vasiliki Kouskouna for her trust and all her advices along the way. Her open heartedness and her will to assist are some of the things that make her one of the favorite teachers I have ever had. Special thanks also to Dr. Ioannis Kassaras for his important lessons and advices. A special mention to Dr. Ritsa Papadimitriou; it was a real opportunity for me to communicate and exchange ideas with her. She is always willing to answer to every question with a smile. My limited time with her was educative and a real pleasure nonetheless. I would like to thank Dr. Kiriaki Pavlou for the fruitful conversations through the years and the educational experience by being her Assistant in teaching activities. For his valuable contribution by providing accelerometric data, I would like to express my gratitude to Dr. Efthimios Sokos. Moreover, I would like to thank Dr. Andreas Karakonstantis for his companion, advices and scientific conversations, but especially Dr. George Sakkas, Dr. Vasilis Kapetanidis, Dr. Maria Mesimeri and Phd Candidate Tasos Kostoglou for their support and assistance in the present Thesis. A very special gratitude goes out to the three Master students that accompanied me for the last two years. For Mr. Ioannis Spingos, I would like to thank him for all the support and assistance and to mention that it was a privilege to collaborate with him. For Msc. Ioannis Fountoulakis, it was a pleasure to be fellow students. Last but not least, I would like to express my gratitude for Mr. Theodoros Aspiotis for our collaboration in the Master's program. Last but not least, I would like to thank my fellow students and friend Pavlos Bonatis for his friendship, assistance and his hospitality.

It is important to thank my family for their moral and financial support, as long as for their patience, which helped me going for all these years. I would also like to express my love to a very special woman, my grandmother. For my friends, it is difficult to describe with words all

the feelings toward them and thus I will not try to. Instead, I would like to express just my love and gratitude to all and especially to those who are really close to me and patiently listened and supported me no matter what. Lastly, I would like to dedicate this Master Thesis to all these individuals that molded and shaped my character through the years, even if some of them are not present in my life any more. I am grateful to all.

Περίληψη

Η εκτίμηση της χωρικής και χρονικής κατανομής της ολίσθησης στην επιφάνεια του ρήγματος αποτελεί σημαντικό εργαλείο για τους σεισμολόγους και όλους τους γεω-επιστήμονες για την κατανόηση της χωροχρονικής εξέλιξης της σεισμικής διάρρηξης. Μια τέτοια διαδικασία απαιτεί δεδομένα τα οποία προσδιορίζονται μετά από ένα ισχυρό σεισμικό γεγονός, δηλαδή τις εστιακές παραμέτρους, συμπεριλαμβανομένου του μηχανισμού γένεσης και τη γεωμετρία του ρήγματος. Η μέθοδος αντιστροφής του τανυστή ολίσθησης μπορεί να συμβάλλει στη δημιουργία αξιόπιστων χαρτών κατανομής εδαφικής κίνησης (shakemaps), στη γρήγορη αντίδραση της πολιτείας μετά από μεγάλο σεισμό και στην εκτίμηση πιθανότητας εκδήλωσης μετασεισμών. Το λογισμικό LinSlipInv (Gallovic and Zahradnik, 2011; Gallovic et al., 2014) εκτελείται χρησιμοποιώντας τοπικά και περιφερειακά δεδομένα που έχουν καταγραφεί από σεισμογράφους του Ενιαίου Εθνικού Δικτύου Σεισμογράφων (ΕΕΔΣ), καθώς και από τα δίκτυα επιταχυνσιογράφων του Γεωδυναμικού Ινστιτούτου του Εθνικού Αστεροσκοπείου Αθηνών (ΓΙ-ΕΑΑ), του Ινστιτούτου Τεχνικής Σεισμολογίας και Αντισεισμικών Κατασκευών (ΙΤΣΑΚ) και, για το Ανατολικό Αιγαίο, δεδομένα από Kandilli Observatory and Earthquake Research Institute (KOERI) και το Κεντρικό Σύστημα Δεδομένων Σεισμών της Τουρκίας (AFAD). Εξετάστηκαν επιλεγμένοι ισχυροί σεισμοί (με $M_w \geq 6.0$) που έγιναν κατά την τελευταία πενταετία σε διάφορες περιοχές της ελληνικής επικράτειας. Κατά τον προσδιορισμό της κατανομής ολίσθησης μέσω του λογισμικού LinSlipInv, εξετάστηκαν οι μηχανισμοί γένεσης, τα μοντέλα ταχύτητας και η γεωμετρία των ρηγμάτων από ήδη δημοσιευμένες εργασίες.

Τα αποτελέσματα της κατανομής ολίσθησης χρησιμοποιήθηκαν ως δεδομένα εισόδου για τον υπολογισμό της εδαφικής παραμόρφωσης, χρησιμοποιώντας το πρόγραμμα DIS3D (Erickson, 1987), λαμβάνοντας υπόψη ότι δεν παρατηρήθηκε ίχνος του ρήγματος στην επιφάνεια. Η προκύπτουσα κατανομή ολίσθησης και η εδαφική παραμόρφωση συγκρίθηκαν με εκείνες που προσδιορίστηκαν από άλλες μελέτες, συμπεριλαμβανομένων εκείνων που χρησιμοποιούν τεχνικές συμβολομετρίας InSAR και GNSS.

Τα αποτελέσματα της κατανομής ολίσθησης κρίνονται ικανοποιητικά. Η κατανομή ολίσθησης για τον σεισμό της Κεφαλονιάς που έλαβε χώρα στις 26 Ιανουαρίου 2014, και προέκυψε από την εφαρμογή του λογισμικού LinSlipInv χρησιμοποιώντας δεδομένα σε τοπικές έως και περιφερειακές αποστάσεις, ανέδειξε ένα επεισόδιο διάρρηξης, ήτοι μία σεισμική πηγή, με μέγιστη ολίσθηση ίση με 40 cm. Όσον αφορά στην εδαφική παραμόρφωση που προέκυψε από την υπολογισθείσα κατανομή ολίσθησης, οι τιμές στην οριζόντια και κατακόρυφη συνιστώσα είναι χαμηλές, κυρίως λόγω του μεγέθους και του εστιακού βάθους του σεισμού. Τα αποτελέσματα έδειξαν μέγιστη τιμή οριζόντιας μετατόπισης 2 cm, ανατολικά του ρήγματος, γύρω από το Αργοστόλι.

Η ολίσθηση για τον σεισμό της Λήμνου στις 24 Μαΐου 2014 ανέδειξε μια πολύπλοκη πηγή, η οποία αποτελείται από τρία διακριτά υπο-γεγονότα. Τα στιγμιότυπα της ολίσθησης αποκάλυψαν ότι αυτή κατευθύνθηκε προς την οροφή του ρήγματος, ενώ η μέγιστη τιμή

έφτασε τα 1.4 m, εμφανίζοντας μια δικαντευθυντική διάρρηξη. Πιο συγκεκριμένα, παρατηρήθηκε μια αρχική διάδοση προς τα δυτικά, ακολουθούμενη από ένα μεγάλο επεισόδιο ολίσθησης προς τα ανατολικά. Η παραγόμενη εδαφική παραμόρφωση στη Λήμνο δείχνει δεξιόστροφη οριζόντια κίνηση.

Τα τοπικά έως περιφερειακά δεδομένα που χρησιμοποιήθηκαν στην αντιστροφή της ολίσθησης για τον σεισμό της Λευκάδας της 17ης Νοεμβρίου 2015 αποκάλυψαν κατευθυντικότητα προς τα ΝΝΔ. Επιπλέον, αναγνωρίστηκαν δύο σεισμικές πηγές, ενώ η μέγιστη τιμή ήταν 1.2 m. Όσον αφορά στην εδαφική παραμόρφωση, η δεξιόστροφη κίνηση επιβεβαιώθηκε με τα αποτελέσματα που προέκυψαν στην παρούσα μελέτη, χρησιμοποιώντας το λογισμικό DIS3D. Παρατηρήθηκαν μικρές τιμές ανύψωσης για το νότιο τμήμα της Λευκάδας (μέγιστη ανύψωση 7 cm).

Σύμφωνα με τα αποτελέσματα αναστροφής του LinSlipInv για τον σεισμό της Λέσβου που συνέβη στις 12 Ιουνίου 2017, η μέγιστη ολίσθηση ήταν ~ 1.0 m και εντοπίστηκε μία μοναδική πηγή. Η εξέλιξη της διάρρηξης, όπως αποκαλύφθηκε από τα στιγμιότυπα ολίσθησης ανά 1 δευτερόλεπτο, έδειξε ένα μοναδικό επεισόδιο ολίσθησης και διάρρηξη προς τα ΒΔ, η οποία θα μπορούσε να εξηγήσει εν μέρει τις βλάβες που παρατηρήθηκαν στο χωριό Βρίσα. Η εφαρμογή του λογισμικού DIS3D ανέδειξε οριζόντια κίνηση προς τα ΒΒΑ στη Νήσο Λέσβο. Επιπλέον, εντοπίστηκε καθίζηση που φθάνει τα 20 cm στα νότια παράλια, πλησίον του σεισμογόνου ρήγματος.

Τα αποτελέσματα κατανομής ολίσθησης που προέκυψαν για τον σεισμό της 20ης Ιουλίου 2017 στην Κω παρουσίασαν μία μοναδική πηγή με μέγιστη τιμή ολίσθησης 1.8 m. Το προτεινόμενο ρήγμα είναι αυτό που κλίνει προς βορρά. Όσον αφορά την εδαφική παραμόρφωση, εντοπίστηκε μετατόπιση με διεύθυνση περίπου Β-Ν. Τιμές οριζόντιας μετάθεσης, της τάξης των 5 cm, εντοπίστηκαν στη Χερσόνησο της Μαρμαρίδας. Στον κόλπο Γκόκοβα εντοπίστηκε καθίζηση που έφθανε τα 30 cm.

Abstract

The temporal and spatial slip distribution assessment is a vital tool for seismologists and other geoscientists towards understanding the spatiotemporal evolution of the earthquake rupture. Such an evaluation requires data which are typically extracted after a large event, meaning the earthquake's source parameters, including focal mechanism, fault geometry and hypocentral relocation. The slip inversion method has application potential for shakemaps, emergency response and aftershock hazard assessment. The LinSlipInv software (Gallovic and Zahradnik, 2011; Gallovic et al., 2014) is implemented using local and near-regional data recorded by seismographs belonging to the Hellenic Unified Seismological Network (HUSN), as well as by the accelerometric network of the Geodynamic Institute of the National Observatory of Athens (GI-NOA), the Institute of Engineering Seismology & Earthquake Engineering (ITSAK) and for the eastern regions, the Kandilli Observatory and Earthquake Research Institute (KOERI) and the Turkey Earthquake Data Center System (AFAD). Selected strong earthquakes (with Mw ≥ 6.0) that occurred during the last decade in various regions of the Hellenic territory are examined. Towards the slip distribution determination via LinSlipInv, focal mechanisms, velocity models and fault geometries, were examined.

The slip distribution results were used as input to extrapolate ground deformation using the DIS3D Program (Erickson, 1987), even in cases where no surficial trace of the fault is observed. The obtained slip distribution and crustal deformation are compared with the ones determined by other studies, including InSAR and GPS.

The slip distribution results were promising. The results for the 26 January 2014 Cephalonia event, derived by the LinSlipInv software utilizing local and near-regional data, indicate a single rupture episode, with the maximum slip calculated at 40 cm. Concerning the ground deformation derived by the obtained slip distribution, the values in the horizontal and vertical component are low, mainly due to the magnitude and the focal depth of the event. The results revealed a maximum of 2 cm of horizontal displacement, to the east of the fault, on Cephalonia Island.

The calculated slip of the 24 May 2014 Lemnos earthquake revealed a complex source, comprised of three discrete patches. The slip snapshots revealed that the slip migrated updip, whereas the total maximum slip value reached 1.4 m. In addition, the slip velocity snapshots identified a bilateral rupture. More specifically, an initial westward rupture propagation was observed, followed by a major slip patch heading to the east. The obtained ground deformation results in Lemnos indicate a right lateral horizontal movement.

The local to near-regional slip inversion results for the 17 November 2015 Lefkada event revealed directivity towards the SSW. In addition, two slip episodes can clearly be identified, whereas the maximum obtained slip value was 1.2 m. Regarding the ground deformation, the dextral movement was verified by the herein obtained results, using the DIS3D software. Small uplift values were obtained for the southern part of the Lefkada Island (7 cm maximum uplift).

According to the LinSlipInv inversion results for the 12 June 2017 Lesvos earthquake, the maximum slip was ~1.0 m and a single patch was identified. The space-time rupture evolution, as revealed by slip velocity snapshots obtained per 1 s, indicated a unique slip patch and rupture directivity towards the NW, which could partly explain the damage observed in the Vrissa village. However, extended destruction is also due to other factors, such as soil conditions and vulnerability of the buildings. An extensional regime and a NNE horizontal movement on the Lesvos Island were identified by the application of the DIS3D software along with subsidence reaching 20 cm offshore, in the vicinity of the causative fault.

The slip distribution results derived by the LinSlipInv software for the 20 July 2017 Kos earthquake presented a unique patch with a maximum slip value of 1.8 m. The suggested causative fault is the one dipping to the north. Regarding the ground deformation, a N-S extension is observed. Values of horizontal movement of the order of 5 cm were obtained in Marmaris. Subsidence up to 30 cm was identified in the Gökova gulf.

1. Introduction

Earthquake physics constitute the wholeness of seismology. During the last decades efforts have been made in order to study and understand the mechanism that drives the earthquake's genesis and rupture pattern. Various methods and approaches have been applied from many branches of Geosciences, from geodesy and geology up to rock mechanics and seismology. The complexity of the problem with the interference of many unstable parameters consist a conundrum of that matter. Therefore, slip distribution is another tool in comprehending the mechanics of the Earth during the occurrence of an earthquake. Although the calculations contain some uncertainties and present limitations (i.e. the need of a given fault plane, the focal mechanism pre-determination, the hypocentral location and the magnitude), slip distribution assessment is the closest we have been in understanding the earthquake processes. It is important to note that the information needed to determine the slip on a fault can be provided either directly by the source and the propagation medium (seismograms/accelerograms) or by the deformation, induced by the earthquake, to the surface (GPS and InSAR Interferometry). In this thesis, the utility and reliability of the slip distribution determination was examined, using local and near-regional seismograms, as well as accelerograms.

In order to calculate the slip distribution on a fault, certain steps should be followed. The first is to determine the focal mechanism, the epicenter, the focal depth and the magnitude of the earthquake. These parameters are included in the routine analysis of seismology and are the first information extracted by the processing. For a more detailed input, a relocation procedure over the foci is very useful. Then, the fault plane that hosted the earthquake must be specified in space (width and length) for the initial model to be complete. As it is obvious, slip distribution assessment is one of the last steps to be performed in a seismotectonic study due to the fact that the input parameters are determined after the main analysis of the mainshock and aftershock sequence. Another application could be a deterministic approach of the problem. In such a point of view, the first step is for the analyst to define the expected values of each parameter and the second step is to run the inversion, for a scenario earthquake. Nevertheless, the results of the slip on the fault can provide, reckoning in all other findings of the seismic analysis of a sequence, valuable information and understanding of the source directivity, duration and complexity, hence of the source behavior.

In the present Master's thesis, regarding the slip distribution assessment, Linear Slip Inversion (LinSlipInv software; Gallovic and Zahradnik, 2011; Gallovic et al., 2014) is implemented using local and near-regional data. There are certain limitations using this program, mainly the acquisition of local data from accelerometers in regions with sparse station density (seismometers usually clip during large earthquakes). However, if the necessary data is acquired, the results provide fine discretization of the slip distribution on the fault.

There are important applications in Geosciences which capitalize the results of the slip distribution procedure. One of them is to determine the surface deformation after the

occurrence of a major event. There are of course other methods and approaches to determine the surficial deformation, such as GPS and InSAR Interferometry, however none of them uses data and information directly related to the source, but observations/data from the surficial effects of an earthquake. In the present work, a different approach was followed. The results obtained by the slip distribution assessment were used as input to the DIS3D program (Erickson, 1987) to extrapolate deformation originated by the slip distribution of the earthquake to the surface. DIS3D calculates the displacement both vertically and horizontally. The displacement results acquired by slip calculations (using the LinSlipInv software) are then compared with the ones derived by GPS and InSAR.

Additional information regarding the methodology and the dataset of this work will be provided in Chapter 3. In Chapter 2 the slip inversion theory and a brief analysis of the approach that is used for the slip distribution assessment are discussed. In Chapter 4 a brief Seismotectonic analysis of each case study is provided, along with the slip results of large earthquakes that occurred in Greece during the last five years by applying the local approach. The results are analyzed regarding both the space and time evolution of the rupture. In the same chapter the extrapolation of the slip distribution to the surface (that is surface displacement) through the DIS3D software is also presented. The discussion over the results is included in Chapter 5. In this chapter you may find a comparison between the obtained results (both slip distribution and crustal displacement) and those by previous work in each case study to find similarities and differentiations of the results. Lastly, in Chapter 6 the conclusions of this Master's thesis are provided: the usefulness, the reliability and the capability of the used programs, along with a brief summary and future goal determination.

2. Slip Inversion and Ground Deformation Theory

In Seismology, the determination of the focal mechanism and of the rupture process are of great importance. There are various methodologies of forward modeling and inversion. Although forward modeling is simpler to understand, it is much more difficult to find the best solution of the seismic parameters. On the contrary, the inverse problem is usually more difficult than the simple question that it reverses, but it is easier to estimate the solution of the problem. With the advance of computer sciences, the capabilities of inversion procedures, to determine the best solution of the problem, were augmented.

The main idea of the inversion theorem is the minimization of the residuals between the observed and the calculated (synthetic) waveforms. The theory of waveform modeling and inversion was well documented by many researchers, such as Chadan et al. (1977), Stein and Wysession (2003) and Aster et al. (2012). In seismology, the observations are derived via waveforms. The recorded waveform, $u(t)$, in each recording station is the convolution (in the time domain) of the source time function, $x(t)$, the elastic wave phenomena (geometrical spreading, reflections and conversions at interfaces along the ray path), $e(t)$, the anelastic attenuation, $q(t)$, and the instrument response of the recording station, $i(t)$:

$$u(t) = x(t) * e(t) * q(t) * i(t) \tag{2.1}$$

The goal of an inverse problem is to obtain the best model parameters m so that:

$$d = G(m) \tag{2.2}$$

where G is an operator describing the explicit relationship between the observed data (d) and the model parameters. In various contexts, the operator G is called forward operator, observation operator or observation function. In the most general context, G represents the governing equations that relate the model parameters to the observed data. To solve for the model parameters that fit the data, it is possible to invert the matrix G to directly convert the measurements into the model parameters:

$$m = G^{-1}d \tag{2.3}$$

However, not all square matrices are invertible (in fact G is almost never invertible). Given that the observation matrix cannot directly be inverted, mathematical methods are used, in a least square sense, to solve the inverse problem. To do so, a goal is defined, also known as an objective function, for the inverse problem. The goal is a function that measures how well the predicted data from the recovered model fits the observed data. In the case where the data (i.e. no noise) and the physical understanding are both perfect, then the recovered model should fit the observed data perfectly. The standard objective function (ϕ) is usually of the form:

$$\varphi = ||d - Gm||_2^2 \tag{2.4}$$

which represents the $L-2$ norm of the misfit between the observed and the predicted data from the model. A norm is a function that assigns a strictly positive length or size to each vector in a vector space, except for the zero vector, which is assigned a length of zero. Lp spaces are function spaces defined using a natural generalization of the p-norm for finite-

dimensional vector spaces. For $p = 2$, the $L - 2$ norm, also known as Euclidean norm or least squares, is determined. It minimizes the sum of the square of the differences ($\boldsymbol{S}$) between the target value ($\boldsymbol{y_i}$) and the estimated values ($\boldsymbol{f(x_i)}$) as:

$$S = \sum_{i=1}^{n} \big(y_i - f(x_i)\big)^2 \tag{2.5}$$

or in order to calculate the distance of the vector:

$$\|x\|_2 = \left(\sum_{i=1}^{n} |x_i|^2\right)^{1/2} \tag{2.6}$$

To minimize the objective function (i.e. to solve the inverse problem) the gradient of the objective function is computed using the same rationale as the one that minimizes a function of only one variable. The gradient of the objective function is:

$$\nabla m\phi = G^T G m - G^T d = 0 \tag{2.7}$$

where G^T denotes the transpose matrix of G. This equation is simplified to:

$$G^T G m = G^T d \tag{2.8}$$

After rearrangement in order to solve m, this becomes:

$$m = (G^T G)^{-1} G^T d \tag{2.9}$$

This expression is known as the Normal Equation, also called generalized inverse of G, and gives a possible solution to the inverse problem. It is equivalent to Ordinary Least Squares. The best fit is usually defined as the model with the smallest residual, or difference between observed and predicted data (Least Square Solution).

2.1. Source time function

The earthquake source signal, $x(t)$ (eq. 2.1), is the source time function produced by the faulting. In the simplest case of a short fault that slips instantaneously, the seismic moment function (eq. 2.10) is a step function whose derivative is a delta function that coincides with the source time function. Real faults, however, give rise to more complicated source time functions. The time derivative of the seismic moment function, $\dot{M}$(t), is defined as the seismic moment rate function or source time function. The seismic moment function is:

$$M(t) = \mu D(t) S(t) \tag{2.10}$$

which describes the faulting process in terms of rigidity, μ (also known as shear modulus), defined as the ratio of the shear stress to the shear strain, of material and history of the slip $D(t)$ and fault area $S(t)$. The latter terms are time-dependent, given that they can vary during an earthquake (Stein and Wysession, 2003).

In reality, a non-point source rupture is to be activated in a rectangular fault. Hence, the source time function can no longer be presented as a delta function, considering that waves arrive first from the initial point of the rupture and later from every point of the fault in the direction of the rupture. In Fig. 2.1, the correlation between the source time function, the azimuth, the rupture velocity and the wave velocity is presented.

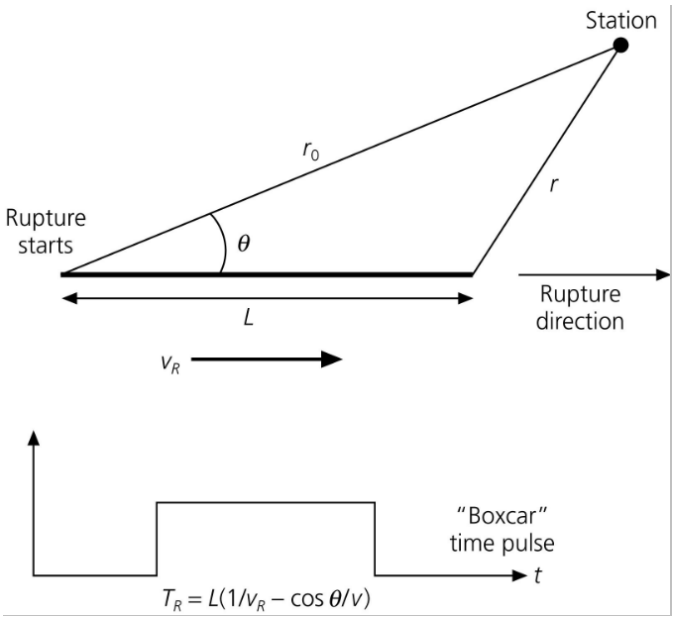

Figure 2.1. For a given fault with length L, the duration of the source time function varies in regard to the observer (station) as a function of azimuth, depending on the ratio of the rupture velocity v_R and the wave velocity v (Stein and Wysession, 2003).

Let a rupture occur with rupture velocity v_R along a fault of length L, and a receiver (station) at distance r_o and azimuth θ from the initial rupture point. The first seismic wave will arrive at time r_o/v, where v is the wave propagation velocity (different for P and S waves). At the time L/v_R the last point of the fault will rupture, giving a seismic arrival at time $(L/v_R + r/v)$, where r is the distance from the far end to the receiver (Fig. 2.1). The law of cosines provides that:

$$r^2 = r_o^2 + L^2 - 2\, r_o L cos\theta \tag{2.11}$$

which for $r >> L$, is approximately:

$$r \approx r_o - Lcos\theta \tag{2.12}$$

Thus, the time pulse due to the finite fault length is a "boxcar" of duration

$$T_R = L(1/V_R - cos\theta/v) = (L/v)(v/v_R - cos\theta) \tag{2.13}$$

where T_R is the rupture time (Stein and Wysession, 2003).

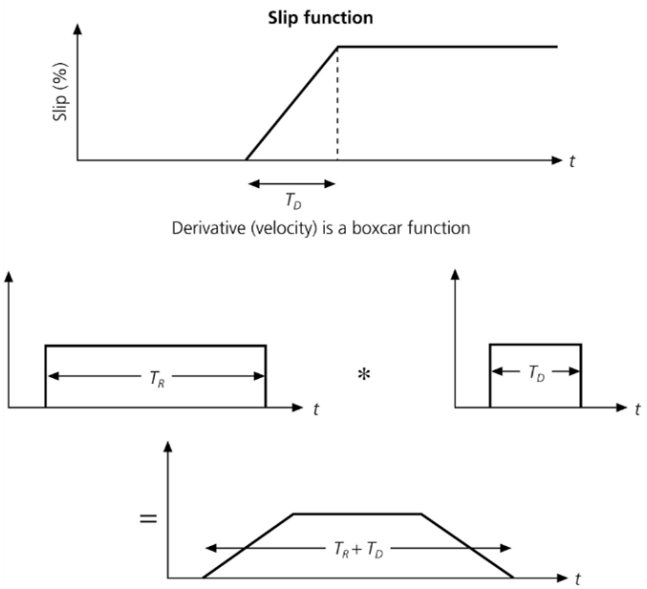

Figure 2.2. The source time function depends on the derivative of the slip history on the fault, i.e. a ramp time history (top) with duration T_D. The time derivative is a "boxcar". When convolved with the "boxcar" time function due to the rupture propagation (center), the source time function takes the shape of a trapezoidal (bottom) (Stein and Wysession, 2003).

Another parameter that changes the delta-like source time function is the fact that slip does not occur instantaneously. The slip history is often modeled as a ramp function (Fig. 2.2) that begins at time zero and ends at the rise time T_D. The source time function depends on the derivative of the slip history, i.e. a ramp function, which is a "boxcar". Convolving the finiteness and rise time effects yields a trapezoid. Its length is the sum of the rise and rupture times, which is often used to represent an earthquake source time function (Stein and Wysession, 2003). For large earthquakes, which are more complex cases, the source time function is more complicated, corresponding to the variation in slip along the fault as a function of space and time. Source time functions could also be approached with other shapes such as triangles (e.g. Hartzell and Heaton, 1983; Hartzell and Langer, 1993; Hartzell et al., 1996; Mendoza and Hartzell, 1999).

The radiated pulse varies in time duration as a function of azimuth from the rupture direction, due to the finite rupture length (eq. 2.13). Taking into account that the area of the pulse is the same at all azimuths, the magnitude of the source time function varies inversely with its duration (Fig. 2.3). In some cases, these directivity effects can be used to identify the fault plane (because no similar effect is associated with the auxiliary plane). Directivity is related to the Doppler effect for sound and light waves, which shifts the frequency of a moving oscillator to higher values when the oscillator moves toward an observer and lower ones when it moves away (Stein and Wysession, 2003).

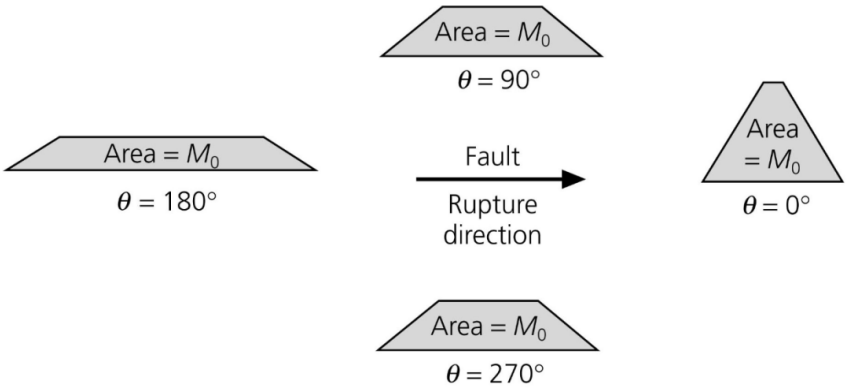

Figure 2.3. Effects of rupture directivity on the source time function at different azimuths from the rupture. The area of each source time function and the seismic moment are the same because the arriving energy is the same (Stein and Wysession, 2003).

If the difference of the arrival time of waves traveling at velocity v from different parts of the fault with length L is the rupture time T_R, which is approximately L/v and is comparable to the period of the seismic wave, T, the arriving waveform will be significantly affected. Thus, when the ratio:

$$\frac{T_R}{T} = \frac{\frac{L}{v}}{\frac{\lambda}{v}} = \frac{L}{\lambda} \tag{2.14}$$

is small, the fault length is short compared to the wavelength, λ, of the seismic waves and the finiteness of the source can be neglected and treated as a point.

2.2. Green's Functions

A widely applied method to estimate source time functions is based on the Green's functions. The mathematical expression of a Green's function is:

$$g(t) = e(t) * q(t) \tag{2.15}$$

with $e(t)$ representing the effect of reflections and conversions of seismic waves at different interfaces along the ray path and the effect of geometric spreading of the rays due to the velocity structure and $q(t)$ describes the anelastic attenuation, whereby a part of the seismic waves' mechanical energy is lost by conversion into heat. In general, $e(t)$ and $q(t)$ correspond to the effects of the Earth structure, combining the elastic and anelastic effects of propagation from the source to the receiver. The Green's function thus describes the signal that would arrive at the seismometer if the source time function was a delta function (Stein and Wysession, 2003). Using the equation (2.1), the source time function can be determined as:

$$x(t) = u(t) * [g(t) * \ i(t)]^{-1} \tag{2.16}$$

The seismogram is treated as the sum of source time functions with different amplitudes C_j at different times τ_j:

$$u(t) = \sum_{j=1}^{k} C_j[x(t-\tau_j) * g(t) * i(t)] \quad (2.17)$$

In all inversion procedures in Seismology, Green's Functions play a crucial role. They constitute the G operator (eq. 2.2), i.e. the synthetic (calculated) waveforms, which are then correlated with the real data.

2.3. Representation theorem

In theory, the rupture process on the fault is assumed to be smooth. However, this is not usually the case. The irregular slip on fault, due to the heterogeneity of the fault plane (e.g. steps and rock heterogeneities) and the source directivity, may yield a more complex source time function. The different behavior of the fault plane can highlight areas of high and low slip, asperities, i.e. areas with very high slip, or even barriers, meaning regions that terminate the rupture progress. The identification of barriers is very important, given that they could possibly host future earthquakes due to stress accumulation. During the last 50 years several slip inversion methods have been introduced (e.g. Hartzell and Heaton, 1983; Dreger and Kaverina, 2000; Ji et al., 2002; Hartzell et al., 2007, Gallovic et al., 2015). They basically differ in how the rupture model is parameterized and which constraints are applied. Certain methods are utilized even routinely for large earthquakes and the results are published online (e.g. the USGS website, www.usgs.gov). However, there is currently no consensus about which of the slip inversion methods is preferable and there are doubts about the reliability of the inferred source models due to the inherent non-uniqueness (i.e. ill-conditioning) of the inverse problem (Hartzell et al., 2007; Shao and Ji, 2012). Therefore, the slip inversion results may differ for the same earthquake by authors utilizing different methods. Moreover, using different type of data (near-field, teleseismic, regional, static co-seismic) or their combination can provide also different models (e.g. Delouis et al., 2002). This makes slip inversion a subject of still active research.

Kinematic seismic source and its radiation is a well investigated theoretical problem in elastodynamics (e.g. Aki and Richards, 2002). A tectonic earthquake can be described by purely shear slip (discontinuity of displacement) $\Delta u(\xi, t)$, describing the rupture propagation along a fault $\Sigma(\xi)$. Such a source can be represented by the seismic moment tensor density:

$$m_{jk}(\xi, t) = \mu(\xi)\Delta u(\xi, t)[n_j(\xi)v_k(\xi) + n_k(\xi)v_j(\xi)] \quad (2.18)$$

where v and n are the unit normal to the fault and the unit vector in the slip direction, respectively. Then displacement, $u(r, t)$, measured at position r caused by the slip, is given by the representation theorem (Aki and Richards, 2002):

$$u(r, t) = \iint_{\Sigma} G_{ij,k}(r, t; \xi) * m_{jk}(\xi, t) d\xi \quad (2.19)$$

where G_{ij} is the Green's tensor composed of solutions of elastodynamic equation in terms of displacement in direction i for force impulse acting at position ξ in direction j.

Introducing the impulse response $H_i(r, t; \xi)$ of the medium to a point double couple dislocation:

$$H_i(r,t;\xi) = \mu(\xi) n_j(\xi) v_k(\xi) [G_{ij,k}(r,t;\xi) + G_{ij,k}(r,t;\xi)] \quad (2.20)$$

the representation integral (2.19) reads:

$$u_i(r,t) = \iint_{\Sigma} H_i(r,t;\xi) * \Delta u(\xi,t) d\xi \quad (2.21)$$

The equation (2.21) is the basic formula used for the earthquake source analyses. Indeed, considering that the crustal model, fault plane geometry and slip direction (rake) are considered to be known a priori (i.e. impulse responses H are known), the equation (2.21) represents a linear relationship between the slip distributed along the fault and the displacement observed at a receiver. Given that, typically, slip rates $\Delta\dot{u}$ are preferred as model parameters in slip inversions, the equation (2.21) can be alternatively expressed as:

$$u_i(r,t) = \iint \widetilde{H}_i(r,t;\xi) * \Delta\dot{u}(\xi,t) d\xi \quad (2.22)$$

where $\widetilde{H}_i$ represents the temporal integral of the impulse response Hi, i.e. $\widetilde{H}_i(r,t;\xi) = \int_0^{\tau} H_i(r,\tau;\xi)\, d\tau$.

2.4. Adopted methods

As it is aforementioned, slip inversion methods differ mainly in how the rupture model is parameterized and which constraints are applied. Depending on how the slip rate functions are parameterized, two general methods can be distinguished. The linear inversion techniques (also called multitime window) are based on a discretized version of the representation theorem (2.19). The slip rate functions are parameterized by elementary functions (overlapping narrow triangles, delta like, etc), acting in several time windows. This procedure requires a large number of model parameters that are linearly related to the wavefield. The inversion is then performed considering regularization by applying smoothing and a positivity constraint. The nonlinear (or parametric) inversion also utilizes the representation theorem, but the shape of the slip rate function is prescribed a priori (such as rupture-onset time, rise time and peak slip rate). The major advantage of nonlinear inversions is that they work with a much lower number of parameters, thus allowing for an efficient uncertainty analysis (Monelli et al., 2009; Cirella et al., 2012; Gallovič and Zahradník, 2012; Razafindrakoto and Mai, 2014). In contrast, although the linear inversion can now be performed fast and efficiently on common desktop computers, any practical uncertainty analysis is prohibited due to the great number of model parameters. In the following chapter (2.4.1.), the adopted approach of slip determination using data from local to near-regional data will be introduced. The rupture surface is represented with a plane divided into subfaults as shown in Fig. 2.4. This parametrization of the fault was introduced by Hartzell and Heaton (1983) for the fault rupture history of the 1979, Imperial Valley earthquake in California, utilizing teleseismic data.

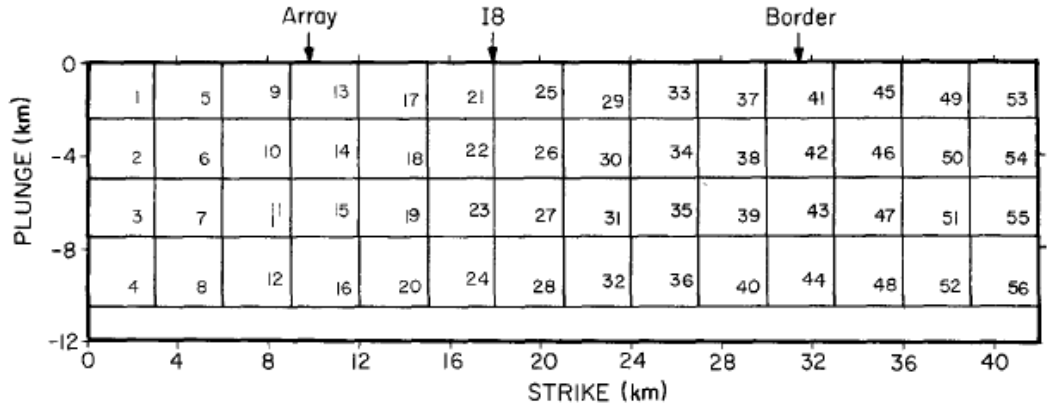

Figure 2.4. A 40 km x 10.5 km fault plane of the Imperial fault, showing the 56 subfaults used in the inversion modeling of the teleseismic records (Hartzell and Heaton, 1983).

Synthetic ground motions are calculated for each subfault for both a right-lateral, strike-slip dislocation and a normal (east-side down) dislocation of constant amplitude. Each of these calculations is repeated for every teleseismic station in the inversion.

2.4.1. Linear Slip Inversion technique (LinSlipInv software)

Regarding the LinSlipInv Software (Gallovic and Zahradnik, 2011; Gallovic et al., 2014), a prior covariance function acting as a smoothing constraint and a constraint on the scalar seismic moment M_0 of the earthquake are considered. In such a case, the $L-2$ misfit function reads:

$$M(m) = \frac{1}{2}(d-Gm)^T C_D^{-1}(d-Gm) + (m-m_A)^T C_M^{-1}(m-m_A) + \frac{1}{2\sigma_{M_0}}(E\cdot m - M_0)^2 \quad (2.23)$$

, where C_D refers to the data and C_M to the prior covariance matrix, σ_{M_0} is the weight of the seismic moment constraint and E is a vector of seismic moments of the elementary subfaults i, $E_i = \mu_i \Delta_L \Delta_W \Delta_t$. We consider $\sigma_{M_0} = M_0$ and $m_A = 0$. Aiming to ensure that the non-negativity constraint on the slip rates is applied, a system of equations in implemented, the misfit function of which is the same as in Eq. (2.23):

$$\begin{pmatrix} U_D^{-T} G \\ U_M^{-T} \\ \frac{1}{\sigma_{M_0}} E \end{pmatrix} m = \begin{pmatrix} U_D^{-1} d \\ 0 \\ \frac{1}{\sigma_{M_0}} M_0 \end{pmatrix} \quad (2.24)$$

In Eq. (2.24) the matrices U_D and U_M are (upper) triangular matrices, obtained by the Cholesky decomposition ($C = U^T U$) of C_D and C_M, respectively. The augmented matrix and augmented data vector in (2.22) are used as inputs to the fast NNLS subroutine, proposed by Luo and Duraiswami (2011). In the LinSlipInv software, C_M is composed of the discretized prior covariance function $\sigma_M^2 c_M(\tau, x, y)$ with temporal lag τ and spatial lags x (along strike) and y (along dip), where σ_M is the marginal standard deviation of the model parameters (c_M itself is

considered to have unit variance). Assuming that the Fourier spectrum of c_M (i.e. slip-rate power spectral density) is proportional to:

$$c_M(f, k_x, k_y) \propto \left(\frac{1}{1+(k_x L)^2+\left(k_y W\right)^2} \right)^2 \quad (2.25)$$

where f is the frequency and k_x and k_y are wavenumbers in the along-strike and along-dip directions, respectively. Given that c_M in (2.23) is independent of f, the prior model parameters are considered to be statistically independent of time. From (2.23) it can also be extracted that the slip rates are considered to have k^{-2} amplitude spectrum in the spatial domain (with radial wavenumber $k = \sqrt{k_x^2 + k_y^2}$). The spectral decay is defined according to theoretical (Andrews, 1980; Gallovic and Brokešová, 2004) and observational (Somerville et al., 1999) studies on spatial properties of earthquake slip distributions. It is worth noting that the covariance function controls the spectral decay (i.e. smoothness) of the solution.

2.4.2. Ground Deformation determination

Ground deformation is focused on the movement of an observation point in time and space. It can be divided into two categories in terms of time; the inter- and co-seismic ground deformation. Regarding the former, the motion of the tectonic plates and of microplates accumulates stress in an area of the Earth's crust. This accumulation is mainly expressed by earthquakes, however, a vast part of the energy in the system is transformed to deformation, either by changing the shape (change on volume, altitude, horizontal distance, etc) or the orientation (rotation) of the mass. The displacement can be measured via GPS instruments and satellites and provide an image of the Earth's procedures in terms of plate movement and strain in an area. We can also identify areas and time periods in which creeping (or aseismic movement) occurs in the upper crust.

Regarding the co-seismic ground deformation, the mechanics are different. Large earthquakes can permanently change the form of the ground if the fault reaches the surface, by generating fault scarps and topographic steps. Even moderate earthquakes generate permanent small surface deformation, which can affect, however, numerous Earth's processes (e.g. changes in the hydrological equilibrium). The source of an earthquake is a fault rupture/dislocation in the Earth's crust, instead of plate movement. There are methods to determine the ground deformation using data from the Earth's surface, such as GPS and InSAR Interferometry, which measure the permanent ground movement caused by the fault slip. Ground deformation due to the seismic event is also calculated by the extrapolation of the slip-on-fault to the surface. This can be achieved by considering the crust as an elastic medium and thus, the rupture on the fault is transferred to the surface.

As it is already explained, ground deformation is the change of the surface both in shape, volume and orientation. Regarding the first, there are limited ways of deforming the shape of an object, that is Distortion. Any non-rigid change in shape is referred as strain and it implies that particles in a rock have changed positions relative to each other. The change in orientation can be due to displacement (translation) or rotation. Translation refers to the

movement of every particle in the rock in the same direction and distance and its displacement field consists of parallel vectors of equal length. Rotation involves a uniform physical rotation of a rock volume (such as a shear zone) relative to an external coordinate system. In Fig. 2.5 the translational component is shown in (b), the rotation component in (c) and the rest (the strain) in (d). Even if the shape of a rock volume is unchanged, it may have shrunk or expanded. Therefore, the volume change has to be added (area change in two dimensions) for a complete description of deformation. Volume change, also referred to as dilation, is commonly considered to be a special type of strain, called volumetric strain (Fossen, 2010). In the present study, the ground deformation is translated only as ground displacement, both vertically and horizontally.

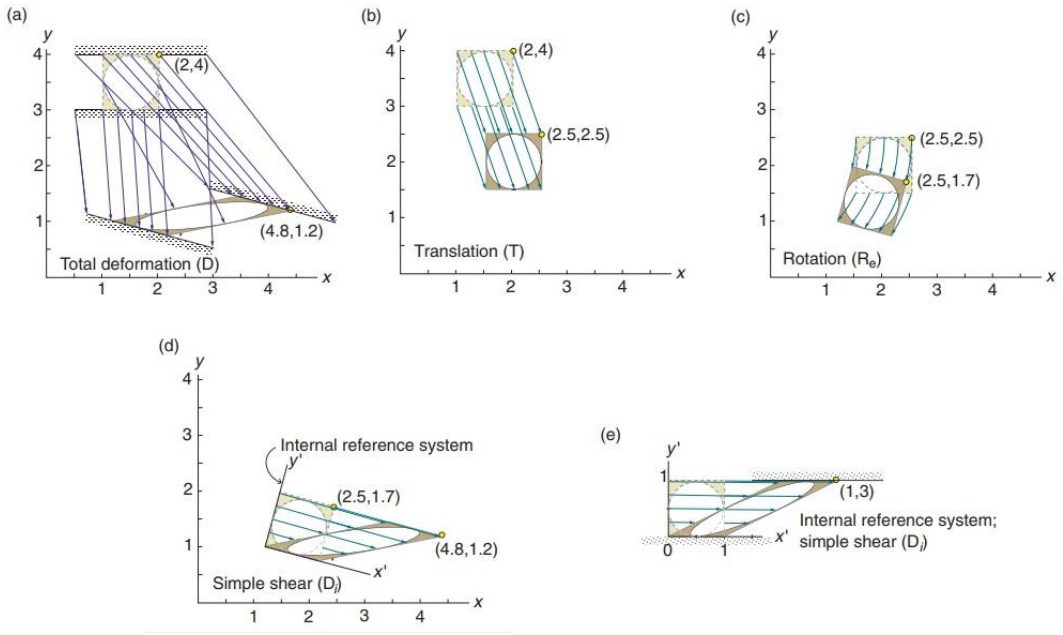

Figure 2.5. (a) The total deformation of an object (square with an internal circle). Arrows in (a) are displacement vectors connecting the initial and final particle positions. Arrows in (b)–(e) are particle paths. (b, c) are the translation and rotation components of the deformation shown in (a). (d) is the strain component. A new coordinate system is introduced (d). The simple shear (e) reveals the strain component (Fossen, 2010).

3. Data and Methodology

The main scope of the present thesis is to determine the slip distribution on faults. In order to apply the algorithm, which utilizes local to near-regional data (LinSlipInv Software; Gallovic and Zahradnik, 2011; Gallovic et al., 2014), that is strong motion records from local and seismograms from near-regional stations, were collected. Data were obtained by the webpages of the Institute of Engineering Seismology and Earthquake Engineering (ITSAK; www.itsak.gr) and the Institute of Geodynamics of the National Observatory of Athens (GI-NOA; bbnet.gein.noa.gr), as well as from the GHEAD database (http://ghead.itsak.gr/map/). Data for the most recent events were acquired from the NOA EIDA node that hosts recordings of ITSAK (HI), as well as of all stations of the Hellenic Unified Seismological Network (HUSN), comprising of the Seismological Laboratory of the National and Kapodistrian University of Athens or SL-NKUA (HA; doi:10.7914/SN/HA), the GI-NOA (HL; doi:10.7914/SN/HL), the Department of Geophysics of the Aristotle University of Thessaloniki (HT; doi:10.7914/SN/HT), the Seismological Laboratory of the University of Patras (HP; doi:10.7914/SN/HP) and the Seismological Network of the TEI of Crete (HC; doi:10.7914/SN/HC). In addition, for the events in the eastern part of Greece, data recorded by stations belonging to the Turkey Earthquake Data Center System (AFAD-TDVMS) and the Kandilli Observatory and Earthquake Research Institute (KOERI) networks were utilized.

Regarding data processing, after acquiring the timeseries, a waveform preparation is carried out in order to construct the suitable input files to fulfill the software requirements. The first step is to demean and detrend the waveforms and then apply a filter (wider than the one used in the inversion procedure). The filter is usually a taper from 0.3 to 50 Hz. After the application of the filter, the timeseries are integrated against time in order to obtain displacement units (one or two times depending on the original data, i.e. seismograms or accelerograms, respectively).

3.1. LinSlipInv Software

The slip distribution assessment using local to near-regional data (Linear Slip Inversion; LinSlipInv program) required the utilization of strong motion recordings due to the fact that the seismometer's recordings in local and, in some cases, in near-regional distances were clipped. The procedure regarding the dataset compilation was quite complex due to its heterogeneity, meaning that the required dataset for the method that utilizes local to near-regional data was comprised by recordings of eight different networks (HI, HA, HL, HT, HP, HC, AFAD-TDVMS, KOERI), which unfortunately do not follow the same format structure. That been said, for the networks of which data were acquired by EIDA Nodes, the waveforms were deconvolved to remove the instruments response. For the data from the HI and AFAD-TDVMS networks, the procedure was quite simpler (detrending and demean was only applied), given that the data were provided already deconvoluted and in the displacement field. In the LinSlipInv software, the rupture process is discretized in space and time along a given fault plane and the model

parameters are the spatiotemporal samples of the slip rates, spanning the whole rupture duration.

Regarding the LinSlipInv's approach for calculating slip distribution, no a priori constraints are required for the source time function. Hence, the necessary input values are few and easy to determine. In more detail, the input files required for LinSlipInv are:

- Processseis.in: In this input file the origin time of the earthquake, the start-time and characteristics of the waveforms (sampling rate, units of measurement, etc.) and the coordinates of each station are given. Additionally, the number and the time-step of the samples that will be used in the inversion procedure are provided (down-sampling).
- Stations.in: The hypocenter of the earthquake is given to the program by this file.
- Crustal.dat: In this input file, a 1-D velocity model, also including the density, Q_s and Q_p (the attenuation factor for S and P waves, respectively) is given. In seismology, the anelastic attenuation factor, or the seismic quality factor, Q (which is inversely proportional to the attenuation factor), quantifies the effects of anelastic attenuation on the seismic wave caused by fluid movement and grain boundary friction. When a seismic wave propagates through a medium, the elastic energy associated with the wave is gradually absorbed by the medium, eventually ending up as heat energy (Stein and Wysession, 2003).
- Input.dat: The fault characteristics (e.g. length and width) and the focal mechanism parameters (azimuth, dip and rake) are inserted in this file. Additional information regarding the inversion parametrization (e.g. slip rate time window, number of computed frequencies and spatial discretization of the fault) is also provided.

The slip distribution assessment follows a simple procedure. First, the Green's functions (GFs) are calculated. In case of considering a 1D velocity model, composed of homogeneous layers, the GFs are calculated by the discrete wavenumber method (DWN; Coutant, 1989; Bouchon, 1981; Kennett and Kerry, 1979) using the axitra code. Following, the waveforms are filtered, demeaned and detrended. Lastly, data are down-sampled to be in accordance with the maximum frequency used in the inversion process, fulfilling the Nyquist criterion, i.e. $\Delta t<1/2f_{max}$. In more detail, the downsampling rate is calculated as follows: first the length of the waveform for the inversion is determined and then the number of samples is defined by the user in order to fulfill the aforementioned criterion (i.e. $\frac{length}{N_{samples}} < f_{Nyquist}$). To stabilize the inverse problem in the least squares sense, two constraints were implemented; spatial smoothing by considering covariance function with k^2 decay at large wave numbers k as a prior for the slip rates and a positivity constraint on the slip rate by means of the nonnegative least squares approach (Lawson and Hanson, 1974). The source description is very general with no a priori constraints on the position of the nucleation point, rupture velocity and shape of the slip-rate functions. It must be noted that, as in any multiparameter inversion, the slip model is sensitive to artifacts and biases imposed by the imperfect station distribution and smoothing.

3.2. Ground deformation (DIS3D Software)

DIS3D (Erickson, 1987) is a fully three-dimensional dislocation program that calculates the elastic fields at specified “observation points” located either at depth or at the surface of a linear elastic half-space. The program's input routines allow the user to specify individual observation points or grids of such points in any plane of half space and permit the calculation of the elastic fields with respect to any reference structure specified by the user. In the present thesis the program is used to convert slip distribution along a fault to ground/surface deformation. The elastic field equations implemented in DIS3D are based on equations derived by Converse (1973).

The input file specifies the coordinates of the "observation points" which are the points where the elastic fields are to be calculated, i.e. X1G: the distance measured at the X1 axis (horizontal axis in the N-S direction) and X2G: the distance measured along the X2 axis (horizontal axis in the E-W direction). In addition, the parameters that describe the dislocation plane in the model are required. These are the dislocation plane's identification number, the half-length of the dislocation plane, the distance measured down-dip from the local coordinate origin to the upper (and lower) edge of the dislocation plane, the dip and strike of the fault and the values of the strike and dip of the slip motion in the dislocation plane. In addition, the database contains the parameters needed for the grid of observation coordinates and the dip and strike of the target fault, according to which the ground displacement will be calculated.

For the present thesis, the obtained slip distribution, determined by the LinSlipInv software, is utilized as input to DIS3D. For that purpose, the fault is discretized in the same way as in the slip calculations. The results (output of DIS3D) are then visualized in a map projection, with a color scale representing the vertical displacement and vectors representing the horizontal one.

4. Case Studies

Greece is the most seismically active region in Europe and one of the most active regions in the globe. However, the distribution of earthquakes in the broader Greek region is not random. In fact, there are areas with significantly more earthquakes, both in terms of quantity and magnitude. Hence, in the present study, major events of the most seismically active regions of the Greek territory are examined. In more detail, for western Greece and particularly for the Cephalonia Transform Fault Zone (CTFZ), which is the outcome of the continental collision between the Eurasian and the Apulian plates, the first main event of Cephalonia 2014 with moment magnitude M_w 6.1 (chapter 4.1) and the earthquake of Lefkada 2015 with M_w 6.4 (chapter 4.3) were analyzed. To the NE borders of Greece, the North Aegean Trough (NAT) is the dominant tectonic feature. The NAT is the extension of the North Anatolian Fault (NAF) to the west and marks the northern tectonic boundary of the expanding Aegean microplate. In order to include this area and tectonic regime, the earthquake of Lemnos 2014 with M_w 6.8 (chapter 4.2) was selected. The destructive earthquake of Lesvos 2017 M_w 6.3 (chapter 4.4) that occurred SW of the homonymous Island was also included. The region presents an extensional regime which is recent from the geological point of view. Lastly, the most recent selected event is the earthquake of Kos 2017 M_w 6.6 (Chapter 4.5), which belongs to an extensional regime in a N-S direction in SW Greece and close to the borders between Greece and Turkey. This extension is attributed to the westerly escape of the Anatolian plate in response to the convergence of the African, Eurasian and Arab plates. All the aforementioned areas are presented in Fig. 4.1. In other highly seismogenic regions, such as the Gulf of Corinth (e.g. Bernard et al., 1997; Papadimitriou et al., 1999; Chouliaras et al., 2015; Kapetanidis et al., 2015; Kaviris et al., 2017, 2018; Mesimeri et al., 2018 a,b; Michas and Vallianatos, 2018), no major earthquakes occurred in the timeframe studied in this Thesis.

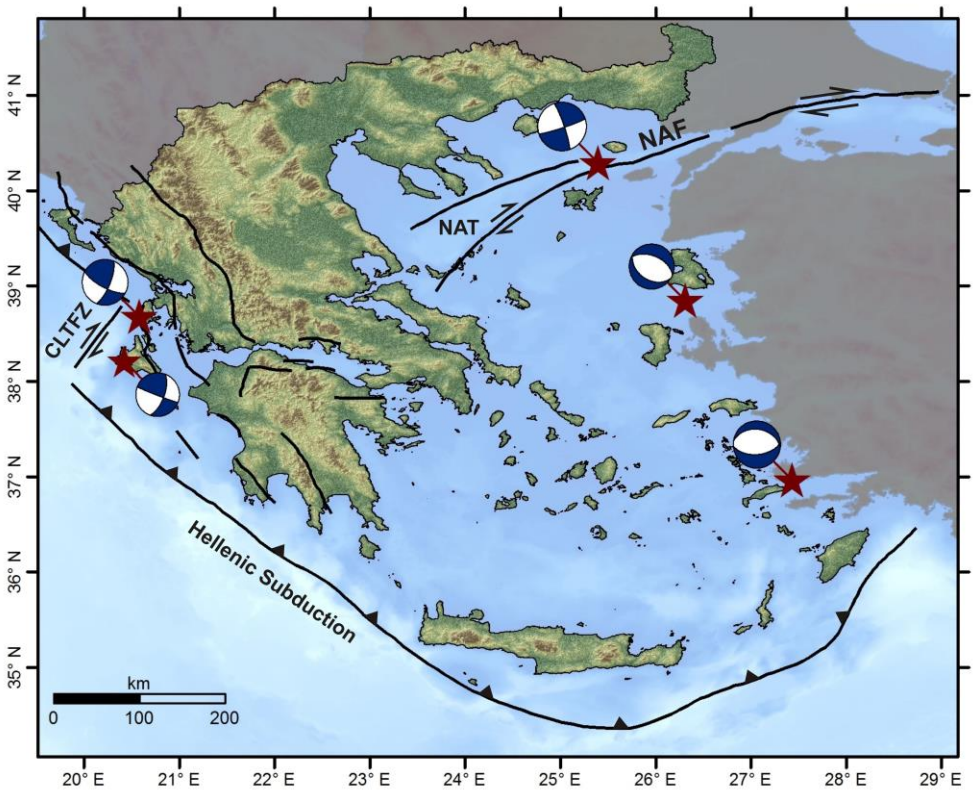

Figure 4.1. Map presenting the focal mechanism of each case study. The black lines represent the major tectonic boundaries in the Hellenic region. The notation represents the areas of the case studies as: A: Cephalonia, B: Lemnos, C: Lefkada, D: Lesvos and E: Kos.

In this chapter, there will be a brief analysis of the seismotectonic setting, followed by the mainshock and aftershock sequence description, for each case study, based on already published research. The results of slip inversion, using the LinSlipInv software, are then presented. For each case study, all the models, suggested in the literature, were examined and the one with the best Variance Reduction (VR) and the best fit of the synthetic and observed waveforms, was selected. An extensive description of the parameters used for each earthquake and the evaluation of the results are also provided. Finally, the derived ground deformation, utilizing as input the determined slip distribution, is presented.

4.1. Cephalonia 2014 (M_w = 6.1)

On January 26, 2014 a shallow crustal earthquake of moment magnitude M_w 6.1 occurred in the western part of the Cephalonia Island, on the Paliki peninsula. One week later, on February 3, 2014, another strong shallow crustal earthquake of magnitude M_w 6.1 was nucleated on the Paliki peninsula, northern of the first and close to the town of Lixouri (Karakostas et al., 2014; Papadopoulos et al., 2014; Sokos et al., 2015; Theodoulidis et al., 2016). Both events, characterized by proximity both in time and space, engendered intense aftershock sequences.

4.1.1. Seismotectonic setting

The main event of January 26, 2014 occurred in the central Ionian Sea, in the western part of the Cephalonia Island, the Paliki peninsula. The activated area is a known branch of the dextral Cephalonia Transform Fault Zone (CTFZ). The CTFZ covers an area of more than 100 km along the western coast of the Cephalonia Island and it can be distinguished into the north and the south segment, i.e. the Lefkada and Cephalonia, respectively (Scordilis et al., 1985; Louvari et al., 1999; Karakostas et al., 2015).

The CTFZ is located west of the island chain from Lefkada to Cephalonia and follows the submarine valley of Cephalonia (Kokinou et al., 2006; Karakostas et al., 2015). However, the main strike-slip motion (often with a thrust component) is expressed not only in the CTFZ but also in a wide zone of about 100 km, up to the western part of Peloponnese (Louvari et al., 1999; Tzanis et al., 2000; Shaw and Jackson, 2010; Sokos et al., 2015). The mapped faults on the island of Cephalonia are in agreement with evidence derived via seismic observations (Kokinou et al., 2006). There are few strike-slip fault segments offshore Cephalonia (Caputo et al., 2012) and an onshore fault zone (Lekkas et al., 2001).

4.1.2. Mainshock and aftershock sequence

The intense aftershock sequence lasted for about three weeks (from 26 January to 16 February), whereas the whole sequence lasted for several months, with the hypocenters revealing the activation of a NNE-SSW plane (Karakostas et al., 2015). This plane is parallel to the Paliki peninsula and the Myrtos gulf. The first major earthquake occurred in the southwestern tip of the peninsula (26/1/2014, M_w 6.1, 20°/65°/177°), producing a very intense aftershock sequence towards the north, however concentrated near the focal area. The distribution of the aftershock sequence suggests a 13 km long plane (Karakostas et al., 2015). Further to the north of this sequence, an area of low seismicity was identified, with absence of $M > 4$ earthquakes. This area hosted the second M_w 6 event (3/2/2014, 12°/45°/154°). In fact, the second major shock occurred at the southern edge of the low seismic area to the north. The aftershock sequence of the latter event was less intense, compared to the first, however it indicates a 10 km long rupture plane. According to Papadimitriou et al. (2014), the entire aftershock sequence is roughly oriented NNE-SSW, covering an area of approximately 32 km long and ~5 km wide on the northern and ~15 km on the southern part. The same authors also suggest that at least two main faults, located on the Paliki peninsula, were activated.

The existence of an area with low seismicity after the occurrence of the first main event and its activation shortly after, may suggest that the northern part remained locked after the first main shock and was activated with the M_w 6 event. Regarding the northern part, the relatively low seismicity, even after the occurrence of the second event, suggests the inexistence of other faults in the area, whereas, for the southern part, the high seismicity could be explained as the consequence of the activation of secondary faults and of stress transfer due to the February 3, 2014 event (Karakostas et al., 2015). In the next figure (Fig. 4.2) the relocated

epicenters as derived by Papadimitriou et al., 2014 are presented. Two groups are defined, with the southern revealing two possible structures with N20°E and N350°E, respectively.

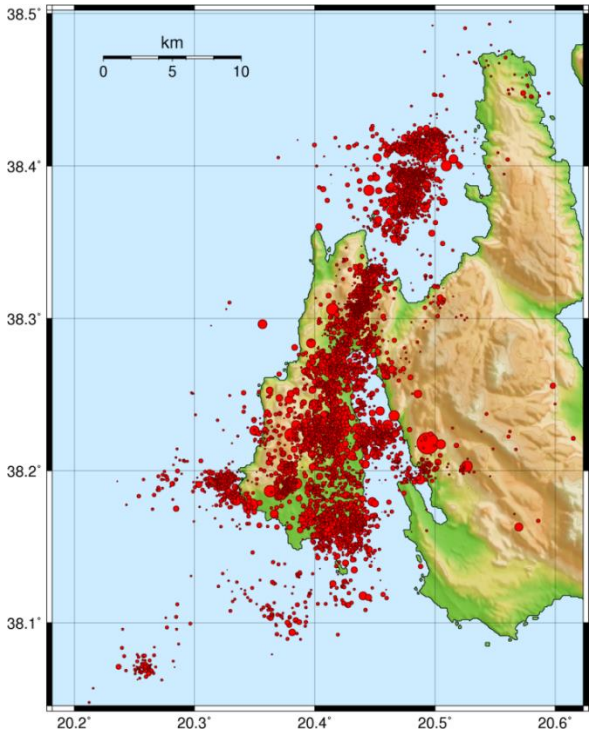

Figure 4.2. Relocated epicenters of the Cephalonia 2014 sequence (Papadimitriou et al., 2014)

4.1.3. Slip Inversion Results

The mainshock coordinates were set as 38.2030°N and 20.4308°E (Karakostas et al., 2015), respectively (Fig. 4.1). The stations used in the inversion are presented with black triangles in the Fig. 4.3. The epicentral distances vary from 1 to 150 km. The results derived using data from local to near-regional distances are presented below (Fig. 4.4 and Fig. 4.5). Regarding the parameters that were used as an input for the LinSlipInv software (Gallovic and Zahradnik, 2011; Gallovic et al., 2014), the fault plane was considered 16 km long and 10 km wide. The focal mechanism of the January 26, 2014 event, which is also an input to the inversion, was 20°/65°/177° (Karakostas et al., 2015) with the focal depth being equal to 16 km. The velocity model used for the inversion was the one suggested by Haslinger et al. (1999).

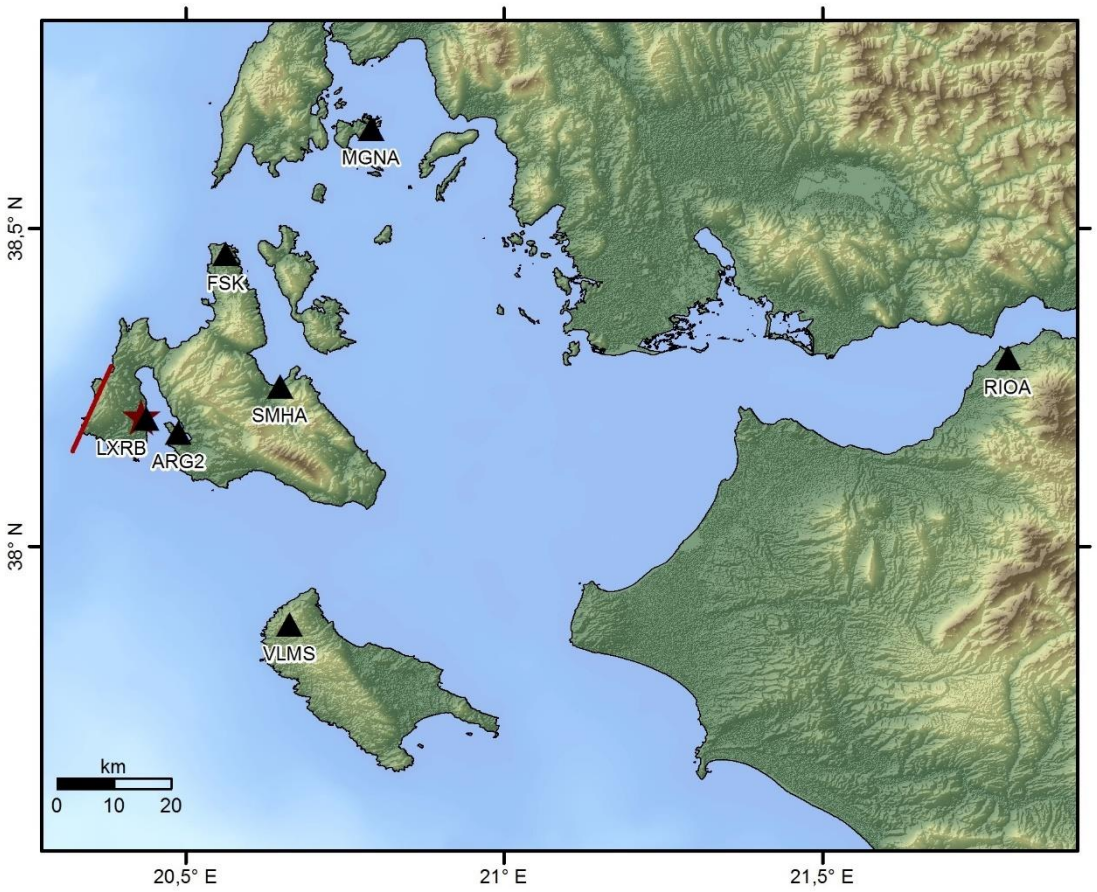

Figure 4.3. The epicenter, the causative fault and the stations used in the slip inversion procedure of the January 26, 2014 Cephalonia earthquake.

The rupture evolution is presented in Fig. 4.4, in terms of slip velocity, with a snap taken every one second. The rupture evolution presents a major patch activated at the beginning, lasting for 2 seconds, and a secondary in the ending of the rupture process. The main rupture lasted for 9 s and the maximum slip velocity occurred during the 1st second. It is worth mentioning that the long duration and the minor patch which is present during the 7th and 8th seconds are possibly due to noise. In any case, if the secondary patch is not taken into account, the duration of the rupture of the January 26, 2014 earthquake is limited to 4 s.

In the next figure (Fig. 4.5), the total slip distribution on the fault is provided. The slip patch is identified at the upper left part of the image, i.e. at the SSW part of the rupture. The focus is located at the edge of the lobe (to the NNE), which may suggest a general orientation of the slip vector towards SSW. The maximum slip value is 0.4 m and is obtained at the center of the lobe. It is important to notice that the figure is up-dip, meaning that it starts from the bottom (0 km) towards the ceiling of the fault (10 km).

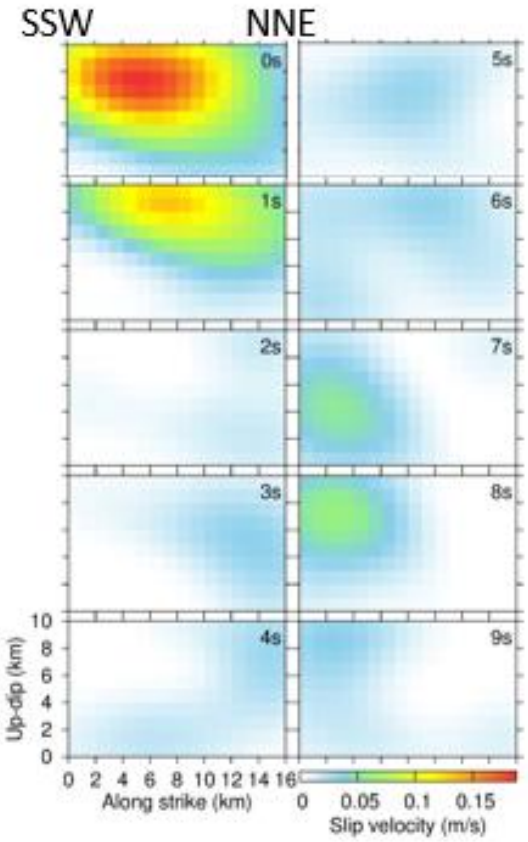

Figure 4.4. The slip distribution evolution is presented by snaps of one second intervals. Note that the maximum slip velocity is 0.15 m/s.

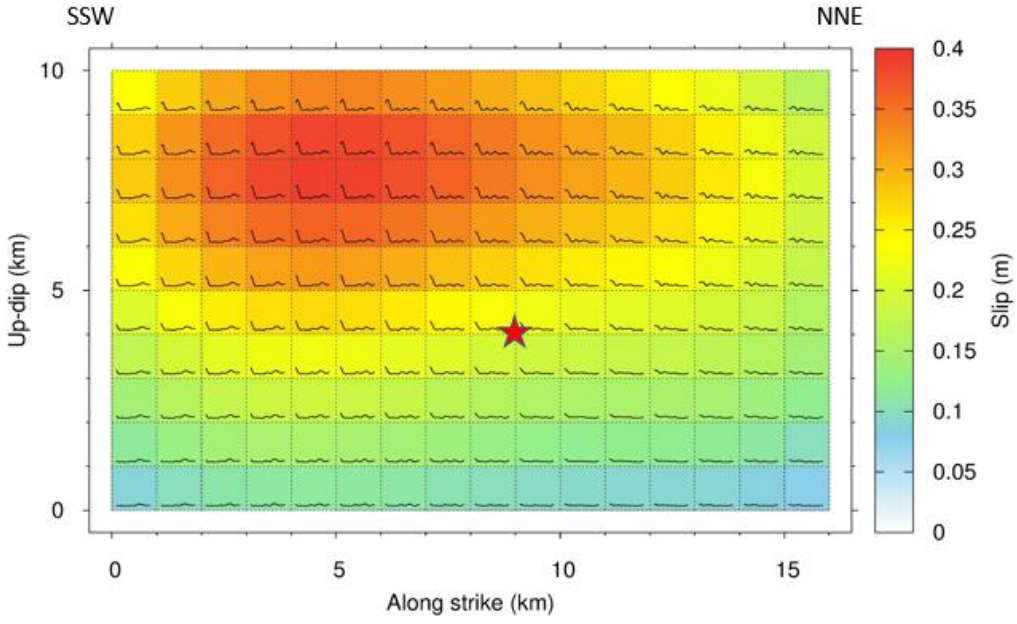

Figure 4.5. The total slip distribution on the fault. The maximum slip reaches 0.4 m.

4.1.4. Ground Deformation Results

Regarding the ground deformation, a right lateral horizontal motion has been determined. Low vertical displacement values were obtained (that is 30 mm of maximum uplift and 50 mm of maximum subsidence), which was expected given the magnitude of the earthquake and, mainly, the focal depth. Small subsidence was calculated for the major part of the Cephalonia Island, with the exception of the southern coasts, where small uplift (less than 1 cm) has been determined. Low values were also the case for the horizontal movement, which revealed a maximum of 2 cm of horizontal displacement, in a WSW direction, close to Argostoli, to the east of the fault (onshore area in the central part of the island).

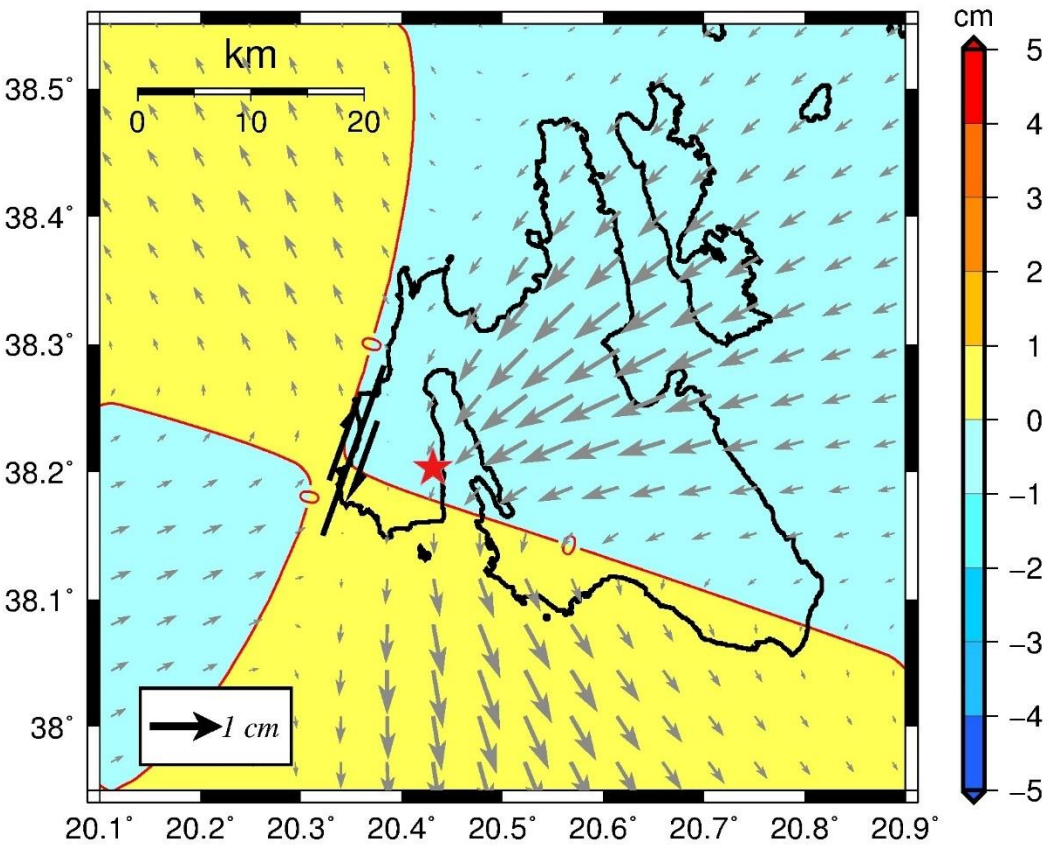

Figure 4.6. Ground deformation determined using the DIS3D software, utilizing the determined slip distribution on the fault, as derived by the LisnSlipInv software, using local to near-regional data. The maximum subsidence is up to 0.5 cm and the maximum uplift reaches 0.3 cm.

4.2. Lemnos 2014 (M_w = 6.8)

The May 24, 2014 M_w 6.8 earthquake occurred southeast of the Samothrace Island, in the offshore area between the islands of Lemnos and Samothrace, in the North Aegean Trough (NAT; Kiratzi et al., 2016; Sboras et al., 2017). According to Kiratzi et al. (2016), the source was complex, comprising of two sub-events (Saltogianni et al., 2015), while the rupture duration was long, varying from 40 s to 65 s (Trabant et al., 2012; Kiratzi et al., 2016; Konca et al., 2018). It is also worth noting that the length of the region where aftershocks occurred was approximately 200 km and that no strong aftershock (M > 5.0) occurred.

4.2.1. Seismotectonic setting

The island of Lemnos is located in the North Aegean Trough (NAT), a very complex tectonic regime, where many earthquakes, with different characteristics, occur. The complexity lies in the fact that in the NAT there are various fault types regarding the dimensions and the kinematics, given that dip – slip and strike – slip faults, with the latter related to large events, are documented (Papazachos and Kiratzi, 1996; Hatzfeld, 1999; Kiratzi and Louvari, 2003; Kokkalas et al., 2006; Mountrakis, 2006; Kiratzi et al., 2007; Rhoades et al., 2010; Leptokaropoulos et al., 2012; Nocquet, 2012; Mitsakaki et al., 2013; Müller et al., 2013; Karakostas et al., 2014; Sakellariou et al., 2016). Secondary faults, parallel to the NAT, are also recognized from seismicity and fault-plane solutions of recent strong earthquakes (Papadimitriou and Sykes, 2001).

The neotectonic history of the Aegean region is rich, with evidence of additional internal deformation, as suggested by geological, geodetic, seismological and palaeomagnetic investigations (Kissel and Laj, 1988; Drakatos and Drakopoulos, 1991; Hatzfeld, 1999; Papazachos, 1999; Taymaz et al., 2007; Le Pichon and Kreemer, 2010; Özeren and Holt, 2010; Nocquet, 2012; Pérouse et al., 2012; Müller et al., 2013; Ersoy et al., 2014; Papadakis and Vallianatos, 2017). It can be considered as a combination of back – arc extension that is driven by slab rollback since the Middle Eocene (45 Ma) and westward extrusion of the Anatolian block into the Aegean Sea along the North Anatolian Fault (NAF) since the Early Pliocene, i.e. about 5 Ma ago (Armijo et al., 1999, 2003; Hubert-Ferrari et al., 2003; Şengör et al., 2005; Papanikolaou et al., 2006; Brun and Sokoutis, 2010; Philippon et al., 2014). The extension of the NAT is associated with the westward prolongation of the NAF into the Aegean Sea (McKenzie, 1970, 1972; Dewey and Şengör, 1979; Lyberis, 1984; Armijo et al., 1999; Papanikolaou et al., 2002, 2006). The NAT marks the northern tectonic boundary of the expanding Aegean microplate, compared to the stable Europe (Mascle and Martin, 1990; Sakellariou et al., 2013; Sakellariou and Tsampouraki-Kraounaki, 2019).

According to geodetic studies that utilize GPS measurements, dextral strike – slip motion along the NAT decreases from the NE (21.2 mm/yr along the Saros basin) to the central part of the basin (12.5 mm/yr south of the Chalkidiki peninsula) and further to the SW (7 mm/yr at the SW corner of the Sporadhes basin; Müller et al., 2013). Thus, the basin is characterized by oblique opening (Mascle and Martin, 1990; Papanikolaou et al., 2002, 2006) due to the

predominantly dextral strike – slip motions and the significant normal components (Kiratzi et al., 1991, 2016; Taymaz et al., 1991; Koukouvelas and Aydin, 2002; Chatzipetros et al., 2013; Leptokaropoulos et al., 2013 Kiratzi and Svigkas, 2013; Kiratzi, 2014).

The seafloor of NAT is segmented by numerous faults and fault splays that consist the uppermost parts of flower structures, either positive or negative, and therefore create uplifted and subsided blocks (Mascle and Martin, 1990; Papanikolaou et al., 2006; Sakellariou et al., 2016). A rough approximation for fault slip rates is 18 – 34 cm/kyr (Roussakis et al., 2004), using Holocene sedimentation rates for the subsided areas (Papanikolaou et al., 2006). Both instrumental data and historical catalogues report many destructive earthquakes in the wider area of the North Aegean Sea (Galanopoulos, 1960; Ambraseys and Finkel, 1995; Papadimitriou and Sykes, 2001; Papazachos and Papazachou, 2003; Makropoulos et al., 2012; Stucchi et al., 2013).

4.2.2. Mainshock and aftershock sequence

The earthquake that occurred in 2014 activated a great part of the NAT, between Mt Athos to the west and the Saros Gulf to the east (Kiratzi et al., 2016). According to Kurt et al. (2000) and McNeill et al. (2004), the geometry of the Saros basin is not simple, given that it is divided by a NW trending fault, striking N310°E, possibly connected with left-lateral motion. Therefore, two sub-basins can be identified. The main expression of the mainshock and the aftershock sequence was located to the East, in the Saros Basin and specifically in the junction of the two sub-basins (Kiratzi et al., 2016). The aftershock distribution provides a blatant description of the operative fault, trending ENE-WSW, parallel to the large axis of the basins, with the expression of the aftershocks presenting clear cluster-like patterns both to the NW and the SW.

Additionally, the location of the clusters indicates a bilateral rupture, with the major aftershocks (M≥4.0) belonging to the eastern part. It is worth mentioning that the first and second major aftershocks of the sequence, with magnitudes equal to 4.9 and 4.6, respectively, occurred at both ends of the entire activated rupture zone. Regarding these aftershocks, no focal mechanisms were obtained, due to the intervention of the mainshock's coda to the recordings (Kiratzi et al., 2016).

The length of the rupture zone, as determined by the aftershock sequence, was L≈95 km (Kiratzi et al., 2016). This evidence is in contrast with the empirical relations introduced by Wells and Coppersmith (1994) and Papazachos et al. (2004) for strike slip earthquakes of relevant magnitudes, according to which the length is expected to be around 50 - 70 km. The results of Evangelidis (2015) indicate that the 2014 Lemnos earthquake ruptured on two fault segments. Regarding the first, the rupture propagated approximately 20 km westward, whereas the second about 65 km eastward with a supershear velocity.

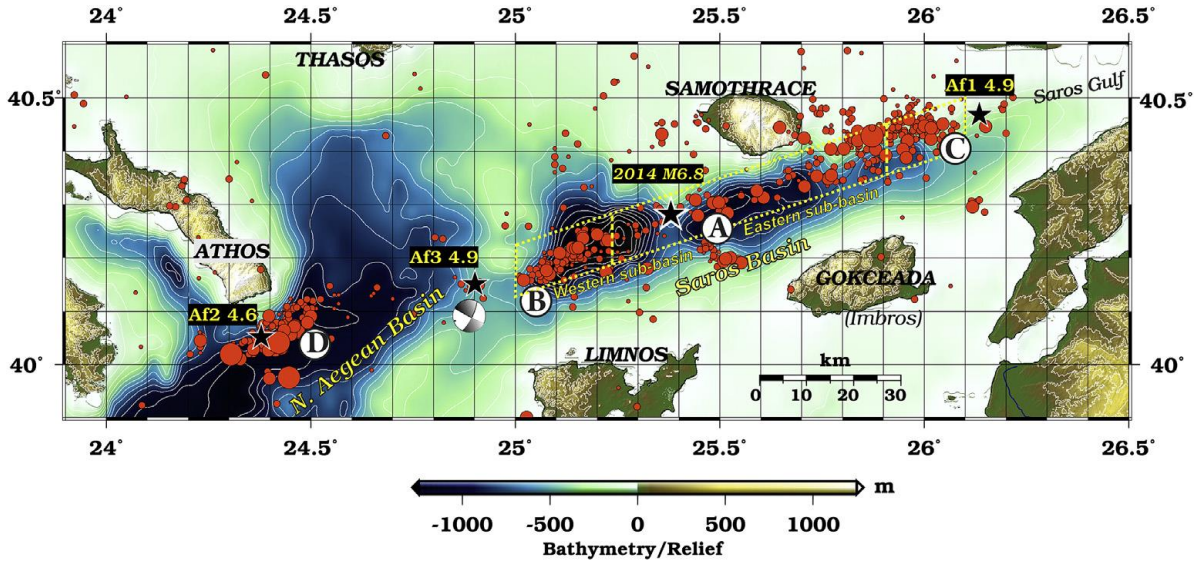

Figure 4.7. Relocated epicenters of earthquakes M≥1.8 which occurred in the North Aegean Trough from 24/5/2014 to 5/9/2014 (Evangelidis, 2015). The mainshock epicenter and the three major aftershocks are denoted by stars. The distinguished clusters are marked with letters A-D (Kiratzi et al., 2016).

4.2.3. Slip Inversion Results

The coordinates of the mainshock were set as 40.29°N and 25.40°E (Kiratzi et al., 2016), respectively (Fig. 4.1). The stations used for the analysis are presented with black triangles in Fig. 4.8. The epicentral distances vary from 25 to 100 km. The results derived using data from local to near-regional distances are presented below (Fig 4.9 and Fig 4.10). The fault plane was considered 40 km long and 15 km wide. The focal mechanism, which is an input to the inversion, was 72°/85°/-173° (Kiratzi et al., 2016) with the focal depth at 14 km. The velocity model utilized in order to calculate the Green's functions was the one determined by Karabulut et al. (2006).

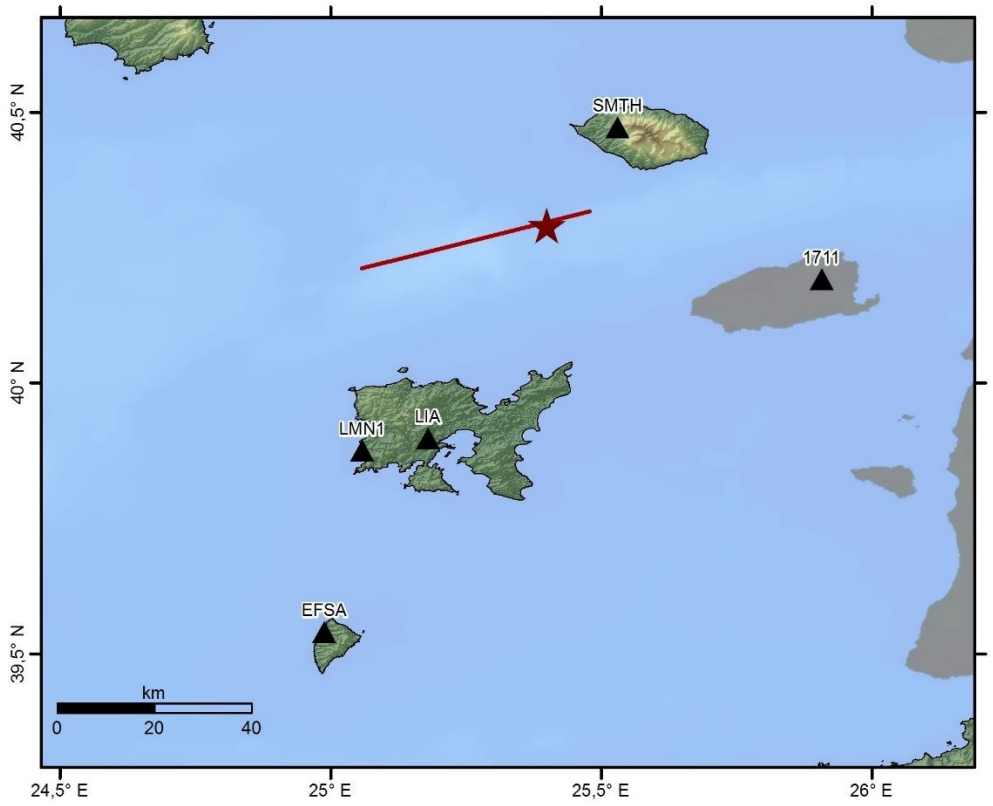

Figure 4.8. The epicenter, the causative fault and the stations used in the slip inversion procedure of the May 24, 2014 Lemnos earthquake.

The rupture evolution is presented in the figure Fig. 4.9, with a snap taken every one second. The rupture evolution presents several patches that were activated at distinct times throughout the total rupture time. The rupture lasted for 11 s and the maximum slip velocity occurred during the 9th and 11th second.

In the Fig. 4.10, the total slip distribution on the fault is provided. It is obvious that there is a lack of a continuum regarding the slip spatial distribution, but four distinguishable patches are observed. From left to right (or from West to East), in the upper part of the image, three patches are identified. In the center of the fault another patch can be distinguished. The last patch is located at the eastern part of the fault at a depth of 13 km. The maximum slip is 1.4 m and is obtained in the central patch. It is important to notice that the figure is up-dip, meaning that it starts from the bottom (0 km) towards the ceiling of the fault (15 km). The existence of a possible barrier is suggested between 7 and 11 km depth from 5 to 22 km along strike, in respect to the upper left corner of the fault plane.

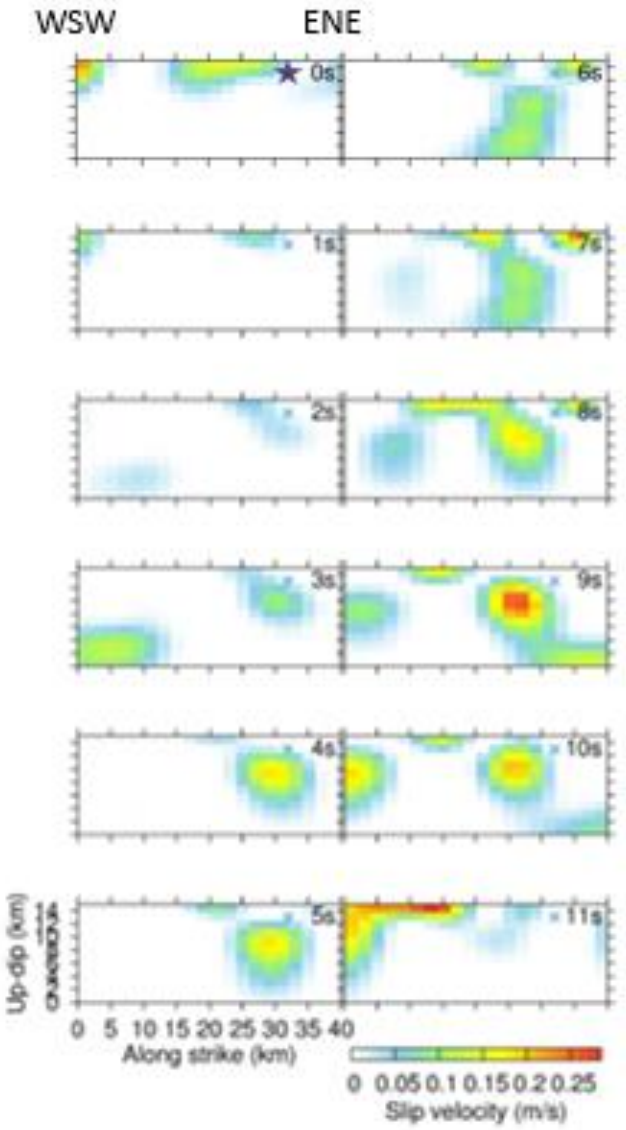

Figure 4.9. The slip distribution evolution is presented by snaps of one second intervals. Note that the maximum slip velocity is 0.15 m/s.

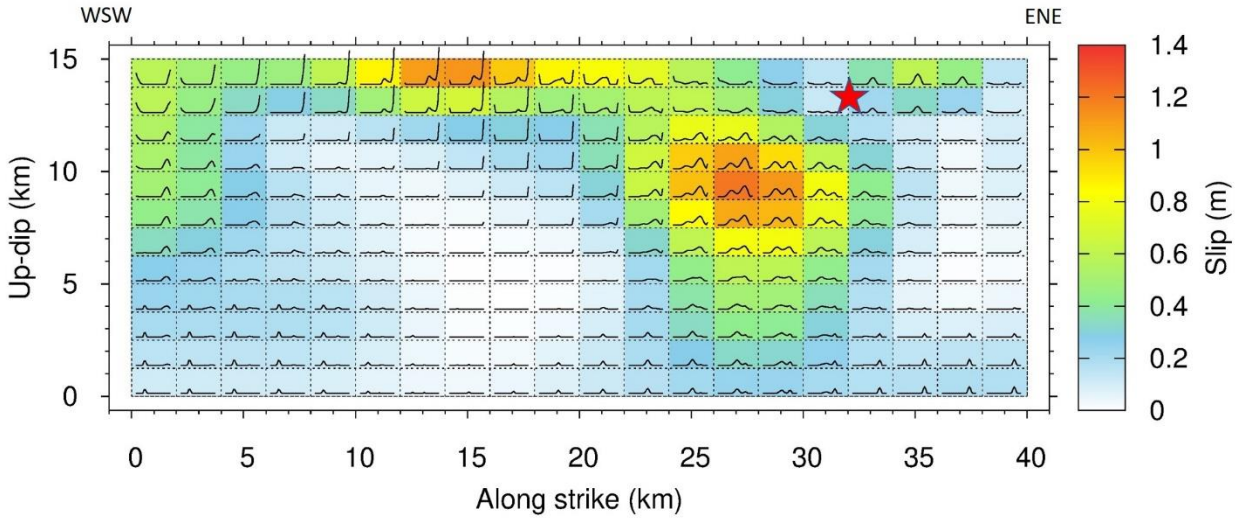

Figure 4.10. The total slip distribution on the fault. The maximum slip reaches 1.4 m. The along strike axis is oriented from the WSW (left) to ENE (right). In the vertical axis, the 0 km indicates the roof of the fault.

4.2.4. Ground Deformation Results

Regarding the derived ground displacement field by the slip model, acquired from the LinSlipInv software, the results are presented below (Fig. 4.11). Three zones can be distinguished in the vicinity of the causative fault. The first lies close to its NE part, towards the Samothrace Island, with an uplift of about 3 cm, the second to its SE, towards the Imbros (Gokceada) Island, with a subsidence of about 4 cm, and the third to the West, with 1 cm of uplift.

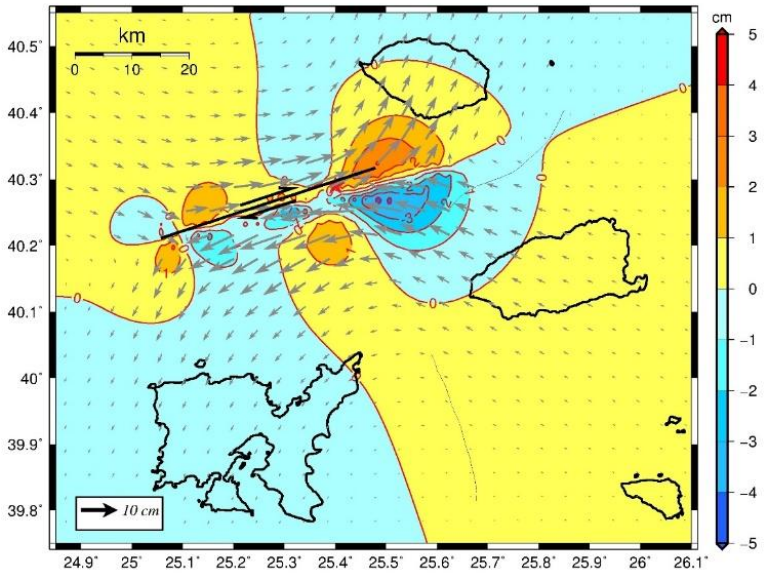

Figure 4.11. Ground deformation determined using the DIS3D software utilizing the determined slip distribution on the fault, as derived by the LisnSlipInv software (using local to near-regional data). The maximum subsidence is up to 4 cm and the maximum uplift reaches 3 cm. The vectors represent the horizontal movement.

4.3. Lefkada 2015 (M_w = 6.4)

The island of Lefkada is located in the Ionian Sea, in Western Greece, which is considered as one of the most seismically active regions in the Mediterranean. The broader Lefkada region, including the neighboring Cephalonia Island, has experienced strong earthquakes (M_w > 6.0), mostly along the Cephalonia Transform Fault Zone (CTFZ; Papadimitriou et al., 2006; Ganas et al., 2016). On November 17, 2015, a shallow M_w 6.5 earthquake occurred in the southwestern part of Lefkada (Papadimitriou et al., 2017).

4.3.1. Seismotectonic setting

The island of Lefkada is considered as one of the most active tectonic areas in Europe and particularly in the eastern Mediterranean region, with often recorded strong ground shaking due to its location near to the 140-km long CTFZ (Scordilis et al., 1985; Kouskouna et al., 1993; Louvari et al., 1999; Kokinou et al., 2006; Papadimitriou et al., 2006; Makropoulos et al., 2012; Ganas et al., 2016). The tectonic framework of the overall area can be described by the combination of the continental collision between the Eurasian and the Apulian plates and the subduction of the Tethys oceanic plate beneath the Aegean continental microplate along the active Hellenic Orogenic Arc to the SW (Papadimitriou et al., 2015). Generally, the islands of Lefkada and Cephalonia are characterized by high seismicity, with frequent strong (M > 6.0) earthquakes, followed by severe casualties and damage during the last six centuries, as revealed by historical records (Papadimitriou et al.,2015; Papadimitriou et al., 2017 and references therein). The western coast of the Lefkada island accommodates the most destructive historical earthquakes, such as the 22 November 1704 (M=6.3), the 12 October 1769 (M=6.7), the 23 March 1783 (M=6.7) and the 28 December 1869 (M=6.4) earthquakes (Kouskouna et al., 1993; Papadimitriou et al., 2006, 2015). It is worth noting that the same fault segment is reactivated almost 3 times per century, producing seismic events. Regarding the historical catalogue of disastrous earthquakes, Stamatelos (1870) listed 13 destructive events in Lefkada Island between 1612 and 1869 (Papazachos and Papazachou 2003; Kouskouna and Sakkas, 2013; Stucchi et al., 2013) that present similarities to the instrumental events located in the western onshore area (Papadimitriou et al., 2017). The first recorded destructive earthquake during the instrumental period was the event that occurred on 27 November 1914, M_w 5.9, where severe onshore damage was reported near the NW coastline. Afterwards, a doublet was recorded in 1948, with the first event on 22 April, with M_w 6.5, destroying the SW part of the island and almost 2 months later, on 30 June, the second event occurred, with M_w 6.5, that damaged the NW part of the Island (Makropoulos et al., 2012). The most recent, before the occurrence of the 2015 event, destructive earthquake, of Mw=6.3, took place on 14 August 2003 NW of the Lefkada Island (e.g. Karakostas et al., 2004; Papadimitriou et al., 2006; Karakostas and Papadimitriou, 2010; Kassaras et al., 2015). It was a shallow event, whose focal mechanism revealed dextral strike–slip faulting, that occurred close to the northern end of the CLTFZ. According to the aftershock's spatial distribution, two clusters were identified

(Papadimitriou et al., 2006): the first in the vicinity of the mainshock's epicenter and the second close to the northwestern coast of the Cephalonia Island.

The island of Lefkada consists of sedimentary rocks (mainly carbonates) of the external Hellenides that belong to the Ionian and Paxos zones (Jacobshagen, 1979), whereas the SW part consists of the limestone of the Paxos zone (Bornovas, 1964). The boundary between the two aforementioned geological zones, the Ionian Thrust (dipping NE), outcrops onshore central Lefkada. South Lefkada is characterized by neotectonic faults (Lekkas et al., 2001; Rondoyanni et al., 2012) striking N-S and NE-SW, with the most important being the NNE-SSW oriented Athani fault (or Athani-Dragano fault). However, the detailed field observations of the area did not lead to the mapping of any major, onshore strike slip fault that could be responsible for events of M> 6.0. Furthermore, no surface expression was identified after the occurrence of the 17 November 2015 mainshock (Ganas et al. 2016; Lekkas et al., 2018).

4.3.2. Mainshock and aftershock sequence

The mainshock occurred on 17 November 2015 07:10:07 (GMT) in the southwestern part of Lefkada Island. The epicenter was determined at 38.6643°N and 20.5845°E by Papadimitriou et al. (2017), whereas at 38.6779°N and 20.5827°E by Sokos et al. (2016). Regarding the damage caused by the mainshock, it was significantly lower compared to the one due to the 2003 event, fact that showcases the good behavior of the local buildings (Kassaras et al., 2018). The aftershock sequence was composed of more than 2600 events up to December 3, 2015 (Papadimitriou et al., 2015). According to Papathanassiou et al. (2017), the earthquake occurred on a near-vertical strike-slip fault with dextral sense of motion; the fault plane strikes N(20 ± 5)°E and dips to the east with an angle of about 70–80° (Ganas et al., 2016; Sokos et al., 2016), in accordance with Papadimitriou et al. (2015). The focal depth was determined equal to 9 km by the latter. Double-difference relocation revealed that the aftershock distribution spanned ~65 km in length in a SSW-NNE direction and is spread over an area far beyond either sides of the mainshock epicenter, parallel to the western coast of the Lefkada Island. Most epicenters are located ~2-3 km onshore Lefkada, while a second, spatially separated group of activity is located to the south, with a more sporadic appearance than in other areas where clusters are formed. The focal depths mainly range between 5 km and 10 km in Lefkada and 5 km - 15 km for the southern spatial group. The activity of the southern group appears to be divided in smaller sub-clusters (Papadimitriou et al., 2015; Papadimitriou et al., 2017). The strongest aftershock of the Lefkada 2015 sequence occurred on 17 November, 08:33 (GMT) with M_w 5.0, about 4 km SSW of the mainshock. The seismic activity was mostly expressed by two dense clusters in central Lefkada and south of the island towards Cephalonia. The temporal distribution of the aftershock sequence followed a smooth exponential decay, with the exception of a small secondary outburst of activity on 29 November at the dense cluster in central Lefkada, including two events of M≈4.0 (Papadimitriou et al., 2015).

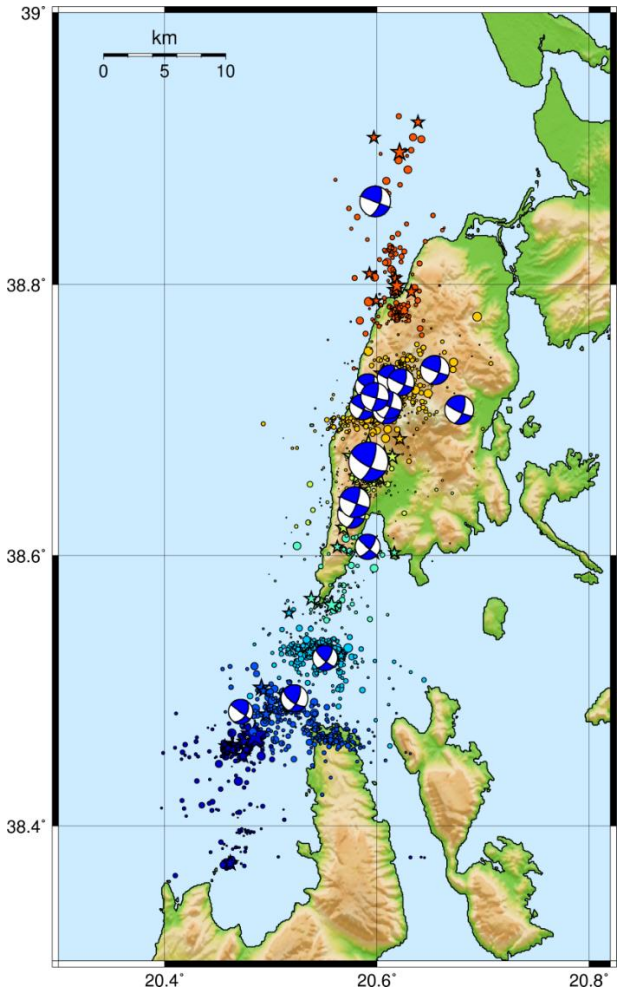

Figure 4.12. Relocated aftershock epicenters using the double difference and cross-correlation techniques (Papadimitriou et al., 2015).

4.3.3. Slip Inversion Results

The coordinates of the mainshock ware taken as 38.6779°N and 20.5827°E (Sokos et al., 2016), respectively (Fig. 4.1). The stations utilized in the inversion scheme are presented with black triangles in Fig. 4.13. The epicentral distances vary, from 5 to 80 km. The results derived using the LinSlipInv software, which requires data recorded in local to near-regional distances, are presented below (Fig. 4.14 and Fig. 4.15). The fault plane was considered 25 km long and 10 km wide. The focal mechanism, utilized as input in the inversion, was 22°/72°/161°, with the focal depth at 14 km (Papadimitriou et al., 2015). The velocity model used in the inversion was determined by Papadimitriou et al. (2017).

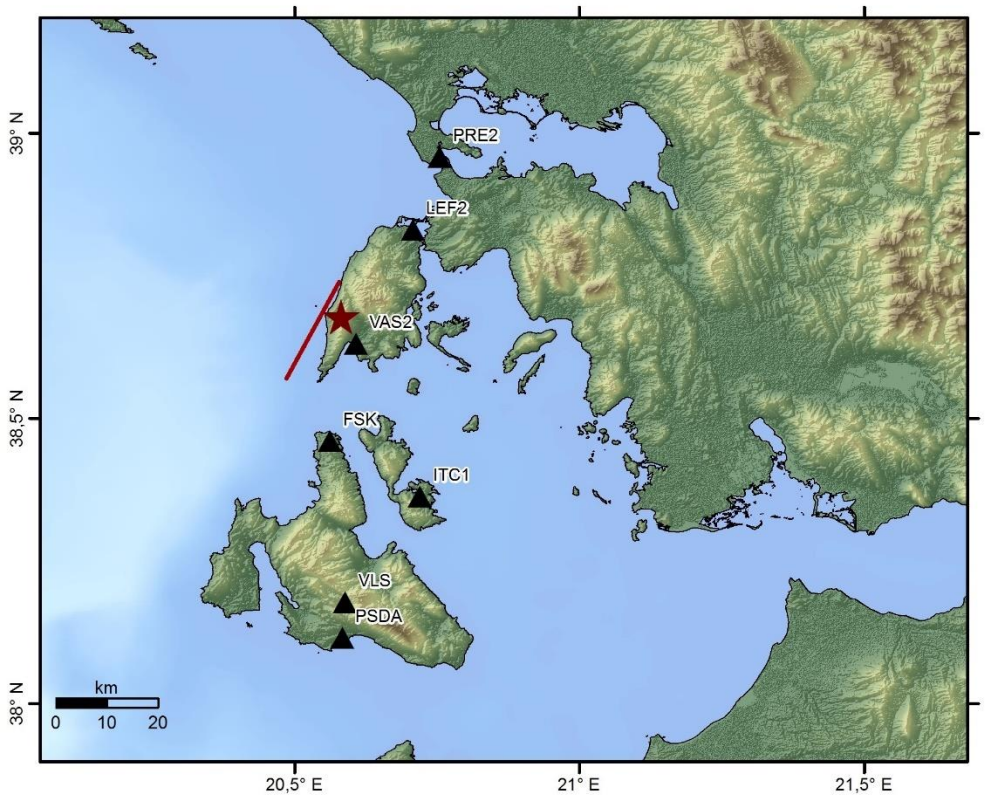

Figure 4.13. The epicenter, the causative fault and the stations used in the slip inversion procedure of the November 17, 2015 Lefkada earthquake.

The rupture evolution is presented in Fig. 4.14, with a snap taken every one second. The rupture is complex, given that it starts from the lowest SSW point of the fault and evolves upward and to the NNE. At the 5th second, a new patch is generated from the lowest NNE part of the rupture, heading also upwards. The rupture related to this patch lasts for about two seconds, until it reaches the ceiling of the fault. Then, a third patch is activated from the NNE heading to the SSW. The rupture ends in the NNE part of the fault. The total rupture lasts for 11 seconds, with the maximum slip rate occurring during the 3rd and the 6th second.

In the Fig. 4.15, the total slip distribution on the fault is given. A single lobe with its principal axis heading from NNE to SSW is identified. The maximum slip is 1.2 m and it is located in the NNE part of the fault. It is important to notice that the figure is up-dip, meaning that it starts from the bottom (0 km) towards the ceiling of the fault (10 km). The total slip is not concentrated in a certain part of the fault, but almost the total fault plane has slipped. A slight directivity to the NNE is evident.

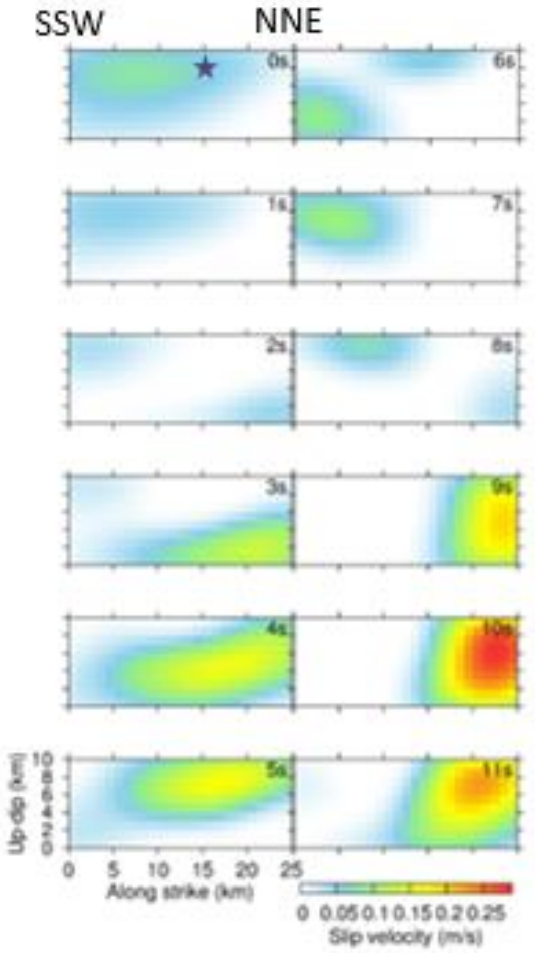

Figure 4.14. The slip distribution evolution is presented by snaps of one second intervals. Note that the maximum slip velocity is 0.2 m/s.

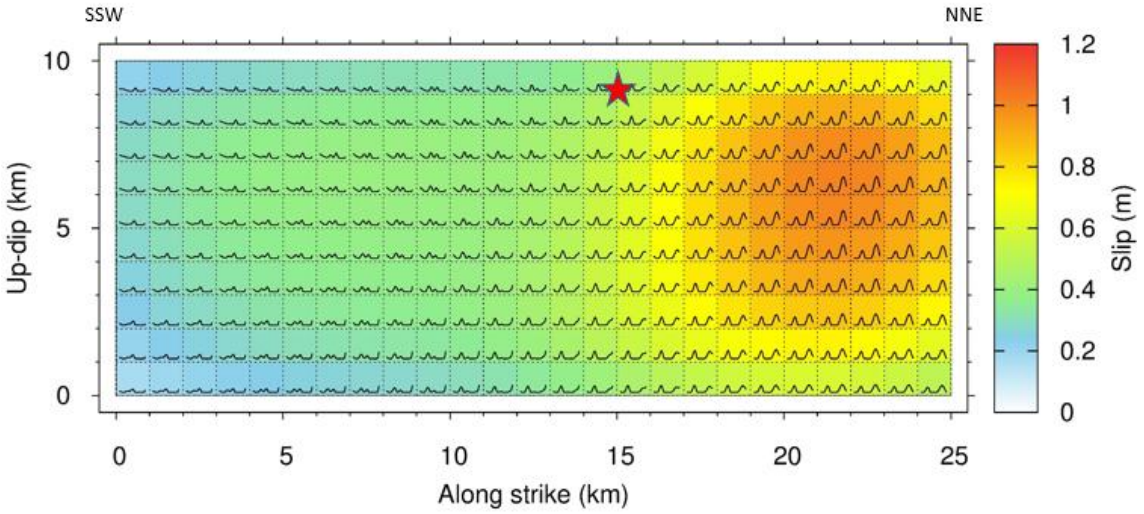

Figure 4.15. The total slip distribution on the fault. The maximum slip reaches 1.2 m. The along strike axis is oriented from the SSW (left) to NNE (right). In the vertical axis, the 0 km indicates the roof of the fault.

4.3.4. Ground Deformation Results

Regarding the ground deformation (Fig. 4.16), a right lateral horizontal movement has been identified. The fault plane controls the calculated uplift and subsidence, with the vertical deformation presenting uplift to the east of the fault and subsidence to the west. Almost the whole island of Lefkada was uplifted, with the exception of the northern part which presents almost no vertical deformation (slight subsidence). The maximum uplift was 18 cm and it is located at the southern coast of the island, between Vassiliki and Syvota.

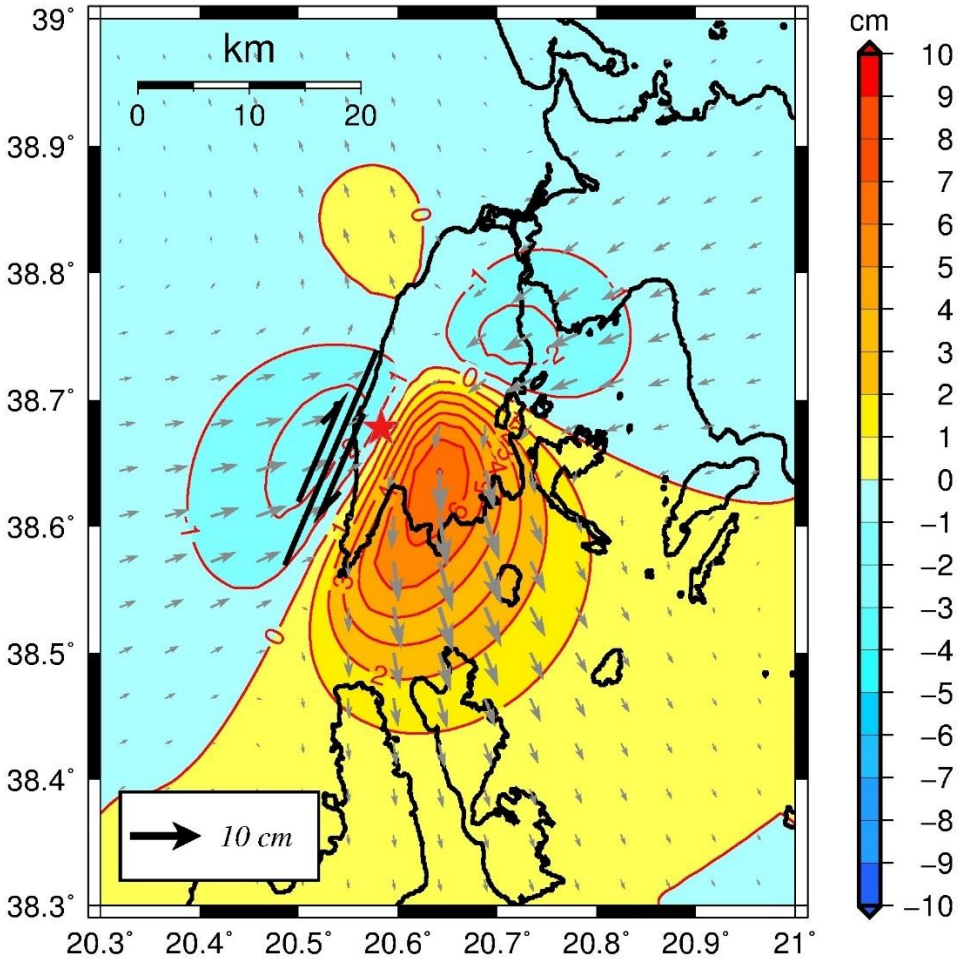

Figure 4.16. Ground deformation determined using the DIS3D software utilizing the determined slip distribution on the fault, as derived by the LinSlipInv software (using local to near-regional data). The maximum subsidence is 2 cm and the maximum uplift reaches 6 cm. The vectors represent the horizontal movement.

4.4. Lesvos 2017 (M_w = 6.3)

On 12 June 2017, a major earthquake occurred S of Lesvos. A rough examination of tectonics in the epicentral area highlights a local extensional regime with normal faulting and an important strike slip component in certain cases. After applying relocation, using the double-

difference HYPODD algorithm (Waldhouser, 2001), the aftershock sequence revealed seven clusters, forming two linear branches (roughly N130°E), in agreement with known faulting in the region. An aftershock that was located SE of the mainshock (5 days later with magnitude M_w 5.2) triggered a secondary aftershock sequence (Papadimitriou et al., 2018).

4.4.1. Seismotectonic setting

The main processes that control the neotectonic history of the Aegean region are responsible for the tectonic evolution of the island of Lesvos, since the Oligocene period (15 Ma). The island is dominated by the presence of three main fault systems striking N40-60°W, N30-60°E and E-W (Hecht, 1974a,b; Katsikatsos et al., 1982). One of the most significant faults of the island is the Agia Paraskevi Fault (APF), characterized by almost pure dextral strike – slip motion, which is related to the formation of elongated NNE – SSW directed depressions (Chatzipetros et al., 2013). It is noteworthy that the APF hosted the Lesvos 1867 event (Papazachos and Papazachou, 2003; Altinok et al., 2012). In the eastern part of Lesvos, the northern margins of the Gulf of Gera (GG) are controlled by normal faults striking NW – SE (Chatzipetros et al., 2013). The Polichnitos Fault is an onshore normal fault that defines the margin of the Lesvos Basin, bounded by normal faults with NW-SE direction, where numerous landslides occur (Mascle and Martin, 1990). The Lesvos Basin is a tectonic asymmetric graben, where the NE marginal fault is dipping towards the SW and antithetic faults exist on the hanging wall, dipping NE (Mascle and Martin 1990). According to Yaltirak and Alpar (2002), the Bababurnu Basin is a transtensional basin, related to the middle branch of the North Anatolian Fault Zone (NAFZ) and is located NW of Lesvos and SW of the Biga Peninsula (Mesimeri et al., 2018c; Papadimitriou et al., 2018). The overall foci in the Lesvos area are shallow and categorized in three seismic zones (Voulgaris et al., 2004):

- The first zone crosses the north coast of Lesvos Island.
- The second zone crosses the south and SE coasts.
- The third zone, being the most active (Delibasis and Voulgaris, 1989), crosses the SW part of Lesvos with a NW orientation (Papadimitriou et al., 2018).

4.4.2. Mainshock and aftershock sequence

The mainshock occurred on 12 June 2017, approximately 15 km south of the South coast of the Lesvos Island. The seismic moment was determined at M_o $3.5 \cdot 10^{18}$ N·m and the centroid depth at 13 km. The acquired focal mechanism by SL-NKUA indicates normal faulting with the fault plane oriented in a N122°E direction with a 40° dip to the SSW and rake equal to -83°. Similar type of faulting is extracted by focal mechanisms of the major events of the sequence, with the exception of the largest aftershock that was characterized by strike-slip faulting (Papadimitriou et al., 2018).

The aftershock sequence covered an area of 20x12 km^2 according to Papadimitriou et al. (2018), whereas according to Kiratzi (2018) the total length of the aftershock sequence spread

for about 40 km, with the epicenters displaying gradual migration to the NW of the mainshock and then to the SE, providing a NW-SE direction. The occurrence of a strong aftershock (M_w 5.2) 5 days later (17 of June) to the eastern part of the aftershock distribution provided a dense cluster (Papadimitriou et al., 2018).

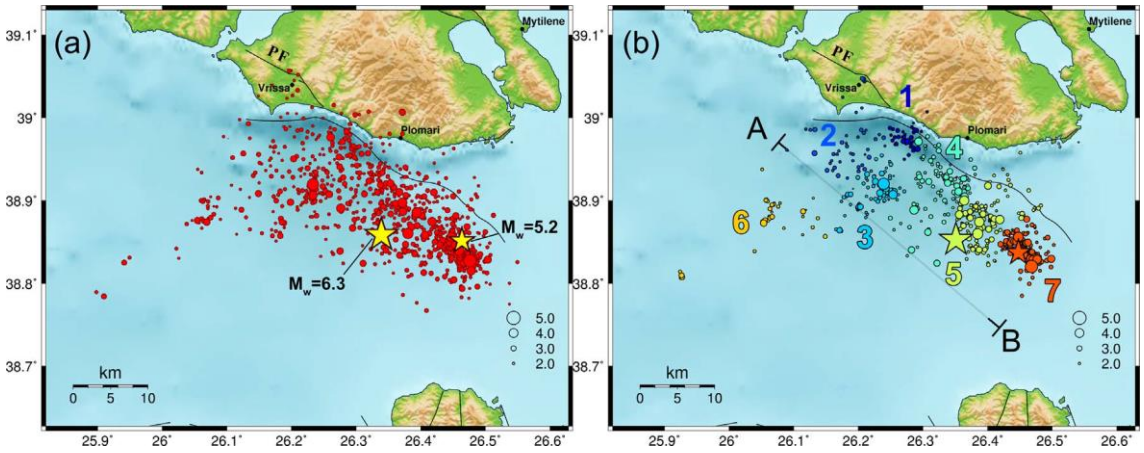

Figure 4.17. a) Map of the manually located events of the June 2017 Lesvos sequence. b) Map of the relocated events. Solid black lines denote active faults. The two stars denote the epicenters of the mainshock and the largest aftershock. Colors and numbers in panel b) refer to the 7 spatial groups determined for the relocated catalogue (Papadimitriou et al., 2018).

In more detail, according to Papadimitriou et al. (2018), seven spatiotemporal groups were identified (Fig. 4.17). Events in groups #1, #2 and #7 started to appear 1, 3 and 7 hours, respectively, after the mainshock. Two days later, group #6 was activated in the western part of the fault plane. The largest aftershock was located roughly in the middle of group #7, oriented NW-SE, with activity spreading gradually outwards, towards its margins. Regarding group #7, its seismic activity remained highly active until 30 June, due to another major aftershock (M_w 4.9) on 22 of the same month, in contradiction to the other groups which slowly diminished, with just group #2 exhibiting a small spatiotemporal cluster until 22 of June (Papadimitriou et al., 2018).

4.4.3. Slip Inversion Results

The focal depth of the mainshock was set 13 km after performing a grid search to obtain the optimum fit, whereas its geographical coordinates, i.e. the longitude and latitude, 38.8488°N and 26.3126°E (AFAD, 2017), respectively (Fig. 4.1). The stations used in the slip distribution analysis are presented with black triangles in (Fig. 4.18). The epicentral distances vary, from 40 to 70 km. The results derived using data from local to near-regional distances are presented below (Fig 4.19 and Fig 4.20). The fault plane was considered 20 km long and 12 km wide, as proposed by Papadimitriou et al. (2018). The dimensions were determined by the spatial distribution of the relocated aftershock sequence. The focal mechanism that was used as input in the inversion is 122°/40°/-83° and was calculated by applying moment tensor inversion in regional distances (Papadimitriou et al., 2018). The utilized crustal model is the one determined by Papadimitriou et al. (2018), consisting of seven horizontal homogeneous layers.

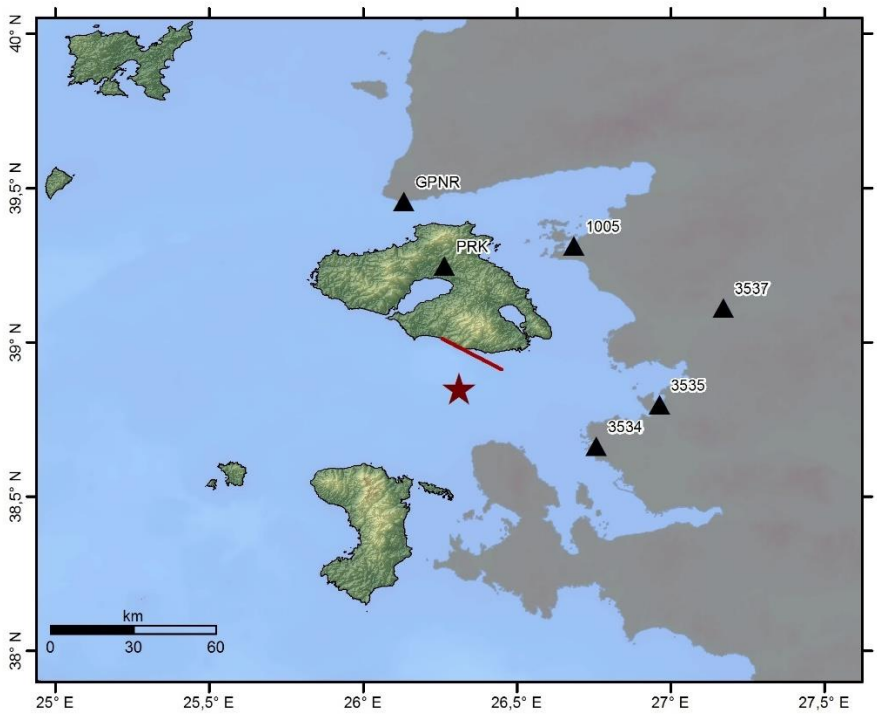

Figure 4.18. The epicenter, the causative fault and the stations used in the slip inversion procedure of the June 12, 2017 earthquake.

In the next figure, the rupture evolution is presented (Fig. 4.19), with a snap taken every one second. The total slip of the fault is concentrated in a limited area in the upper right part (SE) and fades away to the NW end of the fault. The rupture lasts for 7 seconds, with the first 3 seconds being the fastest in terms of the slip rate. The maximum slip velocity occurred during the initiation of the rupture in the central part of the slipping area.

In the Fig. 4.20, the total slip distribution on the fault is presented. A lobe with its principal axis heading from SE to NW is observed. The maximum slip is 1 m and it is located in the left edge of the lobe. It is important to notice that the figure is up-dip, meaning that it starts from the bottom (0 km) towards the ceiling of the fault (12 km). It is observed that the total slip is concentrated within a small area of the fault, i.e. almost the half of the total fault plane. A directivity phenomenon to the NW is evident.

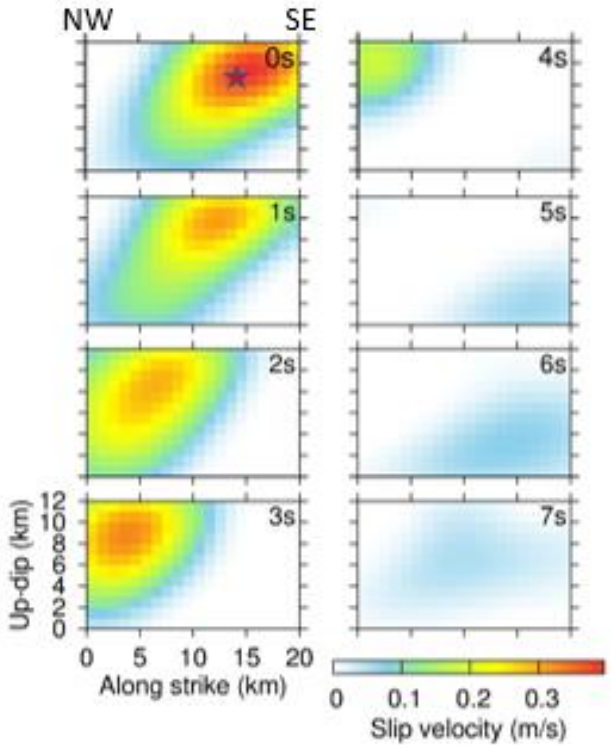

Figure 4.19. The slip distribution evolution is presented by snaps of one second intervals. Note that the maximum slip velocity is 0.35 m/s.

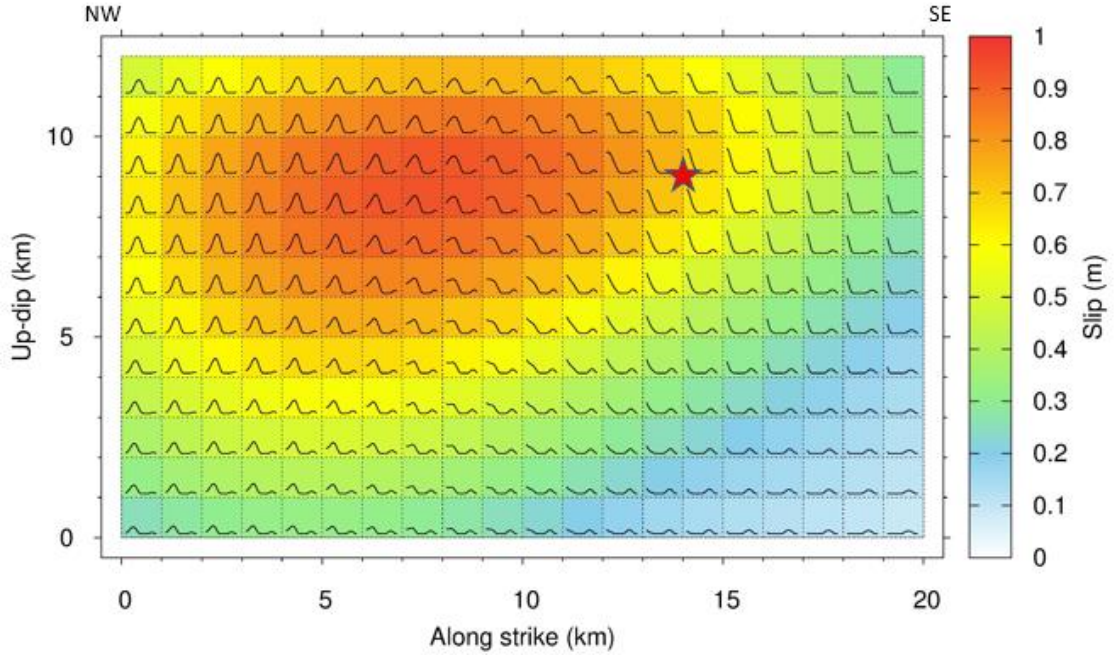

Figure 4.20. The total slip distribution on the fault. The maximum slip reaches 1 m. The along strike axis is oriented from the NW (left) to SE (right). In the vertical axis, the 0 km indicates the roof of the fault.

4.4.4. Ground Deformation Results

Concerning the ground deformation and specifically the horizontal component, an extension in a NNE-SSW direction is evident with the center of the system being the causative fault plane. Thus, horizontal movement in a NNE direction has been determined on the Lesvos Island. As for the vertical component, the entire deformation is located in the vicinity of the fault plane, with the subsidence reaching 20 cm, offshore. Very low uplift values have been obtained for the vast part of the Lesvos Island, with the exception of the SE coasts, including the villages of Plomari and Vatera, where low subsidence has been identified (Fig. 4.21).

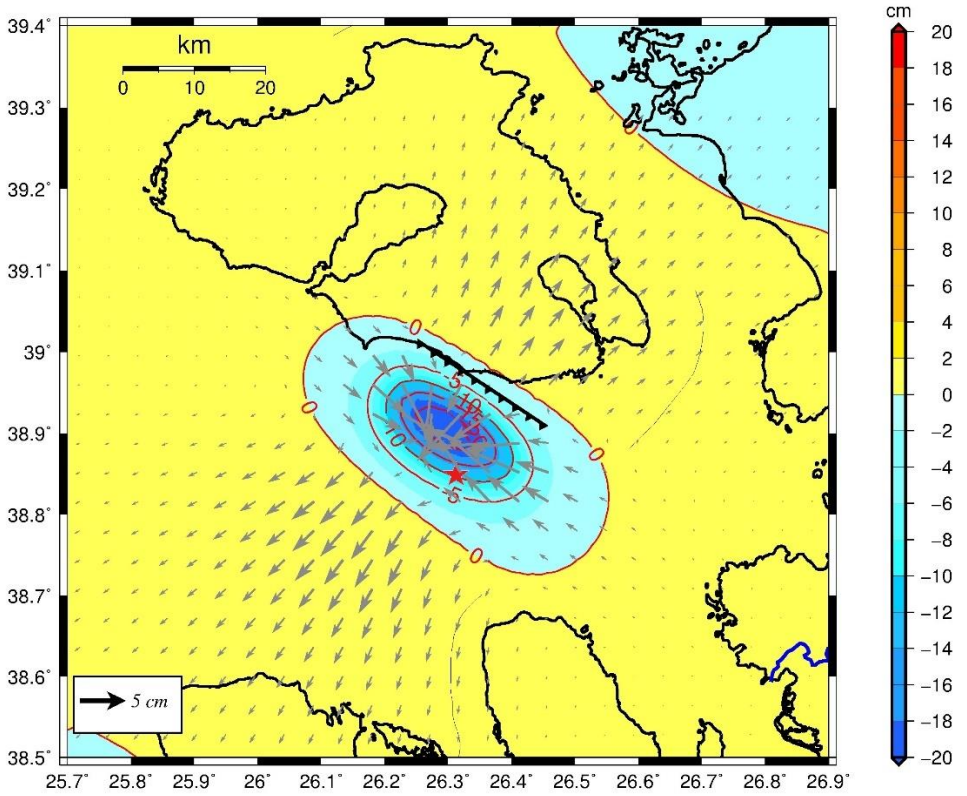

Figure 4.21. Ground deformation determined using the software utilizing the determined slip distribution on the fault, as derived by the LisnSlipInv software (using local to near-regional data). The maximum subsidence is 20 cm. The vectors represent the horizontal movement.

4.5. Kos 2017 (M_W = 6.6)

The M_w 6.6 earthquake that occurred on 20 July 2017 northeast of the Kos Island and south of the Bodrum Peninsula was a destructive one, with two reported casualties and several injured in Kos Island (Ganas et al., 2017). The mainshock is associated with the generation of a moderate tsunami with a, however, significant impact to the surrounding regions (Heidarzadeh et al., 2017; Yalçıner et al., 2017).

4.5.1. Seismotectonic setting

The study area presents high seismic activity, which is supported by the fact that more than 14 earthquakes with M ≥ 6.5 have occurred since 1900 (Makropoulos et al., 2012; Stucchi et al., 2013; Heidarzadeh et al., 2017; Ocakoğlu et al., 2018). The stress regime is extensional with a N-S direction, at a rate of 35 – 40 mm/year (Kurt et al., 1999), 30 mm/year (McKenzie 1972; Şengör 1979; Dewey and Şengör 1979; Le Pichon and Angelier 1981; Reilinger et al. 2010) or 20 mm/yr, as derived by Aktug et al. (2009), which is most probably attributed to the westerly escape of the Anatolian plate in response to the convergence of the African, Eurasian and Arab plates (Heidarzadeh et al., 2017).

Regarding the geology of the study area, the Gökova graben presents an E-W direction with the major part being offshore, i.e. the Gökova Gulf. Two major tectonic features characterize the stress regime: a NW-SE rift and graben system (Görür et al. 1995a,b) and a E-W trending graben developed under a N-S extensional regime (Yılmaz et al. 2000). The Gökova Gulf is about 90 km long (E–W) and 5–30 km wide (N–S) (Ocakoğlu et al., 2018).

The Kos Island is mainly comprised by metamorphic basement rocks, Alpine Mesozoic thrust units and volcanic deposits (Fig. 4.22.; Böger et al., 1974; Böger, 1978; Keller, 1982; Dalabakis, 1987; Bardintzeff et al., 1989; Papanikolaou and Lekkas, 1990; Davis et al., 1993; Triantaphyllis, 1994; Papanikolaou and Nomikou, 1998). Lastly, the Kos Island is a result of a ENE–WSW oriented complex tectonic mega-horst (Nomikou and Papanikolaou, 2010).

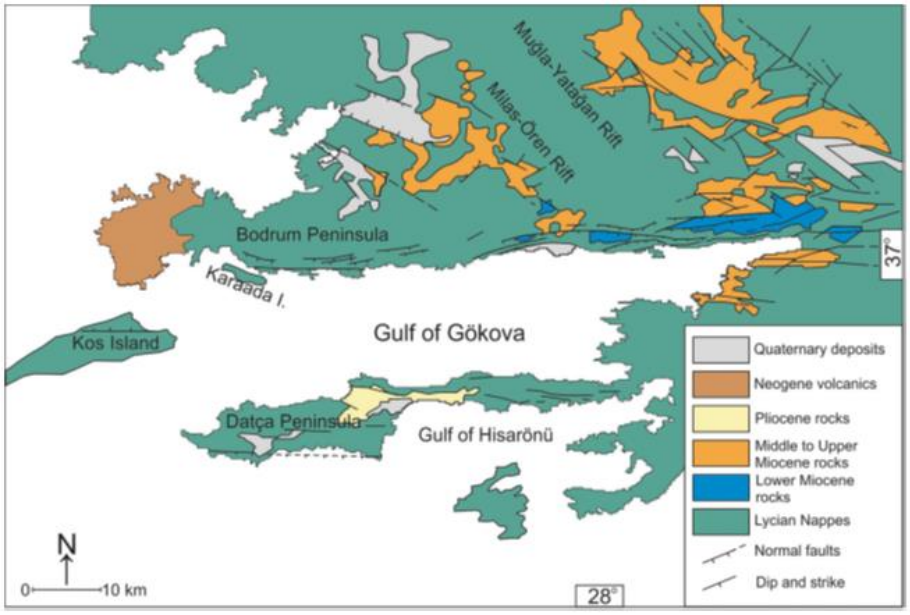

Figure 4.22. Regional on land geology, modified from Görür et al. (1995a,b).

4.5.2. Mainshock and aftershock sequence

The Kos 2017 aftershock sequence was relocated and analyzed in detail in the work of Ganas et al. (2019). According to this study, most of the aftershocks are located outside the area of the main rupture and towards the edges of the inferred fault plane. The sequence

presented spatiotemporal clustering, with two major spatial groups #1 and #3 (Fig. 4.23) being activated right after the occurrence of the mainshock (blue star). The area of the main rupture is delineated by a 15-km gap, nearly void of aftershocks, between these two groups, which suggests that the fault may have ruptured as a single asperity. Most of the activity was concentrated in the eastern cluster (#3), while the cluster #5 was mainly triggered by the largest aftershock (M_w=5.2) that occurred on 8 August, 2017. It is suggested (Ganas et al., 2019) that cluster #5 may belong to an antithetic fault, dipping southwards. However, the lack of local stations and adequate azimuthal coverage did not permit focal depths to be constrained enough to allow for a secure determination of fault dips by the spatial distribution of hypocenters. Only the western cluster (#1), which is also the closest one to the mainshock's hypocenter, indicated a roughly north-dipping plane. Ganas et al. (2019) constrained the fault plane, using a joint inversion of GNSS and InSAR data, striking N283°E and dipping ~37° NNE, with its upwards extension associating its outcrop with the Gökova ridge (Tur et al., 2015). The focal mechanism suggested by Karakostas et al. (2018) is 278°/35°/-80° whereas the one derived by the SL-NKUA is 267°/38°/-110°.

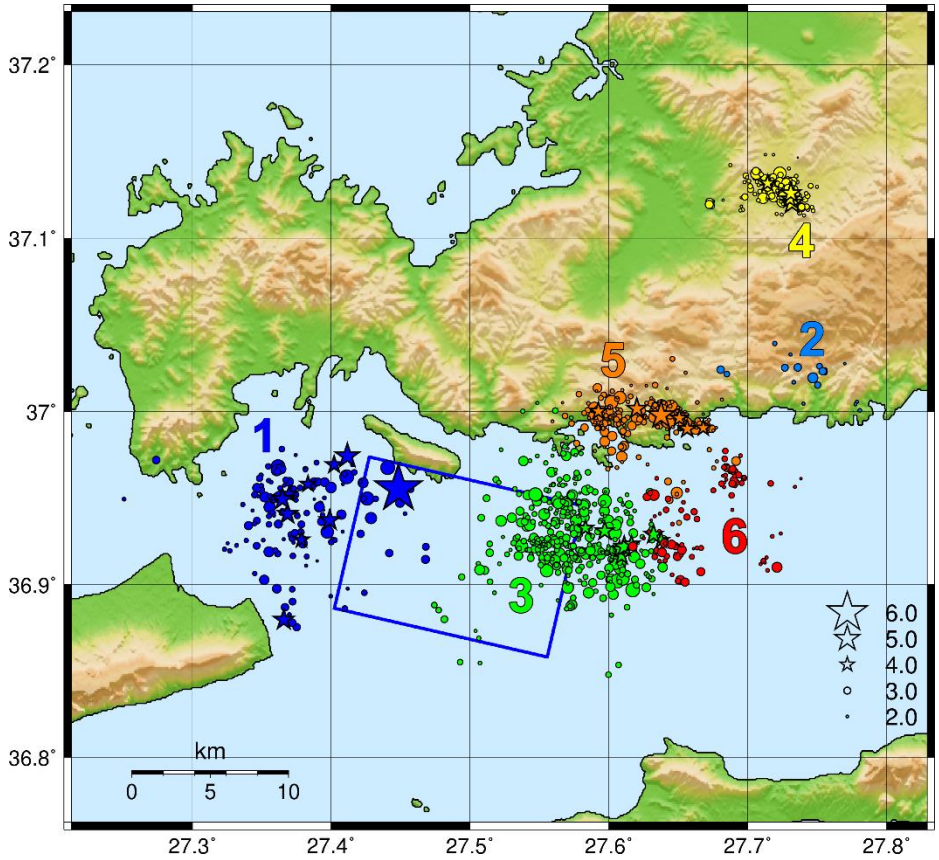

Figure 4.23. Spatial distribution of the relocated Kos 2017 aftershock sequence. Colors represent different spatial groups. The rectangle delineates the inferred fault plane, constrained by inversion of GNSS and InSAR data (modified after Ganas et al., 2019).

4.5.3. Slip Inversion Results

The longitude and latitude of the mainshock (Fig. 4.1) were 36.9643°N and 27.4332°E, respectively, according to Karakostas et al. (2018). The stations used for the analysis are presented with black triangles in Fig. 4.24). The epicentral distances vary from 13 to 90 km. The results derived using data from local to near-regional distances are presented below (Fig 4.24 and Fig 4.25). The fault plane was considered 20 km long and 10 km wide (Karakostas et al., 2018; Karasozen et al., 2018). The focal mechanism that was used as input in the inversion was 278°/35°/-80° (Karakostas et al., 2018) with the focal depth at 11 km (UoA; www.geophysics.geol.uoa.gr).

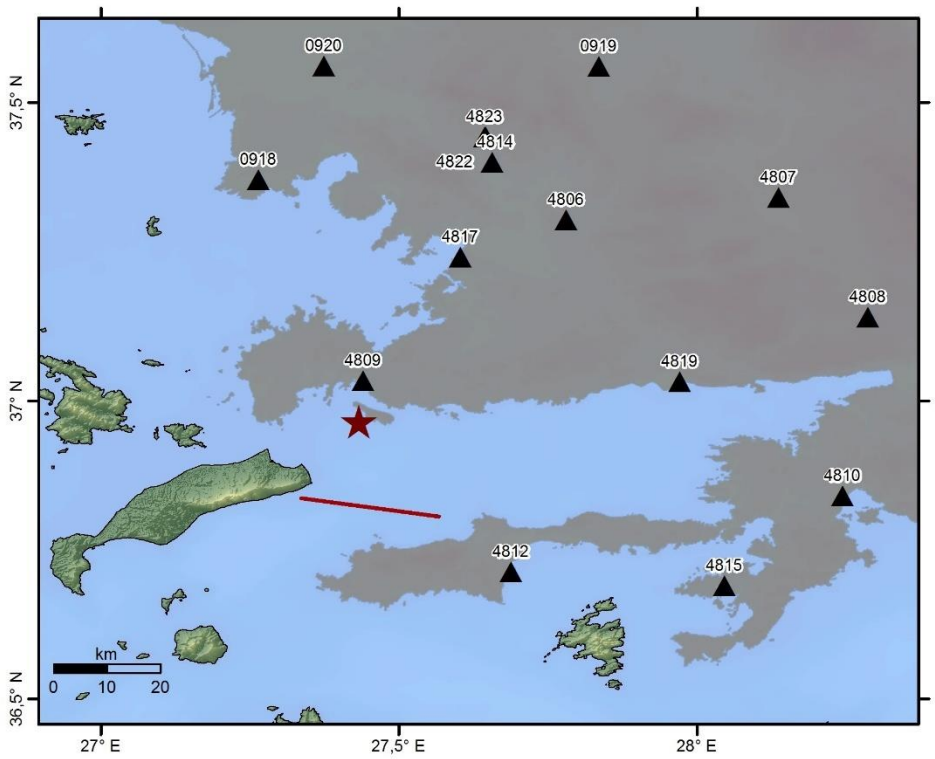

Figure 4.24. The epicenter, the causative fault and the stations used in the slip inversion procedure of the July 20, 2017 earthquake.

In the Fig. 4.25, the rupture evolution is presented, with a snap taken every one second. The total slip of the fault is concentrated in a limited area in the central upper part and fades away to the NW end of the fault. The rupture lasts for 9 s, with the first two seconds being slow in terms of slipping. The maximum slip velocity occurred during the 3rd and 4th second in the central part of the slipping area and is of the order of 0.6 m/s.

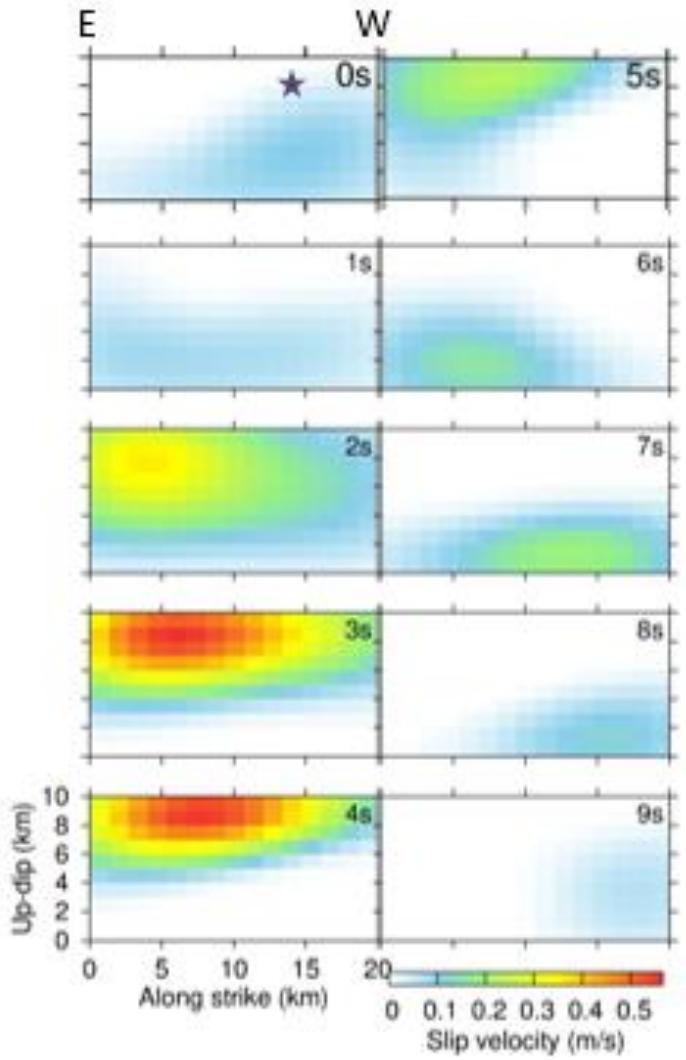

Figure 4.25. The slip distribution evolution is presented by snaps of one second intervals. Note that the maximum slip velocity is 0.56 m/s.

In the next figure (Fig. 4.26), the total slip distribution on the fault is given. A lobe with its principal axis heading from W to E is observed. The maximum slip is 1.8 m and it is located in the SSE part of the lobe. It is important to notice that the figure is up-dip, meaning that it starts from the bottom (0 km) towards the ceiling of the fault (17 km). Again, the total slip is concentrated within a small part of the fault, almost one third of the total fault plane. A non-intense directivity to the East is evident.

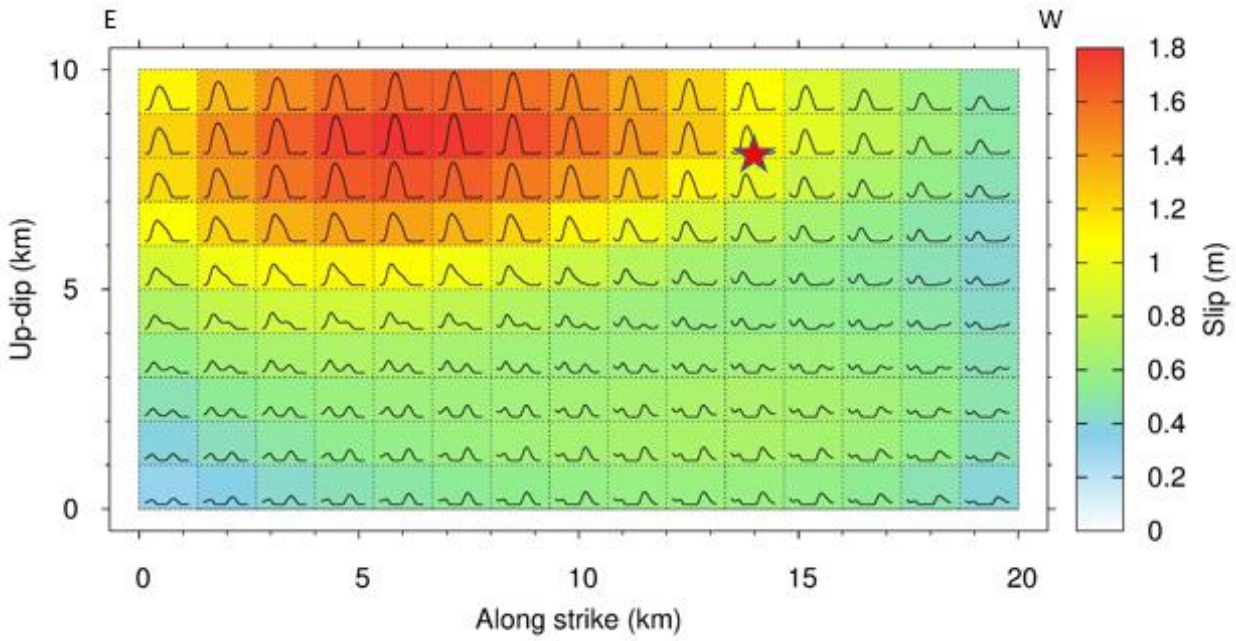

Figure 4.26. The total slip distribution on the fault. The maximum slip reaches 1.8 m. The along strike axis is oriented from the WNW (left) to SSE (right). In the vertical axis, the 0 km indicates the roof of the fault.

4.5.4. Ground Deformation Results

Concerning the ground deformation and specifically the horizontal component, an extension in an almost N-S direction can clearly be identified. Regarding the vertical component, the fault plane has a low dip angle (35°) and thus the projection of the fault to the surface is relatively far to the south, in respect to the actual area where slip occurred. The deformation is mainly located inside the Gökova gulf, with the subsidence reaching 30 cm. The area that subsided also reaches the eastern part of Kos and the Datça peninsula (Fig. 4.27). Regarding the Kos Island, horizontal ground movement is in a ENE direction. In addition, low vertical values have been identified, with the northern part of the island being subsided and the southern uplifted.

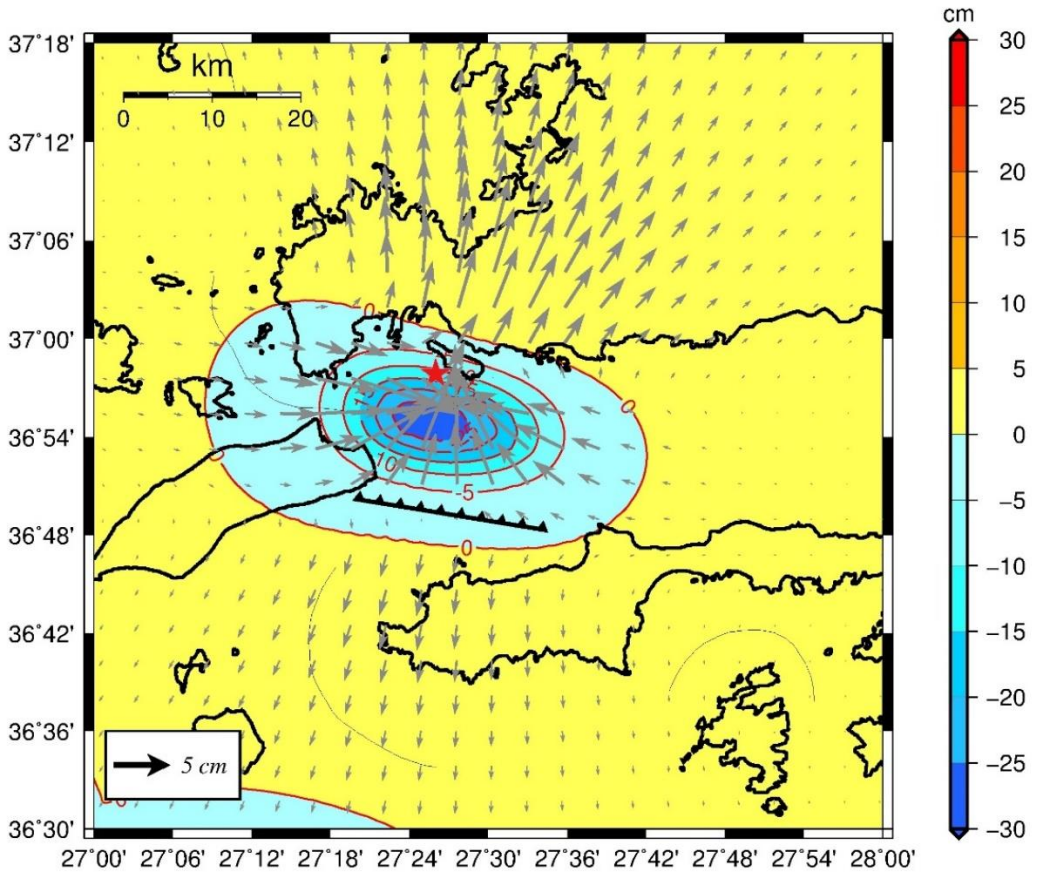

Figure 4.27. Ground deformation determined using the DIS3D software utilizing the determined slip distribution on the fault, as derived by the LisnSlipInv software (using local to near-regional data). The maximum subsidence is up to 30 cm. The vectors represent the horizontal movement.

5. Discussion

The obtained results of the slip distribution and of the ground deformation for the selected Greek earthquakes will be compared in this chapter, with already published work for each case study.

5.1.Cephalonia 2014 Earthquake

The slip distribution of the 26 January 2014 event, derived by the LinSlipInv software utilizing local and near-regional data, indicates a single rupture episode, with the maximum slip calculated at 40 cm. The shape and the maximum slip, suggested by the present Thesis, is in agreement with the results derived by Sokos et al. (2015), according to which the maximum slip was calculated 25 cm. The small maximum value could be due to the difference in the given dimensions of the fault plane, i.e. Sokos et al. (2015) suggest a 30 km x 30 km fault, in contrast to the 16 km x 10 km utilized by the present study. The maximum slip also agrees with Papadopoulos et al. (2014), who determined a maximum value of 60 cm. However, they suggest three distinct patches. Saltogianni et al. (2018) calculated a maximum slip of 1.2 m and two patches, utilizing GPS and InSAR data.

Concerning the ground deformation derived by the slip distribution of the 26 January 2014 Cephalonia earthquake, using the local to near-regional method, the values in the horizontal and vertical component are low, mainly due to the magnitude and the focal depth of the event. However, further investigation is necessary. The results revealed a maximum of 2 cm of horizontal displacement, to the east of the fault, on Cephalonia Island. On the other hand, Boncori et al. (2015) and Saltogianni et al. (2018) determined the ground deformation, utilizing InSAR and GPS data, respectively, suggesting a cumulative horizontal displacement up to 20 - 25 cm, taking into account both large events of 26 January and 3 February. Sakkas and Lagios (2015) derived a horizontal displacement up to 10 cm, in similar directions with the present study.

5.2.Lemnos 2014 Earthquake

Regarding the results obtained by the LinSlipInv software, the calculated slip revealed a complex source, comprised by three discrete patches. The slip snapshots revealed that the slip migrated updip, whereas the total maximum slip value reached 1.4 m. In addition, the slip velocity snapshots identified a bilateral rupture. More specifically, a initial westward rupture propagation was observed, followed by a major slip patch heading to the east, in agreement with Evangelidis et al. (2015). The slip distribution over time, determined by Saltogianni et al. (2015, 2016), presents a resemblance with the obtained slip derived using local to near-regional data, however the maximum slip area presented by the aforementioned study was probably an artifact, given that it did not appear in all solutions and the apparent peak slip corresponds to a relatively low rate of seismic moment release. Konca et al. (2018) suggest a maximum slip of

more than 2 m, using GPS and teleseismic data, whereas Saltogianni et al. (2015, 2016) equal to 2.6 m, yet the slip distribution pattern and the dimensions of the suggested fault of the two studies do not correlate. Kiratzi et al. (2016) proposed that the earthquake hosted two discrete patches, with the maximum slip being significantly smaller, equal to 0.7 m, in respect to all aforementioned studies, including the present one. A possible cause could be the significantly larger dimensions (65x35 km^2) of the utilized fault plane by Kiratzi et al. (2016), taking into account that the respective ones of the present Thesis are 40 x 15 km^2.

The obtained ground deformation results in Lemnos indicate a right lateral horizontal movement, in good agreement with Sboras et al. (2017). Regarding the Lemnos Island, the direction of horizontal displacement determined by the present study (2 cm towards the SW) is in agreement with the results of Ganas et al. (2014), Saltogianni et al. (2015, 2016) and Bitharis et al. (2016), who identified, using GPS data, co-seismic horizontal displacement of about 4-6 cm. Similar results are also obtained for the Samothrace Island. The findings of the present study, as well as the ones of Saltogianni et al. (2015, 2016) and Bitharis et al. (2016), indicate horizontal movement of about 5 cm. Regarding the vertical displacement, the results of the present study derived a maximum uplift of 3 cm and subsidence of 4 cm, in agreement with the 2 cm of uplift and subsidence, suggested in the same areas by Sboras et al. (2017).

5.3.Lefkada 2015 Earthquake

The local to near-regional slip inversion results revealed directivity towards the SSW, in full agreement with the ones obtained by all models applied by Sokos et al. (2016). In addition, three slip episodes can clearly be identified, supporting the conclusion of Sokos et al. (2016), according to which the rupture propagation was complex, consisting of two or three sub-episodes. The slip model of Bie et al. (2017), determined using INSAR observations, indicated that the main slip patches are confined to shallow depths (<10 km), in agreement with the present results, and that the segmentation occurred along strike. The maximum obtained slip value of this Thesis was 1.2 m, in agreement with the values of 1.4 m and 1.5 m, obtained by Sokos et al. (2016) and Bie et al. (2017), respectively. Chousianitis et al. (2016) determined the slip distribution utilizing teleseismic, strong motion and GPS data. The maximum slip was 2.5 m which is a rather high value, taking into account the fault dimensions and the earthquake magnitude. Nevertheless, the maximum value that they obtained using only teleseismic data was about 1.5 m, similar to the previously mentioned studies. In addition, Avallone et al. (2017), who used InSAR and GPS data, determined the maximum slip value equal to 2 m. Last, the results of Saltogianni et al. (2017) agree in terms of the maximum slip value (1.4 m) and directivity, with the ones of the present study, however, the shape of the slip distribution differs.

Regarding the ground deformation, the dextral movement of the fault was verified by the herein obtained results, using the DIS3D software. Small uplift values were obtained for the southern part of Lefkada (7 cm maximum uplift). The direction of horizontal deformation derived by the present study agrees with the results of Saltogianni et al. (2017). The values are

similar at the northern part of the Lefkada Island, whereas they differ at the southern part, with the horizontal vectors of the latter study presenting a dislocation of about 50 cm towards the SSE, in contradiction to the present thesis, in which the derived horizontal dislocation is about 8 cm.

5.4.Lesvos 2017 Earthquake

According to the LinSlipInv inversion results, the maximum slip was ~1.0 m, identical with the one obtained by Kiratzi (2018) and similar to the one (1.2 m) by Chousianitis and Konca (2018) and by Papadopoulos et al. (2017), who utilized teleseismic recordings. The space-time rupture evolution, presented by slip velocity snapshots per 1 s, indicated a unique slip patch and rupture directivity towards the NW, in agreement with the results of the spatiotemporal evolution of the sequence, according to Papadimitriou et al. (2018). Similar directivity effects were also observed by Chousianitis and Konca (2018) and by Kiratzi (2018). In addition, this directivity could partly explain the damage observed in Vrissa village (Mavroulis et al., 2018). However, extended destruction is also due to other factors, such as soil conditions and vulnerability of the buildings. The dimensions of the fault were determined 20 km long and 12 km wide, which coincide with the 20 km x 10 km along strike and dip fault plane derived by Kiratzi (2018) for the main slip patch, after considering dimensions of 50 km x 22 km. However, Papadopoulos et al. (2017) suggest a fault plane of 27 km x 17 km. The focal mechanism (input in the inversion) was 122°/40°/-83° (Papadimitriou et al., 2018), with the optimal solution obtained after a grid search at a focal depth at 11 km. Sokos and Zahradnik (2017) and Kiratzi (2018) suggest that the focal depth is around 7 to 9 km, whereas Papadimitriou et al. (2018) determined the focal depth at 13 km by applying moment tensor inversion.

The obtained low ground deformation values agree with the results of Ganas et al. (2018), according to which surface deformation is not visible with InSAR, but cm-size co-seismic horizontal offsets were recorded by continuous GPS stations in Lesvos. In addition, the NNE horizontal movement not exceeding 3 cm on Lesvos Island, according to the present study, is similar with the values provided by Chousianitis and Konca (2018).

5.5.Kos 2017 Earthquake

The slip distribution results derived by the LinSlipInv software are in agreement with the ones derived by Karasözen et al. (2018) regarding the unique patch of the slip distribution and the maximum slip value (slightly exceeding 1.6 m for Karasözen et al. and 1.8 m in the present study). Both studies consider as causative the fault dipping to the north. Saltogianni et al. (2017) and Kiratzi and Koskosidi (2018) suggest a south dipping fault plane and, thus, the results cannot be compared. The slip distribution assessment of Tiryakioğlu et al. (2017), obtained by GPS measurements, presents very small values (maximum slip of 0.25 m) which cannot be the case for an event with such a magnitude.

Regarding the ground deformation, Tiryakioğlu et al. (2017) derived horizontal displacement by utilizing GPS data. Their results agree with the present ground deformation

derived by DIS3D, providing extension in a N-S direction. Values of horizontal movements, of the order of 3 cm in Marmaris, are also in agreement. The results of the surficial deformation of the present study are also in accordance to the ones of Karasözen et al. (2018), determined via InSAR interferometry. Similar directions of horizontal dislocation have been obtained in Bodrum Peninsula, although the results of the present Thesis provide lower values, given that the ones by Karasözen et al. (2018) are of the order of 10 cm. Sboras et al. (2018) propose that the vertical displacement was spatially constrained and provided a region of about 30 cm of subsidence in the vicinity of the fault area, in full agreement with the results obtained by DIS3D. Horizontal displacement results are in a general agreement with the ones by Sboras et al. (2018). Last, Heidarzadeh et al. (2017) presented an approach of determining the seafloor deformation utilizing "tsunami waveforms" and a mean slip of 0.4 m. The results obtained by this method are similar to the ones from the present study, presenting an uplift (of insignificant values) to the western part of the Bodrum Peninsula and subsidence of 5 – 10 cm in the northeastern part of the Kos Island, in agreement with the present results.

6. Conclusions

In the present Master Thesis, the temporal and spatial slip distribution of major earthquakes that occurred in the Hellenic region during the last five years was examined. The selected events were characterized either by strike-slip or by normal faulting. The investigation of the case studies was not in the framework of a Seismotectonic study and only the derived slip on fault, along with the resulting ground deformation, were examined by this procedure. The slip distribution determination was carried out by using local to near-regional data. The selection of the LinSlipInv software (Gallovic and Zahradnik, 2011; Gallovic et al., 2014) was considered the optimum, considering that there was a number of published studies with satisfactory results, using this program. The procedure for all the case studies was straight forward, considering as fixed variables the results obtained by already published Seismotectonic studies (that is the focal mechanism, the epicenter, the focal depth and the fault dimensions) for each case study. In other words, the evaluation of the slip distribution results was based on the best fit and Variance Reduction of each run, in respect to the other pre-existing solutions. Then, the derived slip was inserted as input to extrapolate slip distribution along a fault to ground/surface deformation using the DIS3D software (Erickson, 1986).

The results obtained using the LinSlipInv and the DIS3D software were quite promising. The Cephalonia, Lesvos and Kos earthquakes presented unilateral rupture, whereas the Lefkada and Lemnos events provided a more complex rupture process. In more detail, for the Cephalonia earthquake, the analysis indicated a single rupture episode, with the maximum slip calculated at 40 cm. The Lemnos earthquake revealed three discrete patches, with the total maximum slip value reaching 1.4 m, whereas the Lefkada event revealed two slip episodes with an evident directivity towards the SSW. For the Lesvos earthquake, a unique slip patch was

derived with rupture directivity towards the NW and a maximum slip of ~1.0 m. Lastly, the slip distribution for the Kos earthquake presented a unique patch of slip distribution and the maximum slip value of 1.8 m.

In the present chapter, the advantages and limitations of the applied approach, regarding slip determination, will be discussed. The conclusions regarding this endeavor were quite encouraging. The approach using local to near-regional data does not require a priori constrains over the source time function (the boxcar geometry) and thus it can identify complex rupture patterns. The LinSlipInv software can also provide satisfactory discretization along the fault (as long as the hardware of the working station is powerful enough) and keeping in mind that the data used in the inversion is the whole waveform and not a specific phase (e.g. P or S), the results provide details regarding the rupture process and the derived value of slip is more secure. The limitations of the LinSlipInv software are strictly dependent on the (mainly accelerometric) networks density, meaning that, in most if not all cases, no satisfactory azimuthal coverage could be established and additionally, in some cases the number of satisfactory recordings was limited.

The future goals, emanated by this endeavor, are the examination of the properties and determination of the source time function as well as the computation of shakemaps utilizing the results from LinSlipInv (slip distribution).

7. Bibliography

Aki, K., Richards, P. G., 2002. Quantitative seismology. Sausalito, Calif: University Science Books.

Aktug, B., Nocquet, J.M., Cingöz, A., Parsons, B., Erkan, Y., England, P., Lenk, O., Gürdal, M.A., Kilicoglu, A., Akdeniz, H., Tekgül, A., 2009. Deformation of western Turkey from a combination of permanent and campaign GPS data: Limits to block-like behavior. J. Geophys. Res. Solid Earth 114, 1–22. https://doi.org/10.1029/2008JB006000

Altinok, Y., Alpar, B., Yaltirak, C., Pinar, A., Ozer, N., 2012. The earthquakes and related tsunamis of October 6, 1944 and March 7, 1867; NE Aegean Sea. Nat. Hazards 60, 3–25.

Ambraseys, N.N., Finkel C.F., 1995: The seismicity of Turkey and adjacent areas. A historical review, 1500-1800, EREN, 34-95-Y-70-061, pp. 240.

Armijo, R., Meyer, B., Hubert, A., Barka, A.A., 1999. Westward propagation of the North Anatolian fault into the northern Aegean: Timing and kinematics. Geology 27, 267–270.

Armijo, R., Flerit, F., King, G., Meyer, B., 2003. Linear elastic fracture mechanics explains the past and present evolution of the Aegean. Earth Planet. Sci. Lett. 217, 85–95. https://doi.org/10.1016/S0012-821X(03)00590-9

Andrews, D. J., 1980. A stochastic fault model. (I) Static case. J. Geophys. Res. 85, 3867-3877.

Aster, R., Borchers, B., Thurber, C., 2012. Parameter Estimation and Inverse Problems, Second Edition, Elsevier. ISBN 0123850487.

Avallone, A., Cirella, A., Cheloni, D., Tolomei, C., Theodoulidis, N., Piatanesi, A., Briole, P., Ganas, A., 2017. Near-source high-rate GPS, strong motion and InSAR observations to image the 2015 Lefkada (Greece) Earthquake rupture history. Scientific Reports, 7, 1, 10358. https://doi.org/10.1038/s41598-017-10431-w.

Bardintzeff, J.M., Dalabakis, P., Traineau, H., Brousse, R., 1989. Recent explosive volcanic episodes on the island of Kos (Greece): associated hydrothermal parageneses and geothermal area of Volcania. Terra Nova 1(1):75–78. https://doi.org/10.1111/j.1365-3121.1989.tb00329.x

Bernard, P., Briole, P., Meyer, B., Lyon-Caen, H., Gomez, J.-M., Tiberi, C., Berge, C., Cattin, R., Hatzfeld, D., Lachet, C., Lebrun, B., Deschamps, A., Courboulex, F., Larroque, C., Rigo, A., Massonet, D., Papadimitriou, P., Kassaras, J., Diagourtas, D., Makropoulos, K., Veis, G., Karakostas V., Papadimitriou, E., Papanastassiou, D., Chouliaras, G., Stavrakakis, G., 1997. The Ms= 6.2, June 15, 1995 Aigion earthquake (Greece: evidence for low angle normal faulting in the Corinth rift). J. Seismol. 1, 131-150.

Bie, L., González, P.J., Rietbrock; A., 2017. Slip distribution of the 2015 Lefkada earthquake and its implications for fault segmentation. Geophys. J. Int., 210, 1, 420–427. https://doi.org/10.1093/gji/ggx171

Bitharis, S., Fotiou, A., Pikridas, C., Rossikopoulos, D., Pavlides, S., Chatzipetros, A., 2016. The Samothrace Earthquake of May 2014 and the displacements estimations using permanent GPS stations data. Bull. Geol. Soc. Greece, 50(3), 1545-1552.

doi:http://dx.doi.org/10.12681/bgsg.11867

Böger H., 1978. Sedimentary history and tectonic movements during the late Neogene. In: Closs H, Roeder D, Schmidt K (eds) Alps, Appenines, Hellenides. Schweizerbart, Stuttgart, pp 510–512.

Böger, H., Gersonde, R., Willmann, R., 1974. Das Neogen im Osten der Insel Kos (Ägäis, Dodekanes) — Stratigraphie und Tektonik. N. Jb. Geol. Paläont. Abh. 145, 129–152.

Boncori, J.P.M., Papoutsis, I., Pezzo, G., Tolomei, C., Atzori, S., Ganas, A., Karastathis, V., Salvi, S., Kontoes, Ch, Antonioli, A., 2016. The February 2014 Cephalonia Earthquake (Greece): 3D Deformation Field and SourceModeling from Multiple SAR Techniques. Seismological Res. Lett., 86, 1. doi: 10.1785/0220140126

Bornovas, J., 1964. Géologie de l'île de Lefkade. Geol. Geophys. Res. (Spec. Publ. Greek Geol. Surv.) 10 (1) (Athens).

Bouchon, M., 1981. A simple method to calculate Green's functions for elastic layered media. Bull. Seismol. Soc. Am. 71, 959–971.

Brun, J.-P., Sokoutis, D., 2010. 45 m.y. of Aegean crust and mantle flow driven by trench retreat. Geology 38, 815–818. https://doi.org/10.1130/G30950.1

Caputo, R., Chatzipetros, A., Pavlides, S., Sboras, S., 2012. The Greek database of seismogenic sources (GreDaSS): state-of-the-art for northern Greece. Ann. Geophys.-Italy 55-5, 859–894. http://dx.doi.org/10.4401/ag-5168.

Chadan, K., Sabatier, P. C., 1977. Inverse Problems in Quantum Scattering Theory. Springer-Verlag. ISBN 0-387-08092-9

Chatzipetros, A., Kiratzi, A., Sboras, S., Pavlides, S., 2013. Active faulting in the Northeastern Aegean Sea Islands. Tectonophysics 597 (SI), 106e122. http://dx.doi.org/ 10.1016/j.tecto.2012.11.026.

Chouliaras, G., Kassaras, I., Kapetanidis, V., Petrou, P., Drakatos, G., 2015. Seismotectonic analysis of the 2013 seismic sequence at the western Corinth Rift. J. Geodyn. 90, 42–57. http://dx.doi.org/10.1016/j.jog.2015.07.001.

Chousianitis, K., Konca, A.O., 2018. Coseismic slip distribution of the 12 June 2017 Mw= 6.3 Lesvos earthquake and imparted static stress changes to the neighboring crust. J. Geophys. Res.: Solid Earth, 123. https://doi.org/10.1029/2018JB015950

Chousianitis, K., Konca, A. O., Tselentis, G.-A., Papadopoulos, G. A., Gianniou, M., 2016. Slip model of the 17 November 2015 Mw = 6.5 Lefkada earthquake from the joint inversion of geodetic and seismic data. Geophysical Research Letters, 43, 7973-7981.

Cirella, A., A. Piatanesi, E. Tinti, M. Chini, and M. Cocco. 2012. Complexity of the rupture process during the 2009 L'Aquila, Italy, earthquake: Geophys. J. Int., 190, 607–621.

Converse, G., 1973. Equations for the displacements and displacement derivatives due to a rectangular dislocation in a three-dimensional elastic half-space, unpublished, U.S. Geological Survey, Menlo Park.

Coutant, O.,1989. Numerical study of the diffraction of elastic waves by fluid-filled cracks. J. Geophys. Res., 94(B12), 17805–17818, doi: 10.1029/JB094iB12p17805.

Dalabakis P., 1987. Une des plus puissante éruptions phréatomagmatiques dans la Méditerranée orientale: l'ignimbrite de Kos (Grèce). C R Acad Sci Paris 303(Série II):505–508

Davis, E., Gartzos, E., Pavlopoulos, A., Tsagalidis, A., 1993. Petrological and geochemical research of perlites and rhyolites from Kefalos peninsula (island of Kos) and their quantitative evaluation (in Greek). In: Special volume in honour of prof. A.G. Panagos, Athens A, pp 284–303

Delibasis, N.D., Voulgaris, N.S., 1989. Microseismic and seismotectonic study of the island of Lesbos. In: Proc. 4th Inter. Semin. Results EC Geothermal Energy Res. And Demon. Florence, 27–30 April 1989. pp. 474–481.

Delouis, B., Giardini D., Lundgren P., Salichon J., 2002. Joint inversion of InSAR, GPS, teleseismic, and strong-motion data for the spatial and temporal distribution of earthquake slip: Application to the 1999 Izmit mainshock. Bull. Seis. Soc. Am 92 (1):278-299.

Dewey, J. F., and Sengor A. M. C., 1979. Aegean and surrounding regions: complex multiplate and continuum tectonics in a convergent zone. Geol. Soc. Am. Bull., 90, 84 – 92, doi:10.1130/0016-7606(1979)90<84: AASRCM>2.0.CO;2.

Drakatos, G., Drakopoulos, J., 1991. 3-D velocity structure beneath the crust and upper mantle of Aegean Sea region. Pageoph, 135:3.

Dreger, D., Kaverina, A., 2000. Seismic remote sensing for the earthquake source process and near-source strong shaking: A case study of the October 16, 1999 hector mine earthquake. Geophys. Res. Lett., 27(13), pp. 1941-1944.

Erickson, 1987. User's manual for DIS3D: A three dimensional dislocation program with applications to faulting in the earth.

Eringen, A. C., Suhubi, E. S., 1975. Chap. 7 of Elastodynamics, Vol. II, Linear Theory, New York: Academic Press.

Ersoy, E. Y., İ. Çemen, C. Helvaci, Billor Z., 2014. Tectonostratigraphy of the Neogene basins in Western Turkey: Implications for tectonic evolution of the Aegean extended region, Tectonophysics, 635, 33–58.

Evangelidis, C.P., 2015. Imaging supershear rupture for the 2014 Mw 6.9 Northern Aegean earthquake by backprojection of strong motion waveforms. Geophys. Res. Lett., 42, 307–315, doi:10.1002/2014GL062513.

Fossen, H., 2010. Structural geology. Cambridge: Cambridge University Press.

Galanopoulos, A. G.: A catalogue of shocks with $I_0 \geq$ VI or M ≥ 5 for the years 1801–1958, 1960.

Gallovič, F., Brokešová, J., 2004. On strong ground motion synthesis with k-2 slip distributions. J. Seismol., 8, 211–224.

Gallovič, F., Zahradník, J., 2011. Toward understanding slip inversion uncertainty and artifacts:

2. Singular value analysis. J. Geophys. Res. Solid Earth 116, 1–16. https://doi.org/10.1029/2010JB007814.

Gallovič, F., Zahradník, J., 2012. Complexity of the M 6.3 2009 L'Aquila (central Italy) earthquake: 1. Multiple finite-extent source inversion, J. Geophys. Res. 117, no. B04307, doi: 10.1029/2011JB008709.

Gallovič, F., Imperatori, W., Mai, P. M., 2014. Effect of three-dimensional velocity heterogeneities and topography on slip inversions: case study of the Mw6.3 2009 L'Aquila earthquake, J. Geophys. Res. 120, 428-449.

Gallovič, F., Imperatori,W., Mai, P.M., 2015. Effects of three-dimensional crustal structure and smoothing constraint on earthquake slip inversions: case study of the Mw6.3 2009 L'Aquila earthquake. J. Geophys. Res. Solid Earth 120 (1), 2169–9356. http://dx.doi.org/10.1002/2014JB011650.

Ganas, A., Roumelioti, Z., Karastathis, V., Chousianitis, K., Moshou, A., & Mouzakiotis, E., 2014. The lemnos 8 january 2013 (Mw = 5.7) earthquake: Fault slip, aftershock properties and static stress transfer modeling in the north aegean sea. J. Seismology, 18(3), 433-455. doi:10.1007/s10950-014-9418-3.

Ganas, A., Elias, P., Bozionelos, G., Papathanassiou, G., Avallone, A., Papastergios, A., Valkaniotis, S., Parcharidis, I., Briole, P., 2016. Coseismic deformation, field observations and seismic fault of the 17 November 2015 M = 6.5, Lefkada Island, Greece earthquake. Tectonophysics, 687, 210–222. https://doi.org/10.1016/j.tecto.2016.08.012

Ganas, A., Elias, P., Valkaniotis, S., Briole, P., Kapetanidis, V., Kassaras, I., Barberopoulou, A., Argyrakis, P., Chouliaras, G., Moshou, A., 2017. Co-seismic deformation and preliminary fault model of the July 20, 2017 M6.6 Kos earthquake, Aegean Sea. Report submitted to EMSC on 30 July 2017, 20 pages. https://www.emsc-csem.org/Files/event/606346/Kos_report_30-7-2017.pdf.

Ganas, G., Elias, P., Kapetanidis, V., Valkaniotis, S., Briole, P., Kassaras, I., Argyrakis, P., Barberopoulou, A. & Moshou, A., 2019. The July 20, 2017 M6.6 Kos earthquake: seismic and geodetic evidence for a north-dipping, low-angle normal fault at the western end of the Gulf of Gökova, SE Aegean Sea. (Submitted to Pure and Applied Geophysics).

Görür, N., Şengör, A.M.C., Sakınç, M., Tüysüz, O., Akkök, R., Yiğitbaş, E., Oktay, F.Y., Barka, A., Sarıca, N., Ecevitoğlu, B., Demirbağ, E., Ersoy, Ş., Algan, O., Güneysu, C., Akyol, A., 1995a. Rift formation in the Gökova region, southwest Anatolia: implications for the opening of the Aegean Sea. Geological Magazine, 132(06): 637–650. https://doi.org/10.1017/S0016756800018884

Görür, N., Şengör, A.M.C., Sakınç, M., Tüysüz, O., Yiğitbaş, E., Oktay, F.Y., Barka, A., Sarıca, N., Ecevitoğlu, B., Demirbağ, E., Aykol, A., Algan, O., Güneysu, C., Ersoy, Ş., 1995b. Cross-cutting rift systems of the Gökova region, SWAnatolia: implications for the formation of the Aegean Sea. Bull Tech Univ Istanbul 47(4):275–292.

Haslinger, F., Kissling, E., Ansorge, J., Hatzfeld, D., Papadimitriou, E., Karakostas, V., Makropoulos, K., Kahle H.G., Peter, Y., 1999. 3D crustal structure from local earthquake

tomography around the gulf of arta (Ionian region, NW greece). Tectonophysics, 304(3), 201-218. doi:10.1016/S0040-1951(98)00298-4

Hartzell, S. H., Heaton T. H., 1983. Inversion of strong ground motion and teleseismic waveform data for the fault rupture history of the 1979 Imperial Valley, California, earthquake, Bull. Seism. Soc. Am. 73, 1553-1583.

Hartzell, S., Langer C., 1993. Importance of model parameterization in finite fault inversions; application to the 1974 Mw 8.0 Peru earthquake. J. Geophys. Res. 98 (12):22,123-22,134.

Hartzell, S., Liu P. C., Mendoza C., 1996. The 1994 Northridge, California, earthquake; investigation of rupture velocity, risetime, and high-frequency radiation. J. Geophys. Res. 101 (9): 20091-20108.

Hartzell, S., Harmsen, S., Frankel, A., Larsen, S., 1999. Calculation of Broadband Time Histories of Ground Motion: Comparison of Methods and Validation using Strong-Ground Motion from the 1994 Northridge Earthquake. Bull. Seism. Soc. Am., 89 (6): 1484-1504.

Hartzell, S., Liu P., Mendoza C., Ji C., Larson K. M., 2007. Stability and Uncertainty of Finite-Fault Slip Inversions: Application to the 2004 Parkfield, California, Earthquake. Bulletin of the Seismological Society of America, 97 (6): 1911-1934. doi:10.1785/0120070080.

Hatzfeld, D., 1999. The present-day tectonics of the aegean as deduced from seismicity doi:10.1144/GSL.SP.1999.156.01.19.

Hecht, J., 1974a. Geological Map of Greece, Eressos Sheet. I.G.M.E., Greece scale 1:50.000.

Hecht, J., 1974b. Geological Map of Greece, Polychnitos Sheet. I.G.M.E., Greece scale 1:50.000.

Heidarzadeh, M., Necmioglu, O., Ishibe, T., Yalciner, A.C., 2017. Bodrum–Kos (Turkey–Greece) Mw 6.6 earthquake and tsunami of 20 July 2017: a test for the Mediterranean tsunami warning system. Geosci. Lett. 4, 1–11. https://doi.org/10.1186/s40562-017-0097-0

Hubert-Ferrari, A., King, G., Manighetti, I., Armijo, R., Meyer, B., Tapponnier, P., 2003. Long-term elasticity in the continental lithosphere; modelling the Aden Ridge propagation and the Anatolian extrusion process. Geophys. J. Int. 153, 111–132. https://doi.org/10.1046/j.1365-246X.2003.01872.x

Jacobshagen, V., 1979. Structure and geotectonic evolution of the Hellenides. Proc. VI Colloq Aegean Region Athens 1977. IGMR, Athens, pp. 1355–1367.

Ji, C., Wald, D.J., Helmberger, D.V., 2002. Source description of the 1999 Hector Mine, California, earthquake, part II: Complexity of slip history. Bull. Seism. Soc. Am., 92(4), pp. 1208-1226.

Kapetanidis, V., Deschamps, A., Papadimitriou, P., Matrullo, E., Karakonstantis, A., Bozionelos, G., Kaviris, G., Serpetsidaki, A., Lyon-Caen, H., Voulgaris, N., Bernard, P., Sokos E., Makropoulos, K., 2015. The 2013 earthquake swarm in Helike, Greece: Seismic activity at the root of old normal faults. Geophys. Journ. Int., 202, 2044–2073.

Karabulut, H., Roumelioti, Z., Benetatos, C., Mutlu, A. K., Özalaybey, S., Aktar, M., Kiratzi, A., 2006. A source study of the 6 July 2003 (Mw 5.7) earthquake sequence in the gulf of Saros

(Northern Aegean Sea): Seismological evidence for the western continuation of the ganos fault. Tectonophysics, 412(3-4), 195-216. doi:10.1016/j.tecto.2005.09.009.

Karakostas, V.G. and Papadimitriou, E.E., 2010. Fault complexity associated with the 14 August 2003 Mw6.2 Lefkada, Greece, aftershock sequence. Acta Geophys. 58: 838. https://doi.org/10.2478/s11600-010-0009-6.

Karakostas, V., Papadimitriou, E., Papazachos, C., 2004. Properties of the 2003 Lefkada, Ionian islands, Greece, Earthquake seismic sequence and seismicity triggering. BSSA 94 (5), 1976–1981.

Karakostas V., Papadimitriou E., Gospodinov D., 2014. Modelling the 2013 North Aegean (Greece) seismic sequence: geometrical and frictional constraints, and aftershock probabilities. Geophys. J. Int., 197 (1), 525–541. https://doi.org/10.1093/gji/ggt523

Karakostas, V., Papadimitriou, E., Mesimeri, M., Gkarlaouni, C., Paradisopoulou, P., 2015. The 2014 Kefalonia Doublet (Mw>6.1 and Mw>6.0), central Ionian Islands, Greece: Seismotectonic implications along the Kefalonia transform fault zone. Acta Geophys. 63, 1–16. https://doi.org/10.2478/s11600-014-0227-4

Karakostas, V., Papadimitriou, E., Mesimeri, M., Begum, C., 2018. The 2017 Kos sequence: Aftershocks relocation and implications for activated fault segments. Abstract, 36th ESC General Assembly, Valetta, Malta, ESC2018-S6-645.

Karasözen, E., Nissen, E., Büyükakpinar, P., Cambaz, M. D., Kahraman, M., Ertan, E. K., Abgarmi , B., Bergman, E., Ghods, A., Özacar, A. A., 2018. The 2017 July 20 Mw 6.6 Bodrum-Kos earthquake illuminates active faulting in the Gulf of Gökova, SW Turkey. Geophys. J. Int., 214(1), 185-199. doi:10.1093/gji/ggy114

Kassaras, I., Kalantoni, D., Benetatos, Ch., Kaviris, G., Michalaki, K., Sakellariou N., Makropoulos, K., 2015. Seismic damage scenarios in Lefkas old town (W. Greece). Bull. Earth. Engin., Vol. 13, Iss. 12, 3669-3711.

Kassaras, I., Kazantzidou-Firtinidou, D., Ganas, A., Tonna, S., Pomonis, A., Karakostas, C., Papadatou-Giannopoulou, C., Psarris, D., Lekkas E., Makropoulos, K., 2018. On the Lefkas (Ionian Sea) November 17, 2015 Mw=6.5 Earthquake Macroseismic Effects. J. Earth. Engin., doi: 10.1080/13632469.2018.1488776.

Katsikatsos, G., Mataragas, D., Migiros, G., Triandafillou, E., 1982. Geological Study of Lesbos Island. Special Report. I.G.M.E., Greece.

Kaviris, G., Spingos, I., Kapetanidis, V., Papadimitriou, P., Voulgaris N., Makropoulos, K., 2017. Upper crust seismic anisotropy study and temporal variations of shear-wave splitting parameters in the Western Gulf of Corinth (Greece) during 2013. Physics of the Earth and Planetary Interiors, 269, 148-164, https://doi.org/10.1016/j.pepi.2017.06.006.

Kaviris, G., Millas, C., Spingos, I., Kapetanidis, V., Fountoulakis, I., Papadimitriou, P., Voulgaris N., Makropoulos, K., 2018. Observations of shear-wave splitting parameters in the Western Gulf of Corinth focusing on the 2014 Mw=5.0 earthquake. Physics of the Earth and Planetary Interiors, 282, 60-76. https://doi.org/10.1016/j.pepi.2018.07.005

Keller, 1982. Mediterranean island arc. In: Thorpe RS (ed) Andesites. Wiley, New York, pp 307–325

Kennett, B., Kerry, N.J., 1979. Seismic waves in a stratified half space. Geophys. J. R. Astron. Soc. 57, 557–583. https://doi.org/10.1111/j.1365-246X.1979.tb06779.x

Kiratzi, A., 2014. Mechanisms of Earthquakes in Aegean, encyclopedia of Earthquake engineering. Article ID: 382074, Chapter ID: 29.9. In: Beer, M., Kougioumtzoglou, I., Patelli, E., Ivan Siu-Kui, Au (Eds.), Encyclopedia of Earthquake Engineering. ISBN: 978-3-642-36197-5.

Kiratzi, A., 2018. The 12 June 2017 Mw 6.3 Lesvos Island (Aegean Sea) earthquake: Slip model and directivity estimated with finite-fault inversion. Tectonophysics 724–725, 1–10. https://doi.org/10.1016/j.tecto.2018.01.003.

Kiratzi, A., Louvari E., 2003. Focal mechanisms of shallow earthquakes in the Aegean Sea and the surrounding lands determined by waveform modeling: a new database, Journal of Geodynamics, 36, 251 - 274.

Kiratzi, A., Svigkas, N., 2013. A study of the 8 January 2013 Mw5.8 earthquake sequence (Lemnos Island, East Aegean Sea). Tectonophysics 608, 452e460. http://dx.doi.org/10.1016/j.tecto.2013.09.002.

Kiratzi, A., Koskosidi A., 2018. Constraints on the near-source motions of the Kos-Bodrum 20 July 2017 Mw6.6 earthquake. Proceeding of the 16th European Conference on Earthquake Engineering, 18-21 June 2018, Thessaloniki, pp.13.

Kiratzi, A., Wagner, G., Langston, C., 1991. Source parameters of some large earthquakes in Northern Aegean determined by body waveform inversion. Pure and Applied Geophysics, 135, 515- 527.

Kiratzi, A., Benetatos, C., Roumelioti Z., 2007. Distributed earthquake focal mechanisms in the Aegean Sea. Bull. Geol. Soc. Greece, Vol. XXXX, 1125-1137.

Kiratzi, A., Tsakiroudi, E., Benetatos, C., Karakaisis, G., 2016. The 24 May 2014 (Mw6.8) earthquake (North Aegean Trough): Spatiotemporal evolution, source and slip model from teleseismic data. Phys. Chem. Earth 95, 85–100. https://doi.org/10.1016/j.pce.2016.08.003

Kissel, C., Laj C., 1988. The tertiary geodynamical evolution of the Aegean arc; a paleomagnetic reconstruction, Tectonophysics, 146, 183–201.

KOERI, 2001. International Federation of Digital Seismograph Networks. Other/Seismic Network. 10.7914/SN/KO. Bogazici University Kandilli Observatory And Earthquake Research Institute.

Kokkalas, S., Xypolias, P., Koukouvelas, I., Doutsos, T., 2006. Postcollisional contractional and extensional deformation in the aegean region. https://doi.org/10.1130/2006.2409(06).

Kokinou, E., Papadimitriou E., Karakostas V., Kamberis E., Vallianatos F., 2006, The Kefalonia Transform Zone (offshore Western Greece) with special emphasis to its prolongation towards the Ionian Abyssal Plain. Mar. Geophys. Res., 27, 4, 241-252,

https://doi.org/10.1007/s11001-006-9005-2

Konca, A.O., Cetin, S., Karabulut, H., Reilinger, R., Dogan, U., Ergintav, S., Cakir, Z., Tari, E., 2018. The 2014,MW6.9 North Aegean earthquake: Seismic and geodetic evidence for coseismic slip on persistent asperities. Geophys. J. Int. 213, 1113–1120. https://doi.org/10.1093/gji/ggy049

Koukouvelas, I.K., Aydin, A., 2002. Fault structure and related basins of the North Aegean Sea and its surroundings. Tectonics, 21, 10-1-10–17. https://doi.org/10.1029/2001TC901037.

Kouskouna, V., Sakkas, G., 2013. The University of Athens Hellenic Macroseismic Database (HMDB.UoA): historical earthquakes. J. Seismol., 17 (4), 1253–1280.

Kouskouna, V., Makropoulos, K.C., Tsiknakis, K., 1993. Contribution of historical information to a realistic seismicity and hazard assessment of an area. The Ionian Islands earthquakes of 1767 and 1769: historical investigation. In: Stucchi, M. (Ed.), "Historical Investigation of European earthquakes," Materials of the CEC project "Review of Historical Seismicity in Europe", vol. 1, pp. 195–206.

Kurt, H., Demirbağ, E., Kuşçu, I., 1999. Investigation of the submarine active tectonism in the Gökova gulf, southwest Anatolia–southeast Aegean Sea, by multi-channel seismic reflection data. Tectonophysics 305(4):477–496. https://doi.org/10.1016/S0040-1951(99)00037-2.

Kurt, H., Demirbag, E., Kuşçu, I., 2000. Active submarine tectonism and formation of the Gulf of Saros, Northeast Aegean Sea, inferred from multi-channel seismic reflection data. Marine Geology 165, 13-26.

Lawson, C. L., Hanson, R. L., 1974. Solving Least Squares Problems, pp. 158-173. Prentice-Hall, Englewood Cliffs, NJ.

Lekkas E., Danamos G., Mavrikas G., 2001. Geological structure and evolution of Cefallonia and Ithaki Islands. Bull. Geol. Soc. Greece, XXXIV, 1:11–17

Le Pichon, X., Angelier, J., 1981. The Aegean Sea. Philos. Trans. R. Soc. Lond. A 300, 357–372.

Le Pichon, X., Kreemer, C., 2010. The Miocene-to-Present Kinematic Evolution of the Eastern Mediterranean and Middle East and Its Implications for Dynamics. Annu. Rev. Earth Planet. Sci. 38, 323–351. https://doi.org/10.1146/annurev-earth-040809-152419.

Lekkas E., Danamos G., Lozios S., 2001. Neotectonic structure and evolution of Lefkas Island. Bull. Geol. Soc. Greece, 34(1):157–163

Lekkas, E., Mavroulis, S., Carydis, P., Alexoudi, V., 2018. The 17 November 2015 Mw 6.4 Lefkas (Ionian Sea, Western Greece) Earthquake: Impact on Environment and Buildings, Geotechnical and Geological Engineering. Springer International Publishing. https://doi.org/10.1007/s10706-018-0452-8

Leptokaropoulos, K. M., Papadimitriou, E. E., Orlecka-Sikora, B. and Karakostas, V. G., 2012. Seismicity rate changes in association with the evolution of the stress field in northern Aegean Sea, Greece. Geophys. J. Int., 188: 1322-1338. doi:10.1111/j.1365-

246X.2011.05337.x.

Leptokaropoulos, K. M., Karakostas, V. G., Papadimitriou, E. E., Adamaki, A. K., Tan, O., Inan S., 2013. A homogeneous earthquake catalog for western turkey and magnitude of completeness determination. Bulletin of the Seismological Society of America 103, no. 5: 2739-2751

Louvari, E., Kiratzi A., Papazachos B.C., 1999. The Cephalonia Transform Fault and its extension to western Lefkada Island (Greece). Tectonophysics 308, 1-2, 223-236. https://doi.org/10.1016/S0040-1951(99)00078-5

Lyberis, N., 1984. Tectonic evolution of the North Aegean Trough, in: The Geological Evolution of the Eastern Mediterranean. Geological Society Special Publications, pp. 709–725.

Makropoulos, K., Kaviris, G. and Kouskouna, V., 2012. An updated and extended earthquake catalogue for Greece and adjacent areas since 1900. Nat. Hazards Earth Syst. Sci., 12, 1425-1430.

Mascle, J., Martin, L., 1990. Shallow structure and recent evolution of the Aegean Sea: A synthesis based on continuous reflection profiles. Mar. Geol. 94, 271–299. https://doi.org/10.1016/0025-3227(90)90060-W.

Mavroulis, S., Andreadakis, E., Antoniou, V., Skourtsos, E., Lekkas, E. (2018). Geodynamic phenomena and ESI 2007 intensities of the 2017 June 12, Mw 6.3 Lesvos (North Aegean Sea, Greece) earthquake. Geophys. Res. Abstr., Vol. 20, EGU2018-9254.

McKenzie, D., 1970. Plate tectonics of the Mediterranean region, Nature, 226, 239–243.

McKenzie, D., 1972. Active tectonics of the Mediterranean region, Geophys. J. R. Astron. Soc., 30, 109 – 185.

McNeill, L. C., Mille, A., Minshull, T. A., Bull, J. M., Kenyon, N. H., & Ivanov, M. (2004). Extension of the north anatolian fault into the north aegean trough: Evidence for transtension, strain partitioning, and analogues for sea of marmara basin models. Tectonics, 23(2), TC2016 1-12. doi:10.1029/2002TC001490

Mendoza, C., Hartzell, S., 1999. Fault-slip distribution of the 1995 Colima-Jalisco, Mexico, earthquake. Bull. Seismol. Soc. Am. 89, 1338–1344

Mesimeri, M., Karakostas, V., 2018a. Repeating earthquakes in western Corinth Gulf (Greece): Implications for aseismic slip near locked faults. Geophysical Journal International, 215 (1), pp. 659-676.

Mesimeri, M., Karakostas, V., Papadimitriou, E., Tsaklidis, G., Jacobs, K., 2018b. Relocation of recent seismicity and seismotectonic properties in the Gulf of Corinth (Greece). Geophysical Journal International, 212 (2), pp. 1123-1142.

Mesimeri, M., Kourouklas, C., Papadimitriou, E., Karakostas, V. and Kementzetzidou , D., 2018c. Acta Geophys., 66: 479. https://doi.org/10.1007/s11600-018-0157-7

Michas, G., Vallianatos, F., 2018. Modelling earthquake diffusion as a continuous-time random walk with fractional kinetics: The case of the 2001 Agios Ioannis earthquake swarm

(Corinth Rift). Geophys. J. Int., 215 (1), pp. 333-345.

Mitsakaki, C., Sakellariou, M. G., Tsinas, D., 2013. A study of the crust stress field for the Aegean region (Greece). Tectonophysics, 597-598, 50-72. doi:10.1016/j.tecto.2012.10.003.

Monelli, D., Mai, M. P., Jónsson, S., Giardini, D., 2009. Bayesian imaging of the 2000 Western Tottori (Japan) earthquake through fitting of strong motion and GPS data. Geophys. J. Int., 176, 135–150.

Mountrakis, D., 2006. Tertiary and Quaternary tectonics of Greece, in Dilek, Y., Pavlides, S., eds. Postcollisional tectonics and magmatism in the Mediterranean region and Asia. Geological Society of America, Special Paper, v. 409, p. 125-136. https://doi.org/10.1130/2006.2409(07).

Müller, M.D., Geiger, A., Kahle, H.G., Veis, G., Billiris, H., Paradissis, D., Felekis, S., 2013. Velocity and deformation fields in the North Aegean domain, Greece, and implications for fault kinematics, derived from GPS data 1993-2009. Tectonophysics 597–598, 34–49. https://doi.org/10.1016/j.tecto.2012.08.003

Nocquet, J. M., 2012. Present-day kinematics of the Mediterranean: A comprehensive overview of GPS results, Tectonophysics, 579, 220–242.

Nomikou, P., Papanikolaou, D., 2010. A comparative morphological study of the Kos-Nisyros-Tilos volcano sedimentary basins. Bull. Geol. Soc. Greece, 43:464–474

Ocakoğlu, N., Nomikou, P., İşcan, Y., Loreto, M.F., Lampridou, D., 2018. Evidence of extensional and strike-slip deformation in the offshore Gökova-Kos area affected by the July 2017 Mw6.6 Bodrum-Kos earthquake, eastern Aegean Sea. Geo-Marine Lett. 38, 211–225. https://doi.org/10.1007/s00367-017-0532-4

Özeren, M. S., Holt, W. E., 2010. The dynamics of the eastern Mediterranean and eastern Turkey, Geophys. J. Int., 183(3), 1165–1184.

Papadakis, G., Vallianatos, F., 2017. Non-extensive statistical physics analysis of earthquake magnitude sequences in North Aegean Trough, Greece. Acta Geophysica, 65 (3), pp. 555-563.

Papadimitriou, E., Sykes, L.R., 2001. Evolution of the stress eld in the northern Aegean Sea (Greece). Geophys. J. Int. 747–759.

Papadimitriou, E., Karakostas, V., Mesimeri, M., Chouliaras, G., Kourouklas, C., 2017. The Mw6.5 17 November 2015 Lefkada (Greece) Earthquake: Structural Interpretation by Means of the Aftershock Analysis. Pure Appl. Geophys. 174, 3869–3888. https://doi.org/10.1007/s00024-017-1601-3

Papadimitriou, P., Kaviris G. and Makropoulos, K., 1999. Evidence of shear wave splitting in the eastern Corinthian Gulf (Greece). Physics of the Earth and Planetary Interiors, 114, 3-13.

Papadimitriou, P., Kaviris, G., Makropoulos, K., 2006. The Mw= 6.3 2003 Lefkada earthquake (Greece) and induced stress transfer changes. Tectonophysics 423, 73–82. https://doi.org/10.1016/j.tecto.2006.03.003

Papadimitriou P., Voulgaris N., Kouskouna V., Kassaras I., Kaviris G., Pavlou K., Karakonstantis A., Bozionelos G., Kapetanidis V., 2014. The Kefallinia Island earthquake sequence January – February 2014. Abstract, 2nd ECEES, Istanbul, Turkey.

Papadimitriou, P., Karakonstantis, A., Bozionelos, G., Kapetanidis, V., Kaviris, G., Spingos, I., Millas, C., Kassaras I., Voulgaris, N., 2015. Preliminary report on the Lefkada 17 November 2015 Mw = 6.4 earthquake. Report published by EMSC. http://www.emsc-csem.org/Doc/Additional_Earthquake_Report/470390/20151117_lefkada_report_nkua.pdf.

Papadimitriou, P., Kassaras, I., Kaviris, G., Tselentis, G.-A., Voulgaris, N., Lekkas, E., Chouliaras, G., Evangelidis, C., Pavlou, K., Kapetanidis, V., Karakonstantis, A., Kazantzidou-Firtinidou, D., Fountoulakis, I., Millas, C., Spingos, I., Aspiotis, T., Moumoulidou, A., Skourtsos, E., Antoniou, V., Andreadakis, E., Mavroulis, S., Kleanthi, M., 2018. The 12th June 2017 Mw = 6.3 Lesvos earthquake from detailed seismological observations. J. Geodyn. 115, 23–42. https://doi.org/10.1016/j.jog.2018.01.009

Papadopoulos, G. A., Karastathis, V.K., Koukouvelas, I., Sachpazi, M., Baskoutas, I., Chouliaras, G., Agalos, A., Daskalaki, E., Minadakis, G., Moshou, A., Mouzakiotis, A., Orfanogiannaki, K., Papageorgiou, A., Spanos, D., Triantafyllou, I., 2014. The Cephalonia, Ionian Sea (Greece), sequence of strong earthquakes of January-February 2014: a first report. Res. Geophys. 4, 3–5. https://doi.org/10.4081/rg.2014.5441.

Papadopoulos, G. A., Agalos, A., Charalampakis, M., Novikova, T., Triantafyllou, I., Annunziato, A., Probst, P., Proietti, Ch., Kleanthi, M., Necmioğlu, Ö., Sozdinler, C. Ö., Dogan, G. G., Yalciner, A. C., 2017. The Lesvos Isl. (NE Aegean Sea) strong (Mw6.3) earthquake of 12 June 2017 and its associated tsunami. International Conference on the Recent Tsunami Events in the Aegean Sea. 12th - 13th December 2017, Ispra, Italy.

Papanikolaou D., Nomikou P., 1998. The Palaeozoic of Kos: a low grade metamorphic unit of the basement of the external Hellenides terrain. IGCP project no 276. Newsletter 6:155–166

Papanikolaou D., Lekkas E., 1990. Miocene tectonism in Kos. Dodekanese islands. Int earth sciences Congr on Aegean. The Region:179–180

Papanikolaou, D., Alexandri, M., Nomikou, P., Ballas, D., 2002. Morphotectonic structure of the western part of the North Aegean Basin based on swath bathymetry. Mar. Geol. 190, 465–492. https://doi.org/10.1016/S0025-3227(02)00359-6

Papanikolaou, D., Alexandri, M., Nomikou, P., 2006. Active faulting in the North Aegean basin. Geol. Soc. Am. Bull. 409, 189–209. https://doi.org/10.1130/2006.2409(11).

Papathanassiou, G., Valkaniotis, S., Ganas, A., Grendas, N., Kollia, E., 2017. The November 17th, 2015 Lefkada (greece) strike-slip earthquake: Field mapping of generated failures and assessment of macroseismic intensity ESI-07. Engineering Geology, 220, 13-30. doi:10.1016/j.enggeo.2017.01.019

Papazachos, C. B., Kiratzi, A. A., 1996. A detailed study of the active crustal deformation in the aegean and surrounding area. Tectonophysics, 253(1-2), 129-153. doi:10.1016/0040-1951(95)00047-X.

Papazachos, B.C., Papazachou, C., 2003. The Earthquakes of Greece. Ziti Publ., Thessaloniki, Greece.

Papazachos, B. C., Papaioannou C., Papazachos C., Savvaidis A. S., 1999. Rupture zones in the Aegean region, Tectonophysics, 308, 205–221.

Papazachos, B.C., Scordilis, E.M., Panagiotopoulos, D.G., Papazachos, C.B., Karakaisis, G.F., 2004. Global relations between seismic fault parameters and moment magnitude of earthquakes. Bull. Geol. Soc. Greece 36, 8.

Pavlides, S.B., Papadopoulos, G.A., Ganas, A., Papathanassiou, G., Karastathis, V., Keramydas, D., Fokaefs, A., 2004. The 14 August 2003 Lefkada (Ionian Sea) Earthquake. 5th International Symposium on Eastern Mediterranean Geology, Thessaloniki, Greece, 14–20 April 2004, Reference T5–34.

Pérouse, E., Chamot-Rooke, N., Rabaute, A., Briole, P., Jouanne, F., Georgiev, I., Dimitrov, D., 2012. Bridging onshore and offshore present-day kinematics of central and eastern Mediterranean: Implications for crustal dynamics and mantle flow. Geochemistry, Geophys. Geosystems 13, 1–25. https://doi.org/10.1029/2012GC004289

Philippon, M., Brun, J.-P., Gueydan, F., Sokoutis, D., 2014. The interaction between Aegean back-arc extension and Anatolia escape since Middle Miocene. Tectonophysics 631, 176–188. https://doi.org/10.1016/j.tecto.2014.04.039.

Razafindrakoto, H. N. T., Martin Mai, P., 2014. Uncertainty in earthquake source imaging due to variations in source time function and earth structure. Bull. Seism. Soc. Am., 104(2), 855-874. https://doi.org/10.1785/0120130195

Reilinger, R., McClusky, S.C., Paradissis, D., Ergintav, S., Vernant, P., 2010. Geodetic constraints on the tectonic evolution of the Aegean region and strain accumulation along the Hellenic subduction zone. Tectonophysics 488, 22–30.

Rhoades, D.A., Papadimitriou, E.E., Karakostas, V.G., Console, R., Murru, M., 2010. Pure Appl. Geophys., 167: 1049. https://doi.org/10.1007/s00024-010-0092-2

Rondoyanni Th., Sakellariou M., Baskoutas J., Christodoulou N., 2012. Evaluation of active faulting and earthquake secondary effects in Lefkas Island, Ionian Sea, Greece: an overview. Nat. Hazards, 61:843–860

Roussakis, G., Karageorgis, A.P., Conispoliatis, N., Lykousis, V., 2004. Last glacial - Holocene sediment sequences in N. Aegean basins: structure, accumulation rates and clay mineral distribution. Geo-Marine Lett. 24, 97–111. https://doi.org/10.1007/s00367-004-0167-0.

Sakkas, V., Lagios, E., 2015. Fault modelling of the early-2014 ~M6 earthquakes in cephalonia island (W. greece) based on GPS measurements. Tectonophysics, 644, 184-196. https://doi.org/10.1016/j.tecto.2015.01.010.

Sakellariou, D., Tsampouraki-Kraounaki, K., 2019. Plio-Quaternary Extension and Strike-Slip Tectonics in the Aegean, in: Transform Plate Boundaries and Fracture Zones. Elsevier, pp. 339–374. https://doi.org/10.1016/B978-0-12-812064-4.00014-1

Sakellariou, D., Mascle, J., Lykousis, V., 2013. Strike Slip Tectonics and Transtensional Deformation in the Aegean Region and the Hellenic Arc : Preliminary Results. Bull. Geol. Soc. Greece XLVII, 647–656.

Sakellariou, D., Rousakis, G., Vougioukalakis, G., Panagiotopoulos, I., Morfis, I., Zimianitis, E., Athanasoulis, K., Mpardis, D., Karageorgis, A.P., 2016. Deformation Pattern in the Western North Aegean Trough: Preliminary Results. Bull. Geol. Soc. Greece, L, 1799–1807.

Saltogianni, V., Gianniou, M., Yolsal-çevikbilen, S., Eken, T., Taymaz, T., 2015. Seismological and Geodetic Modeling of the 2014, Mw 6. 8 Earthquake of North Aegean Trough 17, 4839.

Saltogianni, V., Gianniou, M., Moschas, F., Stiros, S., 2016. Pattern of dynamic displacements in a strike-slip earthquake. Geophys. Res. Lett., 43(13), 6861-6868. https://doi.org/10.1002/2016GL069507.

Saltogianni, V., Taymaz, T., Yolsal-Çevikbilen, S., Eken, T., Moschas, F., Stiros, S., 2017. Fault model for the 2015 leucas (aegean arc) earthquake: Analysis based on seismological and geodetic observations. Bull. Seism. Soc. Am., 107(1), 433-444. doi:10.1785/0120160080.

Saltogianni, V., Moschas, F., Stiros, S., 2018. The 2014 Cephalonia Earthquakes: Finite Fault Modeling, Fault Segmentation, Shear and Thrusting at the NW Aegean Arc (Greece). Pure Appl. Geophys., 1-20. https://doi.org/10.1007/s00024-018-1938-2

Sboras, S., Chatzipetros, A., Pavlides, S., 2017. North Aegean Active Fault Pattern and the 24 May 2014, Mw 6.9 Earthquake. Act. Glob. Seismol. Neotectonics Earthq. Potential East. Mediterr. Reg. 239–272. https://doi.org/10.1002/9781118944998.ch9

Scordilis, E.M., Karakaisis, G.F., Karacostas, B.G., Panagiotopoulos, D.G., Comninakis, P.E., Papazachos, B.C., 1985. Evidence for transform faulting in the Ionian Sea: the Cephalonia island earthquake sequence of 1983. Pageoph, 123, 387–397.https://doi.org/10.1007/BF00880738

Şengör, A.M., 1979. The North Anatolian transform fault: its age, offset and tectonic significance. J. Geol. Soc. London. 136, 269–282. https://doi.org/10.1144/gsjgs.136.3.0269

Şengör, A.M., Tüysüz, O., İmren, C., Sakınç, M., Eyidoğan, H., Görür, N., Le Pichon, X., Rangin, C., 2005. the North Anatolian Fault: a New Look. Annu. Rev. Earth Planet. Sci. 33, 37–112. https://doi.org/10.1146/annurev.earth.32.101802.120415

Shao, G., Ji, C., 2012. What the exercise of the SPICE source inversion validation BlindTest 1 did not tell you. Geophys. J. Int. 189, 569–590. https://doi.org/10.1111/j.1365-246X.2012.05359.x

Shaw, B., Jackson, J., 2010. Earthquake mechanisms and active tectonics of the Hellenic subduction zone. Geophys. J. Int. 181, 966-984. https://doi.org/10.1111/j.1365-246X.2010.04551.x

Sokos, E., Kiratzi, A., Gallovič, F., Zahradník, J., Serpetsidaki, A., Plicka, V., Janský, J., Kostelecký, J., Tselentis, G.A., 2015. Rupture process of the 2014 Cephalonia, Greece, earthquake doublet (Mw6) as inferred from regional and local seismic data. Tectonophysics 656, 131–141. https://doi.org/10.1016/j.tecto.2015.06.013.

Sokos, E., Zahradník J., 2017. Lesvos June 12, 2017, Mw 6.3 event, a quick study of the source. Report published by EMSC. https://www.emsc-csem.org/Files/news/Earthquakes_reports/Lesvos_Source_Study_Sokos_and_Zahradnik.pdf.

Sokos, E., Zahradník, J., Gallovič, F., Serpetsidaki, A., Plicka, V., Kiratzi, A., 2016. Asperity break after 12 years: The Mw6.4 2015 Lefkada (Greece) earthquake. Geophys. Res. Lett. 43. https://doi.org/10.1002/2016GL069427.

Somerville, P., Irikura, K., Graves, R., Sawada, S., Wald, D., Abrahamson, N., Iwasaki, Y., Kagawa, T., Smith, N., Kowada, A., 1999. Characterizing crustal earthquake slip models for the prediction of strong ground motion. Seismological Research Letters, 70(1), 59-80.

Stein, S., Wysession, M., 2003. An introduction to seismology, earthquakes, and earth structure. Malden, MA: Blackwell Pub.

Stucchi, M., Rovida, A., Gomez Capera, A.A., Alexandre, P., Camelbeeck, T., Demircioglu, M.B., Gasperini, P., Kouskouna, V., Musson, R.M.W., Radulian, M., Sesetyan, K., Vilanova, S., Baumont, D., Bungum, H., Fäh, D., Lenhardt, W., Makropoulos, K., Martinez Solares, J.M., Scotti, O., Zivcic, M., Albini, P., Batllo, J., Papaioannou, C., Tatevossian, R., Locati, M., Meletti, C., Viganò, D., Giardini, D., 2013. The SHARE European Earthquake Catalog (SHEEC) 1000–1899. J. Seismol. 17 (2), 523–544.

Taymaz, T., Jackson, J., McKenzie, D., 1991. Active tectonics of the north and central Aegean Sea. Geophys. J. Int. 106 (2), 433e490. http://dx.doi.org/10.1111/j.1365-246X.1991.tb03906.x.

Taymaz, T., Yilmaz Y., Dilek Y., 2007. The geodynamics of the Aegean and Anatolia: introduction, in The Geodynamics of the Aegean and Anatolia, edited by T. Taymaz, Y. Yilmaz, and Y. Dilek, 1–16, Geological Society, London, Special Publications., 291.

Theodoulidis, N., Karakostas, C., Lekidis, V., Makra, K., Margaris, B., Morfidis, K., Papaioannou, C., Rovithis, E., Salonikios, T., Savvaidis, A., 2016. The Cephalonia, Greece, January 26 (M6.1) and February 3, 2014 (M6.0) earthquakes: near-fault ground motion and effects on soil and structures. Bull. Earthq. Eng. 14, 1–38. https://doi.org/10.1007/s10518-015-9807-1.

Tiryakioglu, I., Yigit, C. O., Yavasoglu, H., Saka, M. H., Alkan, R. M., 2017. The determination of interseismic, coseismic and postseismic deformations caused by the gökçeada-samothraki earthquake (2014, Mw: 6.9) based on GNSS data. Journal of African Earth Sciences, 133, 86-94. https://doi.org/10.1016/j.jafrearsci.2017.05.012.

Trabant, C., Hutko, A.R., Bahavar, M., Karstens, R., Ahern, T., Aster, R., 2012. Data products at the IRIS DMC: stepping stones for research and other applications. Seismol. Res. Lett. 83 (5), 846e854. http://dx.doi.org/10.1785/0220120032.

Triantaphyllis M., 1994. Geological map of Greece, western Kos, sheet (Kefalos) 1:50,000. Inst, Geology Mineral Exploration (IGME), Athens

Tzanis, A., Vallianatos, F., Makropoulos, K., 2000. Seismic and electrical precursors to the 17-1-

1983, M7 Kefallinia Earthquake, Greece: Signatures of a SOC system. Phys. Chem. Earth 25:281-287.

Tur, H., Yaltirak, C., Elitez, T. And Sarikavak, K.T., 2015. Pliocene-Quaternary tectonic evolution of the Gulf of Gökova, southwest Turkey. Tectonophysics, 638(1), pp. 158-176.

Voulgaris, N., Parcharidis, I., Pahoula, M., Pirlis, E., 2004. Correlation of tectonics, seismicity and geothermics of Lesbos Island using remote sensing data and geographical information systems. Bull. Geol. Soc. Greece XXXVI, 938–947.

Waldhauser, F., 2001. HypoDD-A Program to Compute Double-Difference Hypocenter Locations. U.S. Geol. Surv. Open File Rep.01-113. 25 p.

Wells, D.L., Coppersmith, K.J., 1994. New empirical relationships between magnitude, rupture length, rupture width, rupture area, and surface displacement. Bull. Seism. Soc. Am. 84, 974e1002.

Yılmaz Y., Genç Ş. C., Gürer F., Bozcu M., Yılmaz K., Karacık Z., Altunkaynak Ş., Elmas A., 2000. When did the western Anatolian grabens begin to develop? In: Bozkurt E,Winchester JA, piper JDA (eds) tectonics and magmatism in Turkey and surrounding area. Geological Society of London, Special Publication 173(1):353–384. https://doi.org/10.1144/GSL.SP.2000.173.01.17

Yalciner, C.A., Annunziato, A., Papadopoulos, G.A., Guney Dogan, G., Gokhan Guler, H., Eray Cakir, T., Ozer Sozdinler, C., Ulutas, E., Arikawa, T., Suzen, L., Kanoglu, U., Guler, I., Probst, P., Synolakis, C., 2017. The 20th July 2017 (22:31 UTC) Bodrum/Kos Earthquake and Tsunami; Post Tsunami Field Survey Report 2017, 115.

Yaltirak, C., Alpar, B., 2002. Evolution of the NAF Middle segment and shallow seismic investigation of the Southestern Sea of Marmara (Gemlik Bay). Mar. Geol. 190, 307–327.